Design and Performance Comparison of Novel High Q Coaxial Resonator Filter for Ka-band High Throughput Satellite

Thesis

Submitted by

Vineet Kumar Dad
(201321004)

in partial fulfillment of the requirements

for the degree of

Doctor of Philosophy

to

Dhirubhai Ambani
Institute of Information and Communication Technology,
Gandhinagar, Gujarat, India

June, 2021

Author's Declaration

This is to certify that

1. The thesis comprises my original work towards the degree of Doctor of Philosophy in Information and Communication Technology at DA-IICT and has not been submitted elsewhere for a degree,
2. Due acknowledgment has been made in the text to all other material used.

Signature of Student

Certificate

This is to certify that the thesis work entitled "Design and Performance Comparison of Novel High Q Coaxial Resonator Filter for Ka-band High Throughput Satellite" has been carried out by Vineet Kumar Dad (201321004) for the degree of Doctor of Philosophy in Information and Communication Technology at this Institute under my supervision.

Thesis Supervisor

Prof. (Dr.)Sanjeev Gupta

Dedicated to

My wife Ushma, My son Aarav, My In-laws and My Parents

Acknowledgments

First and foremost, I thank my family for providing me inspiration, strength, energy, constant support and patience to start and accomplish my goal. The work described in this thesis cannot accomplish without the help, and support of others, a few of them, I am trying to acknowledge.

First of all, I would like to thank my research advisor, Prof. (Dr.) Sanjeev Gupta, for his guidance and support. I am especially grateful to him for providing an extraordinary research environment, resources, and continuous discussion regarding the direction of workflow. His result-oriented nature always inspires me. Without his motivation and valuable suggestions, this research could not have been possible.

I am also grateful to the members of my Research Progress Committee members Prof. Biswajit Mishra and Prof. Deepak Ghodgoankar for their patience and suggestions which help in determining the direction of my research.

I am also grateful to the members of my Synopsis Review Committee members Prof. Deepak Ghodgaonkar and Prof. Biswajit Mishra for reviewing my synopsis and providing valuable guidance to improve the work related to my thesis.

I am grateful to the Director Space Applications Centre for approving study leave to enroll for PhD program at DAIICT. I would like to thank Shri Tushar Gajjar to overcome the issue regarding practical realization of filter, my

colleagues and seniors who provide facility for testing of filter and suggestion to improve the research results. I would also thank mechanical engineer Shri. Keyur Trivedi for mechanical design and support needed for realization of filter. Moreover, I would like to thank the mechanical and electrical fabrication facility staff at Space Applications Centre (SAC), ISRO for providing valuable help and support.

I would like to thank the staff members of DA-IICT Resource Centre for their cooperation related to literature survey required for my work.

Finally, I would like to express my appreciation to my parents and my in-laws for encouragement which have been a source of strength for me to finish the presented work.

Abstract

The filters deployed in the satellite are high-performance filters that have very stringent in-band and out of band performance. They require high Q resonators with spurious free-range for their realization. But, the Q factor decrease with an increase in frequency. Currently, Ka-band high throughput satellite uses cavity filters in its payload because of its known performance and well-established realization process. This thesis presents novel high Q filters, which provide an alternative to conventional cavity filters.

The Ka-band filters developed using two different technologies. The first is a fully tunable Non-radiative dielectric waveguide filter, and the second is the High Q coaxial resonator filter. For the first time, high Q TM_{012} mode of the coaxial resonator used at Ka-band for filter realization. The direct and cross-coupled filters have designed to demonstrate the concept of higher-order modes of the coaxial resonator for filter development. The high power analysis has done for the identical configuration cross-coupled coaxial resonator and cavity filter; compare their performance over operating temperature from -15^0C to 65^0C. These filters fabricated from metal and their frequency drift depend on the coefficient of thermal expansion of metal, which should be minimum to have a stable response in the space environment. The analytical tool used to minimize the frequency drift of the coaxial resonator filter and compensate it over the operating temperature. The temperature-compensated coaxial resonator filter has developed with this tool, and its performance is compared with the identical uncompensated filter. This temperature-compensated filter provides more design margin without increasing the complexity.

Contents

List of Figures

List of Tables

List of Acronyms

BPF	Bandpass Filter
BW	Bandwidth
CF	Center Frequency
CPW	Coplanar Waveguide
CTE	Coefficient of Thermal Expansion
DA	Driver Amplifier
DPLXR	Diplexer
DR	Dielectric Resonator
FBW	Fractional Bandwidth
HRF	Harmonic Reject Filter
HTS	High Throughput Satellite
HYB	Hybrid
IL	Insertion Loss
IMUX	Input Multiplexer
LTWTA	Linearized Travelling Wave Tube Amplifier
MIC	Microwave Integrated Circuit
MNRD	Modified Non-Radiative Dielectric Waveguide
NRD	Non-Radiative Dielectric Waveguide
OMUX	Output Multiplexer
PSF	Pre-Select Filter
Q	Quality Factor
RF	Radio Frequency
RL	Return Loss
Rx	Receiver
SOI	Silicon on Insulator
SSPA	Solid State Power Amplifier
SW	Switch
SWM	Switch Matrix
TC	Test Coupler

Chapter 1

Introduction

1.1. Motivation

The demand for broadband is rapidly exhausting the available capacity of existing Ku-band and leads to the evolution of High throughput satellite (HTS) in Ka-band Large and small enterprises increasingly depend on media-rich applications to grow their businesses and retain their competitive edge. Governments need high-bandwidth applications to deliver services to their citizens, and consumers want to watch movies, make VoIP phone calls, and browse the Web—all at the same time. The first generation of high throughput satellite operate in Ku-band, but the Ku-band spectrum is saturated, and the next generation of HTS operate in Ka-band due to uncrowded available spectrum in the Ka-band. The high bandwidth available in the Ka spectrum and frequency re-use capabilities across multiple beams enable the delivery of more capacity at faster speeds to smaller dishes—opening the door to upgraded services at lower costs for more users [1]. These HTS require high-performance filters, which used both at transmitting and receiving end. The demand for high-performance filters requires high Q-factor resonator makes it challenging to design them at higher frequency bands. Simultaneously, these resonators

should have a very wide spurious-free range and good thermal stability to be used for filtering applications in the satellite.

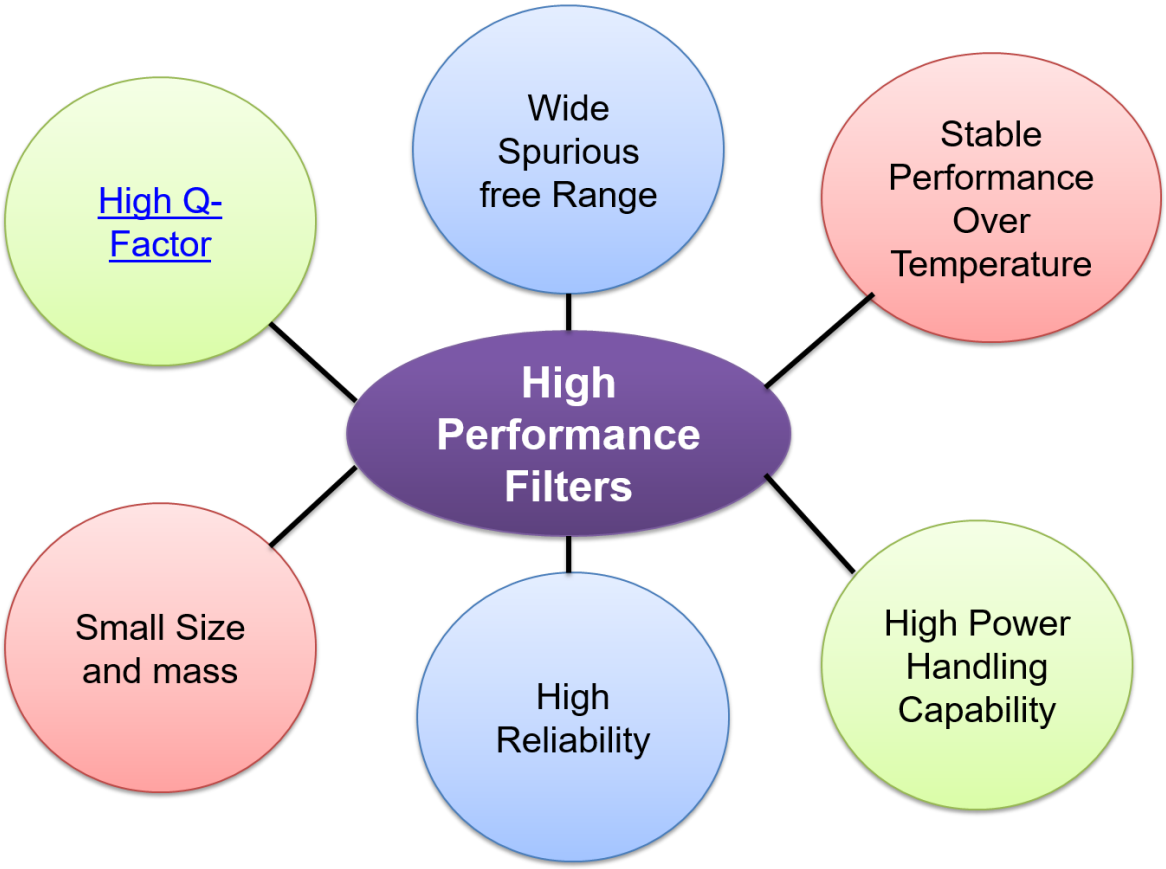

Figure 1.1 *Requirement for high performance filter.*

Figure 1.1 shows the requirement for a high performance filter. These high-performance filters use high-quality factor resonator to achieve the specifications, which are either direct-coupled or cross-coupled resonator based filters. The quality factor decreases as the frequency increases and is proportional to the ratio of volume to the surface area. The commonly used microwave resonators are planar resonators and three-dimensional resonators. The planar resonators with different shapes and topologies realized on the microstrip substrate have low Q (Q<200) and seldom used at Ka-band for high-

performance filters. The three-dimensional resonators are MEMS resonator, coaxial resonator, waveguide resonator, gap waveguide resonator, cavity resonator, and dielectric resonators. These resonators offer moderate to very high Q depending upon its type. The resonators used for high-performance filters should have reasonably high Q, small size, less mass, wide spurious free range; stable performance over the operating temperature range, high power handling capability and high reliability that is must for filters used in satellite applications. Figure 1.2 shows the insertion loss variation of different types of resonator considering their size. The MEMS resonators are compact but have moderate Q at Ka-band [2-3]. The dielectric resonators are being used till Ku-band in payloads due to its small size, high-Quality factor, and better performance over the temperature, but they suffer from the problem of inferior spurious free range and better suited for narrowband filters [4].

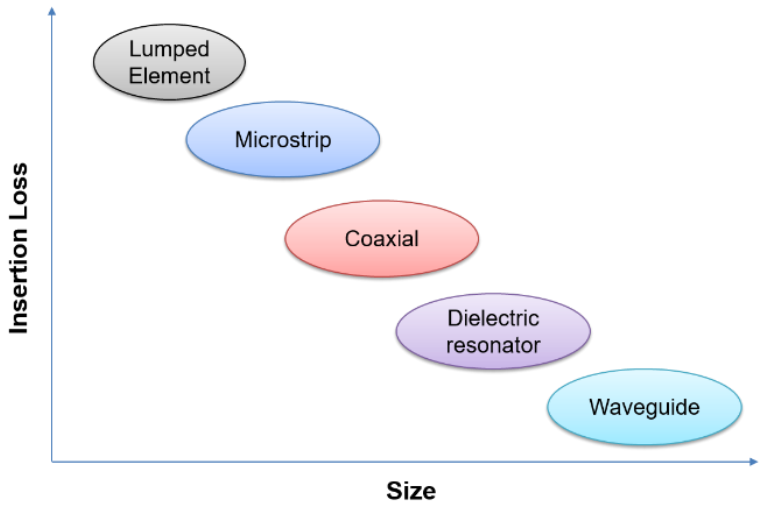

Figure 1.2 *Variation of insertion loss with size of resonator.*

Moreover, DR size and Q-factor decreases with an increase in frequency, and they are difficult to handle at Ka-band. The cavity resonators are the state of

art for very high-frequency filters due to their high Q, fairly good size, better power handling capability and its predictable performance over the temperature [5]. They offer wide spurious-free window if operated in the dominant mode, else the higher order spurious mode is to be suppressed, which is bit tedious task. The coaxial resonators' dominant TEM mode offer high Q, small size, good power handling capability and very wide spurious free range, but the TEM mode coaxial resonator filter application is limited to C-band because their Q decreases drastically with increase in the frequency. The filters developed with the TEM mode coaxial resonator are direct-coupled or cross-coupled, and in each form, the emphasis is on performance improvement and size reduction [6-9]. From many decades, in the gyrotron application, the higher order Transverse electric (TE) or Transverse magnetic (TM) modes of the coaxial resonators are used [10]. These higher order modes have very high Q and never explored for the filter application. Recently, the higher order mode of the coaxial resonator uses for filter realization at Ka-band. This thesis explores the novel approaches to realize high Q high-performance filters at Ka-band for high throughput satellite.

1.1.1. Importance of filters in Satellite

The heart of the communication satellite is a payload, which consists of many transponders responsible for providing communication link. The different types of filters cover more than 60% of the payload, and without filters, it is difficult to imagine a communication payload. They have shown as a shaded region in figure 1.3. The low power filters

deployed at the front-end of the payload before the TWTA and high power filters at the back end.

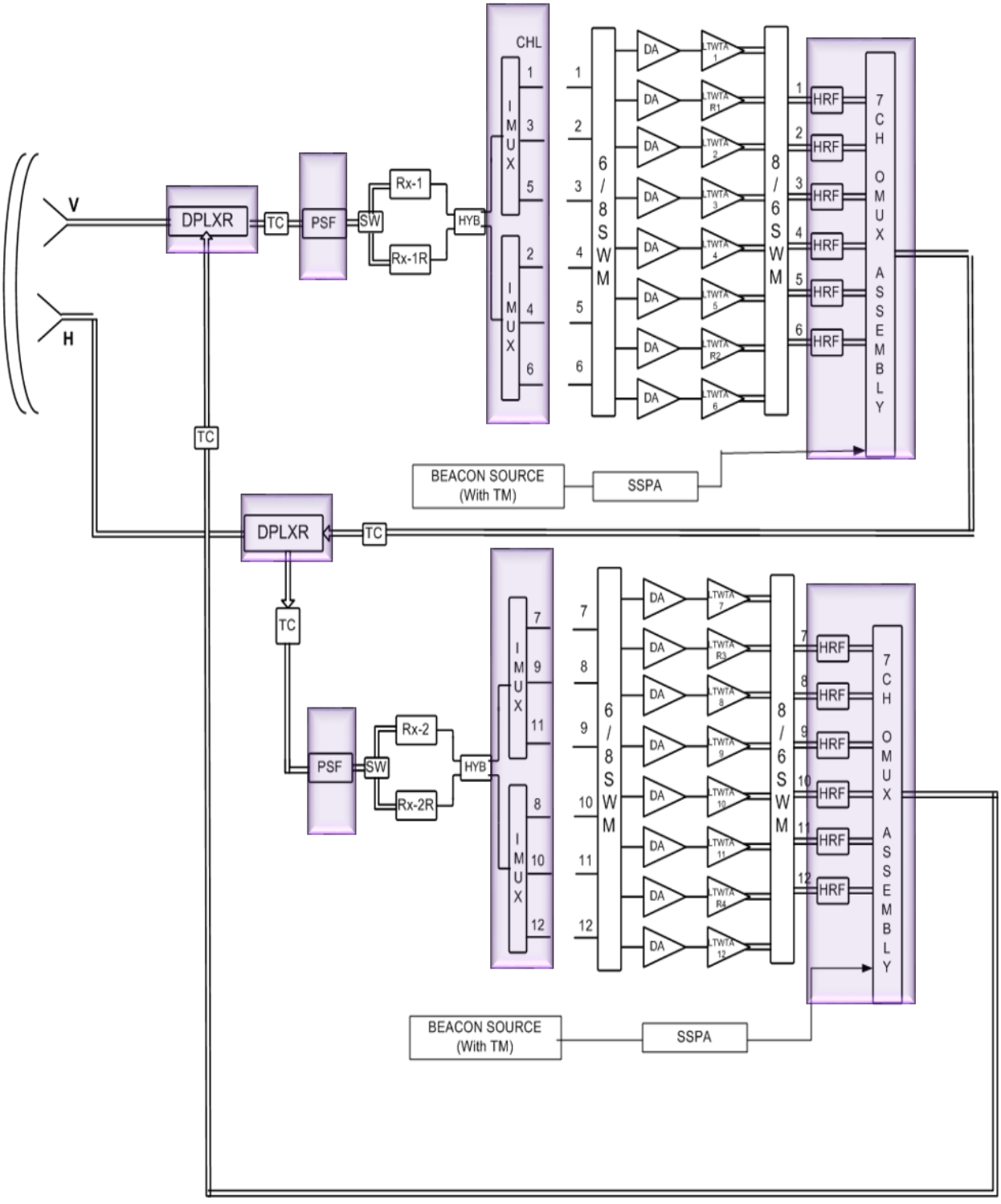

Figure 1.3 *Communication payload block diagram (12-channel transponder).*

These filters are high-performance filters as their specifications are stringent and have superior passband (in-band) and stopband (out-of-band) performance with an insignificant impairment to the signal. These filters require high-quality factor, wide spurious free range, small mass and size, high power handling capability and stable thermal behaviour.

The pre-select filter is a bandpass filter deployed after antenna should have low insertion loss and offer very high isolation to the transmit band. It requires high Q and wide spurious free resonators for their realization. There are many different types of filters used in the receiver for rejection only with a minimal insertion loss. After receiver, the incoming frequency band channelized into different RF channels by Input multiplexer (IMUX), which is a bank of bandpass filters tuned at different channel frequencies. The IMUX filters are high Q filters as it has very good bandpass flatness and offers very high isolation to the adjacent channels. The IMUX filters have a wide spurious free response, so that spurious may not fall in the frequency band of operation. The output multiplexer (OMUX) filter used to combine the channels after being amplified by TWTA. They have very low insertion loss and have signification isolation for the combining signal. They require high Q resonator, which can handle very high power with a wide spurious free performance. The harmonic reject filters which are inherently lowpass filters are used at the output of the payload to reject the harmonics of TWTA.

1.1.2. Communication Satellite filters

The satellite communications started with the Intelsat series, and the Intelsat IV was the first to use a channelized architecture in which 500-MHz uplink around 6 GHz has received by satellite, amplified using a low-noise amplifier (LNA) and down convert downlink band from 3.7 to 4.2 GHz. This 500 MHz band is channelized into 36 MHz bandwidth channels using an input multiplexer. These individual channels are known as transponders, and each channel is amplified and recombined using an output multiplexer. After recombining, they are feed to the transmit antenna [5] which creates the need for high-performance filters and multiplexers. The insertion loss of the input multiplexers is of relatively little importance as the noise figure depends on the Low noise amplifier. On the other hand, the insertion loss of the output multiplexer is critical, as it directly affects the link budget. The output multiplexers use rectangular waveguide filters constructed from Invar (for temperature stability), which combined in a common waveguide manifold, with each channel filter providing high isolation to signals in non-adjacent bands. These multiplexers were very large and heavy, weighing about 4 kg per channel. The methods of reducing this weight were of paramount importance. The first breakthrough was the use of dual-mode filters, where two orthogonal degenerate modes in the same physical cavity are excited. Comsat Laboratories, Canada developed the first practical devices [11–13]. The Triple mode and quad-mode filter

designs offer further size reduction, but they are very sensitive and suffer from poor temperature stability. The next stimulus to research was the adoption of higher frequencies, in particular, the 14/12-GHz band for direct broadcast satellites. Standard designs at these frequencies would have an unacceptable 1 dB more loss than the 6/4-GHz band. This led to the development of TE_{10N} and TE_{11N} filters, where N is an integer corresponds to the number of half-wavelength cavity lengths [14]. Then the advancement was made in the methods and theory of multiplexing from non-contiguous to contiguous [15-17]. Satellite communications also stimulated work on filter transfer functions and network synthesis. The use of high permittivity and high Q ceramics termed as dielectric resonators were used to construct single mode filters, which offer very good size, volume, and mass reduction [18]. The further development in this area was the use of dual-mode dielectric resonator filter, which matches the performance of single mode and has significant size, volume, and mass reduction. The other major development was High-temperature superconductor filter where ultra-high Q resonators cooled to 77 K [19]. They offer huge mass saving at the expense of cryo-coolers. The major focus on communication filters is to reduce the footprint and mass without any compromise on its performance. Moreover, the power of communication satellite is increasing pose a major challenge to dissipate the heat, which requires an efficient thermal design with minimum frequency drift in the filter over the operating temperature.

1.2. Research Contribution

The satellite filters are high performance and high Q filters, which have low loss and steep rejection over the operating temperature. The prime objective of the thesis is to explore and implement the novel high Q resonator-based filters at Ka-band for high throughput satellite.

Also, the filters must have comparable performance compared to the conventional waveguide filters used in the satellite. The contributions are as follows:

1) The high Q resonators are explored and found that the three-dimensional resonator offers the highest Q-factor among different types of microwave resonator. The LSM_{01} mode of Non-Radiative Dielectric Waveguide and higher-order modes of coaxial resonators has explored.

2) Besides high Q, the modes should have a wide spurious free window and tunability to be used for the filter application. The NRD guide based filter reported in the literature lacks tuning. So, the LSM_{01} mode of E-plane resonator with mechanical tuning proposed for the filter design. The fabricated MNRD guide filter offers for both centre frequency and bandwidth tunability. The TM_{012} mode of coaxial resonator offers ultra-wide spurious-free window, use for the first time for filter application. The TM_{012} mode used to design and realize direct and cross-coupled filters at Ka-band to validate the concept of higher-order coaxial resonator modes for filter application.

3) The cross-coupled waveguide filter design with the overmoded cavity to achieve cross-coupling. Here, a solution has proposed to use a non-resonating post instead of overmoded cavity to realize cross-coupling in the waveguide filter, which makes the waveguide filter compact.

4) The proposed 5-2-0 TM_{012} mode coaxial resonator filter to be used for satellite must comply with the performance that can achieve with the conventional waveguide filter. So, an identical waveguide configuration compact waveguide filter has designed, and its performance compared with the proposed filter.

5) The filters deployed at the output section of the payload can able to withstand high power. The rigorous high power analysis of both the filters done, so that, they can be used for high power applications.

6) The filter response should be stable over the operating temperature in the satellite. The thermal stability of the filter determined by the frequency drift of the filter. The proposed temperature compensated coaxial resonator filter uses Invar metal post to minimize its frequency drift without any compromise on the RF performance. The high Q temperature compensated coaxial resonator filter at Ka-band has proposed for the first time. This approach does not degrade the resonator Q, and at the same time provide excellent design margin without increasing the overall filter weight.

1.3. Organization of the Thesis

The thesis has organised into six different chapters. Chapter 2 is the literature survey which discussed the work done for various types of filters at Ka-band. To emulate a low Q resonator to behave as high Q, Predistortion technique employed in the filter has discussed. Since the filters deployed in the satellite have a stable response over the operating temperature. So, temperature compensated filters and approaches of temperature compensation have discussed.

Chapter 3 describe the method to realize the transfer function for direct and cross-coupled microwave filters. The filters synthesized through the coupling matrix whose elements give the coupling between the resonators.

Chapter 4 describe the mechanically tunable Non-Radiative Dielectric Waveguide filter. The low loss LSM_{01} mode of E-plane resonator used to design a filter at Ka-band. The filter centre frequency, as well as bandwidth, can be tuned with the help of screws.

Chapter 5 discussed in detail about the higher-order modes of the coaxial resonator. The high Q TM_{012} mode with an ultra-wide spurious-free window has used to realize the filter at Ka-band. The concept of high Q higher-order mode for filter realization is validated through the direct and cross-coupled filter. The compact cross-coupled waveguide filter designed for the identical configuration TM_{012} mode based coaxial resonator filter and their RF performance compared along with the high power analysis.

Chapter 6 provide the method for temperature compensation of High Q coaxial resonator-based filter at Ka-band. Here, the analytical tool of sensitivity analysis used to calculate the temperature compensation. The coaxial post of Aluminium is replaced by Invar metal post to achieve temperature compensation without any impact on the RF performance of the filter. The performance of temperature compensated and uncompensated filters have compared for the identical configuration filter.

Finally, conclusion and future scope are provided in chapter7.

1.4. List of Publications

1) V. K. Dad and S. Gupta, "**Novel High Q Coaxial Resonator Filter for Millimeter Wave Application**," *2017 IEEE MTT-S International Microwave and RF Conference (IMaRC)*, 2017, pp. 1-4, doi: 10.1109/IMaRC.2017.8449676.
2) Vineet K. Dad and Sanjeev Gupta, Sanjeev, "**Design and performance comparison of a novel high Q coaxial resonator filter and compact waveguide filter for millimeter wave payload applications.**" *International Journal of RF and Microwave Computer-Aided Engineering, Wiley* ***Publications Inc.***; Vol. 29, No. 8, August 2019. https://doi.org/10.1002/mmce.21773
3) Dad, Vineet K., and Gupta, Sanjeev, "**Temperature compensated high Q coaxial resonator filter for high throughput satellite.**" submitted for review to Engineering Reports.

Chapter 2

Literature review

2.1. Introduction

The microwave filters are resonator coupled filter, which is either directly coupled or cross-coupled. This chapter introduces the various filter technologies, especially Ka-band, and their feasibility in realizing payload filter. Apart from the technologies, the techniques like Predistortion to improve the in-band performance of filter are also introduced. Moreover, the payload filter has to operate satisfactorily in the space environment facing temperature excursion. The various temperature compensation techniques for filters reported in the last three decades has been reviewed.

2.2. Ka-band Filters

The resonant cavities or three-dimensional resonators are used to realize Ka-band filters for satellite applications. There are different technologies for realization of cavity filters, and they are as follows:

1) Micromachined cavity filters
2) Substrate Integrated waveguide filters
3) Cavity Filters

2.2.1. Micromachined Cavity filters

The work on micromechanical resonator and silicon micromachined structure start with the fabrication of plated-metal cantilever beam in 1967 by Nathanson [20], but the micromachined filter gained popularity last two decades because of the their small size, use of IC technology process for fabrication, low mass and good RF performance. In this technology, metallized cavities and suspended membranes have realized in Silicon or SOI (Silicon on Insulator) substrates. The multilayer approach of stacking multiple cavities by bonding reduces the footprint. The flexibility of designing input and output ports on the same layer gives the surface mountable filters provides good ease of integration with monolithic circuits. Despite their advantages, the single-layer filters have high losses (i.e. low Q-factor) compared to 3D resonators, prone to fabrication process tolerances, no tunability because of their small size, thermal drift, and their cavity wall surface roughness which mainly determine their Q-factor.

The work started with the micromachined components developed on a microshielded line [21-26]. The microshield is a quasi-planar half-shielded design, which uses a thin dielectric membrane to support the conducting lines. The W-band filter developed with the microshield lines. A 90 GHz low pass filter and 95 GHz bandpass filter has been presented at W-band and their performance is at par with the planar filter technologies like microstrip and CPW [27].

The WR-10 rectangular waveguide has been fabricated from (100) silicon wafer using micromachining technique for 75 GHz–115 GHz [28]. The waveguide split in two half along the broadside to ease fabrication. This opens the way for the design of a micromachined cavity filter with a high Q and small footprint. The micromachined cavity resonators are the building block of the filter. A high Q micromachined filter consisting of input and output microstrip lines and rectangular cavities on different dielectric layers in vertical stacking greatly reduces the occupied area. The cavities made by Si micromachining and are metallized by conventional micromachining techniques. Coupling between the cavities and the microstrip line is achieved via the slots etched at appropriate locations with respect to the microstrip lines [29-31]. The micromachined cavity has Q similar to a metallic waveguide cavity with the same dimensions, but it has the advantage of maintaining a planar form that allows for easy integration for MIC. This concept of vertical stacking resonator was used to fabricate a three-pole filter with 3.7% bandwidth at 10.01 GHz. The measured de-embedded insertion loss of the filter is 2.0 dB attributed to the CPW-microstrip transition line length and the fabrication process reduced the conductivity [32].

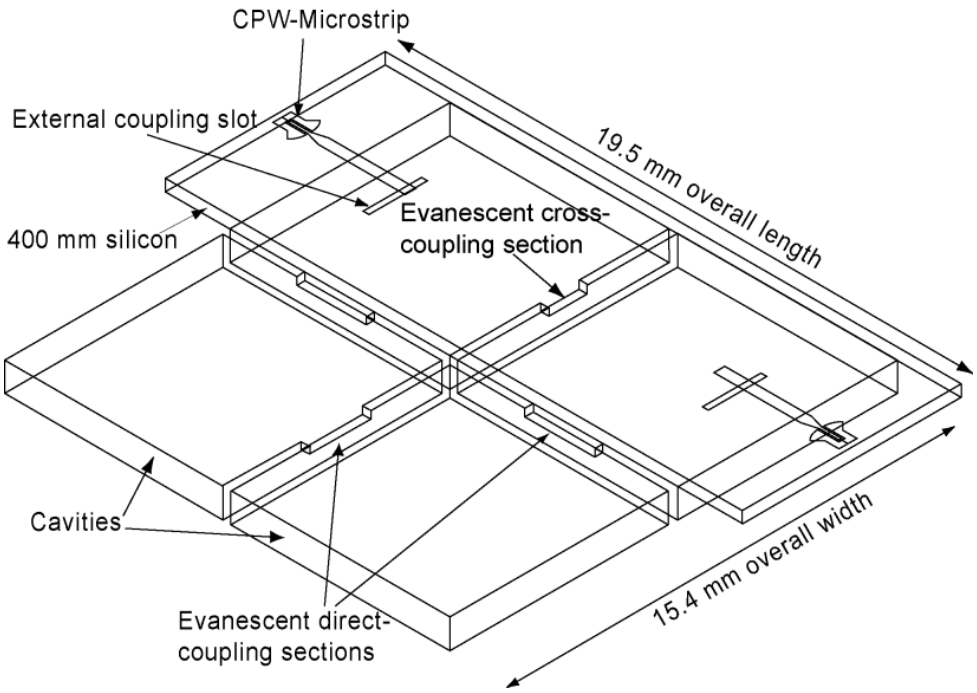

Figure 2.1 *Cross-sectional schematic of four-pole linear phase filter [32].*

The good work was done [32] by the authors used horizontal integration of cavity where resonators are placed side by side and coupled by evanescent waveguide shown in fig. 2.1. They have designed a four-pole filter at 27 GHz. The filter has 1.9% fractional bandwidth centered at 27.604 GHz with an insertion loss of 1.6 dB. The unloaded Q-factor was 1465. The same concept with a similar coupling scheme was used to design a bandpass filter around 20 GHz [33]. However, this approach produces an inclined or non-vertical sidewall cavity due to the etching. Moreover, the processing condition affects the surface roughness, which increases the conductor losses of the metallized cavity, affects Q-factor. The multilayer micromachined cavity resonators and filters at 38 GHz demonstrated where each layer made of gold-coated

silicon, structured by deep reactive etching. The measured unloaded Q-factor was 343 at 38 GHz, which is poor to realize front-end filters for high throughput satellite [3].

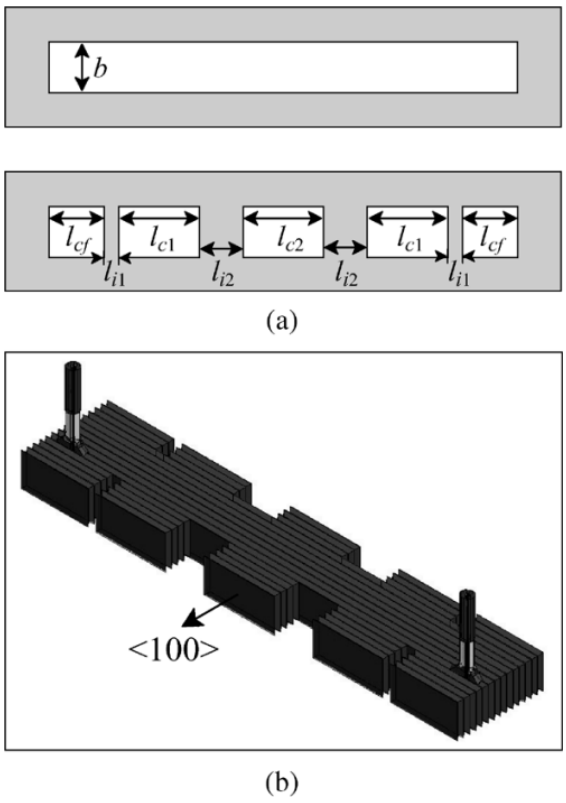

Figure 2.2 *(a) Layout of etched silicon wafer pieces, and (b) perspective view of width-stacked filter design [35].*

Another work to improve the Q of the micromachined cavity was done by Micah Stickel, et. al. They fabricate a micromachined cube cavity of dimension 7.071 mm*7.071 mm* 7.5 mm with a measured Q of 4500 at 29.314 GHz, where wafers are bonded by electroplating thick copper [34]. Later on, they demonstrate a three-pole bandpass filter at 29.7 GHz with 654 MHz bandwidth. In this filter, the width of the rectangular waveguide structure is created through the stacking of etched silicon wafer pieces shown in figure 2.2. The measured

insertion loss of the filter is 1 dB, while the predicted passband insertion loss was 0.45 dB [35]. The etching and metallization was the major drawback to achieve desired performance.

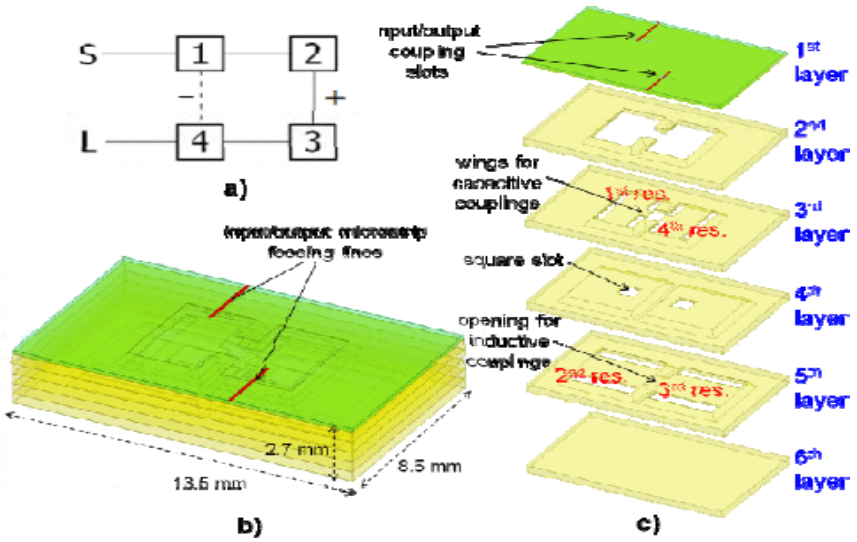

Figure 2.3 *(a)Fourth order filter topology with a negative sign coupling between 1st and 4th resonators, (b) perspective view of the 4th order filter, and (c) details of the layers [37].*

The compact and low loss 4th order pseudo-elliptic filter at Ka-band in multilayer micromachined technology is designed and fabricated, which is having good reproducibility. The stacking of six silicon layers reduces the footprint. The filter design on λ/2 TEM Si membrane resonators placed inside shielding cavities, and short-circuited at both anchored ends. The fourth-order filter shown in figure 2.3. It has a 50%-footprint reduction compared to TE_{101} resonant mode cavity filter but has a poor Q-factor of about 500 [36-37]. This filter has been used by European Space Agency (ESA) for their project, and they are suitable when they used in integration with active packages like a receiver for rejection of

harmonics and unwanted signal. They meant for unwanted signal suppression where there is no emphasis on in-band filter performance, which largely depends on the Q-factor of the resonator. The micromachined 3D filter designed has a wide-bandpass characteristic of 39%; with an insertion loss of 1.7 dB at 33.2 GHz is suitable for high power MMIC applications. This filter is compact but has a low Q [38]. Apart from this, work is going on in the submillimeter-wave and Terahertz frequency for High Q filters, where there is a limitation of conventional machining. One such filter developed at 450 GHz with 1% bandwidth and Q of more than 700 [39].

2.2.2. Substrate Integrate Waveguide (SIW) filters

Over the past decade, Substrate integrated waveguide (SIW) has received much attention due to its low cost, small size, integration potential and superior performance over planar filter technologies. SIW is a dielectrically filled waveguide transmission line formed with microwave laminate (Printed Circuit Board) substrate material. The top and bottom metal surfaces of the substrate are electrically connected using two parallel sets of collinearly arranged metal-plated via holes, which function as the waveguide sidewalls [40]. The resultant structure has modes and propagation characteristics the same as their conventional metal waveguide. The configuration of SIW was initially introduced as a post-wall waveguide [41] or laminated waveguide [42],

which could be fabricated with the easily fabricated with commonly printed circuit board (PCB) fabrication method. SIW has less radiation loss and better quality factor than conventional planar circuits. It is also easier to fabricate, more compact and cost-effective than the traditional rectangular waveguides. Due to its quasi-planar structure, it provide an upper hand to design and integrate passive components, active circuits and radiating elements in a dielectric substrate, which led to the development of various microwave and millimeter-wave components in SIW technology, such as antennas [43-45], power dividers [46-48], couplers [49, 50], filters [51- 53] and diplexers [53, 54]. The separation between the vias in the transverse direction, the diameter of the vias and the pitch length (vias centre to centre distance) are the parameters use for designing SIW. Like rectangular waveguide, the dominant mode of SIW is TE_{10} [55].

Different types of filters with different topologies have been developed based upon SIWs [53, 56, 57]. In [58], a direct-coupled SIW filter with irises operating at 60 GHz was designed and fabricated. In [59, 60], cross-coupled filters developed on rectangular and circular SIW cavities. SIW elliptic filters with high selectivity were proposed in [61] using a two-layer substrate to realize the elliptic response with four cavities; compact and super-wideband SIW bandpass filters employing electromagnetic band-gap (EBG) structures were designed and experimentally verified in [61]. These filters have lower losses than the corresponding planar filters in the millimeter-wave frequency range,

and they exhibit a substantial size reduction compared to their implementation in conventional waveguide structures.

The research was going on to reduce the size of SIW filters and improve their performance. The different modified waveguide configurations that have been proposed are as follows:

a) **Folded SIW**: In [62] author used a double-folded SIW with multilayer structures in a low-temperature co-fired ceramic (LTCC) technology to design a quasi-elliptic and Chebyshev filter. The coupling between the vertically SIW resonators is controlled using U- and L-shaped slots in the middle metallic layer, as shown in figure 2.4. The size reduction of 74% and 88% are noted for quasi-elliptic and Chebyshev respectively compared to conventional SIW. The author uses quadri-folded SIW (QFSIW) [63] to develop a fourth-order bandpass filter with a size reduction of 89%.

b) **Slot Loaded SIW**: The inductive and capacitive loading of slot in SIW lower shift its fundamental resonant mode. The authors of [64] designed three different miniaturized dual-mode filters with rectangular cross-slot, H-slot and T-shaped slots respectively in the SIW technology. The slot induces a capacitive effect to the cavity and thus miniaturization is achieved. The fabricated prototypes of all types of the reported filters are shown in figure 2.5. Similarly, the square ring slot, ramp shaped slot [65], open-ended semi-circular slot [66] and E-shaped slot-loaded SIW [67] has been reported with

miniaturized size and improved performance.

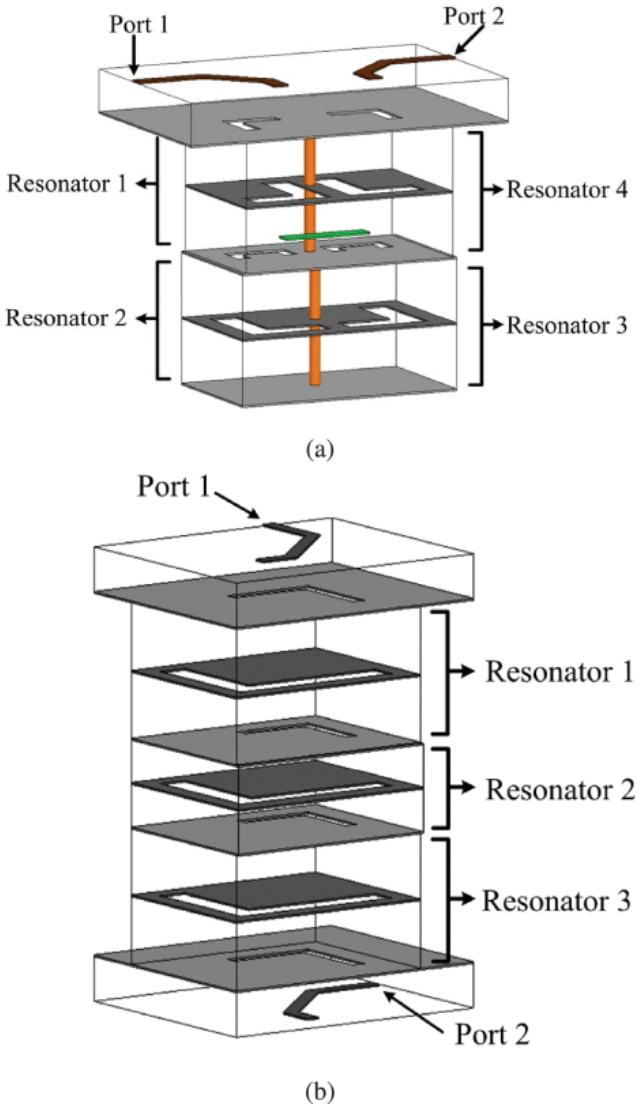

Figure 2.4 Exploded view of the (a) quasi-elliptic, and (b) Chebyshev filter [62].

c) **Stepped impedance metamaterial structure (SIMMS):** The SIMMS works on evanescent mode propagation [68]. It states that an electric dipole (above the waveguide) can be used to achieve a passband below the cutoff frequency of the waveguide. By loading SIMMS on the SIW components, a negative permittivity is expected. Based on its negative permittivity, SIMMS can be considered as an

electric dipole [68]. The author [68] incorporate SIMMS in half mode SIW to design a filter and diplexer with a 75% reduction in the size compared to conventional SIW. In [69] author uses different geometry of SIMMS to miniaturize the filters and diplexers with high selectivity. The other work to reduce size and improve Q is done by incorporation of composite left/right-handed (CLRH) structure in SIW [70]. The CLRH structure behaves as a series capacitance and shunts inductance, thus achieves CLRH functionality. The CLRH structure generates the resonance below the cut-off frequency of the SIW resonator.

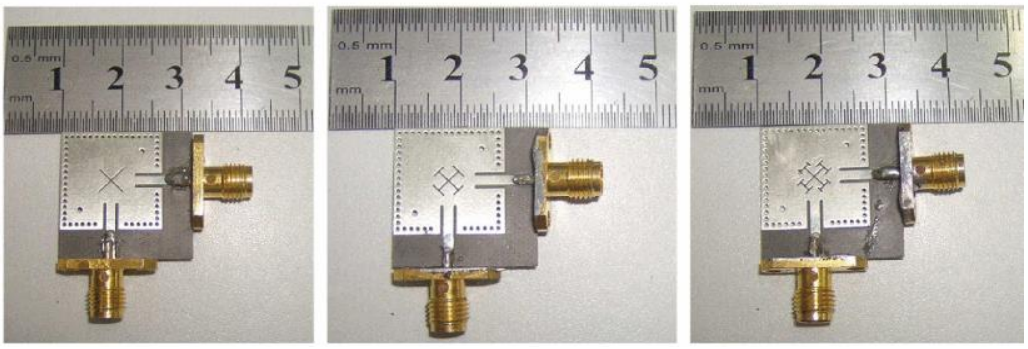

Figure 2.5 Fabricated prototypes of the miniaturized dual-mode SIW filters with the rectangular cross-slots, T-shaped cross-slots, and H-shaped cross-slots. [64].

d) Sub modes of Full mode SIW: Electric field patterns of the fundamental TE_{101} mode in a conventional full-mode circular-SIW cavity resonator, half-mode SIW (HMSIW), quarter-mode SIW (QMSIW), eighth-mode SIW (EMSIW), sixteenth-mode SIW (SMSIW), and thirty-two-mode SIW (HMSIW) are shown in figure

2.6 [71]. The solid line is considered as an electrical wall and the dashed line as a magnetic wall, as shown in figure 2.6. Symmetrical planes of A-A1, B-B1, C-C1, and D-D1 in figure 2.6a are considered as magnetic walls. The half-mode SIW (HMSIW) can be realized from the full mode SIW by cutting it along the symmetrical A-A1 line, as shown in figure 2.6b. As a result, the field pattern of the fundamental mode remains unchanged with a size reduction of 50%.

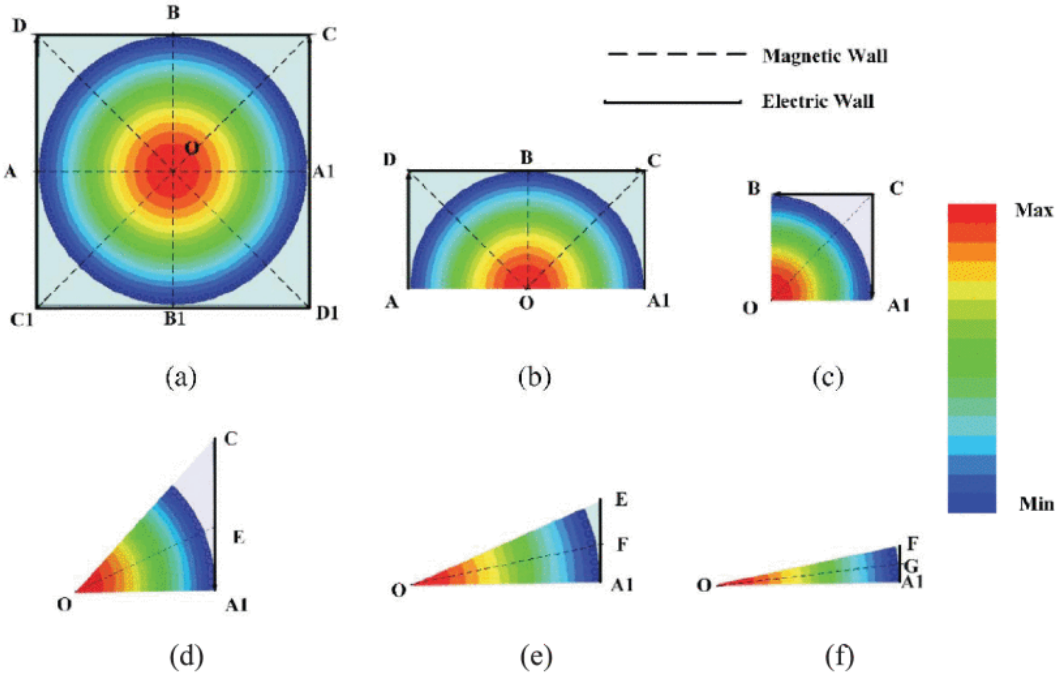

Figure 2.6 *Field distribution of the circular SIW cavity resonator (a) full-mode, (b) half-mode, (c) quarter-mode, (d) eighth-mode, (e) sixteenth-mode, and (f) thirty-second-mode [71].*

In [72] wideband filter is designed by coupling the four QMSIW cavity resonators with H-shaped slots on each cavity to suppress the higher-order modes, which enhance the upper stopband

performance and 75% size reduction compared to full mode SIW. In [73] a bandpass filter with controllable transmission zeros designed with EMSIW cavity resonator. The filter in the multilayers configuration is designed where resonators are arranged vertically through a slot for coupling. The author of [74] uses the SMSIW cavity resonator with fundamental TM_{01} mode. The spacing between resonators is adjusted to achieve coupling, and a rectangular slot is etched on the ground plane to suppress higher-order mode.

Table 2.1 Comparison of different miniaturization techniques in SIW filters

Ref.	Miniaturization Technique	Size Reduction	Order	Centre Frequency (GHz)	FBW (%)	IL (dB)	Selectivity
[62]	Double-Folded SIW-1	75	3	30	2.9	0.1	Low
	Double-Folded SIW-2	88	3	60	10	0.1	Low
[63]	Quadri-folded SIW	89	4	3.2	9.3	1.6	Medium
[64]	Rectangular slots	22.15	2	14.09	9.1	0.79	High
	T-shaped slots	30.56	2	13.30	8.12	0.96	High
	Cross-slots	56.25	2	12.25	6.86	1.21	High
[66]	Open-ended slots	70	2	11.7	68.4	0	Low
[67]	E-shaped Slot	33	2	3.6, 6.4	8.2,6.7	1.2	High
[68]	SIMMS	69	2	5.8	7.8	1.1	Medium
[70]	CLRH	80	4	5.3	6.2	1.5	Medium
[71]	TMSIW	96.87	2	2.45	36.7	0.25	Medium
[72]	QMSIW	75	4	3.25	21.2	1.02	High
[73]	EMSIW	87.5	4	1.02	8.35	1.55	High
[74]	SMSIW	93.75	2	2.05	7	1.2	Medium

The fabricated filter has a 93.75% size reduction compared to the conventional full mode SIW cavity filter. The table compares the various miniaturization techniques in SIW filters [75].

The author of [74] uses the SMSIW cavity resonator with fundamental TM_{01} mode. The spacing between resonators is adjusted to achieve coupling, and a rectangular slot is etched on the ground plane to suppress higher-order mode. The fabricated filter has a 93.75% size reduction compared to the conventional full mode SIW cavity filter. The table compares the various miniaturization techniques in SIW filters [75].

2.2.3. Cavity Filters

The low losses and high power handling capability of cavity filters make them popular for many decades for onboard application. Their metallic cavity structure made from either Invar or Aluminium makes them bulky, and significant advances were made in the past to reduce their mass and volume and improve RF performance. The mass and volume reduction have done by employing various lightweight material instead of metals, while the RF performance has improved due to advancement in the filter synthesis [76]. The advancement done in the last few decades in the field of cavity filters are as follows:

a) **Inductively Coupled waveguide filter** [77]: The rectangular waveguide resonator coupled to other resonators through a thick iris.

Each resonator operates in a single mode and is the most common use cavity filter configuration.

b) **Lightweight Material Cavity filters**: The cavity filters fabricated from metal makes them bulky. So, other structurally stiff, lightweight and conductive materials explored for the filter development, which led to the development of composite materials like Kevlar and graphite fiber epoxy composite (GFEC) for cavity filters [78-80] fabrication. The manufacturing process established successfully, but the graphite filters are difficult to manufacture than invar filters and require elaborate quality control and mechanical design. This limits its use for spaceborne applications.

c) **Multi-mode cavity filters**: Lin [82] first illustrated the use of degenerate mode with identical natural frequency in a single cavity. However, the first practical dual-mode waveguide filter was developed by suppressing the unwanted mode and control the degenerate mode independently [83]. The use of a dual-mode cavity filter provides identical performance to the single-mode cavity filter. Also, the dual-mode filters have significant mass and volume reduction due to the reduction of the physical cavity by half. A variety of dual-mode filters has developed using the principle of spatial symmetry [11]. The quest for further mass and volume reduction led to the development of triple and quad mode filters. Comsat labs was the first to realize a triple-mode filter [83] using two orthogonal TE_{111}

modes and a TM_{010} mode to construct a two-cavity six-pole filter. The quadruple mode filters required two orthogonal modes that could use twice within a square or circular cavity. The quad-mode filter using TE_{113} and TM_{010} mode has been demonstrated [84, 14]. The reported multi-mode filter like triple and quad mode filters are sensitive to temperature variation and are not suitable for deployment in the payloads.

d) Low loss mode filters: The need for low loss filter at Ku-band leads to the invention of TE_{11n} and TE_{10n} (n>1) cavity filter [14, 85]. The implementation of these filters are same as iris coupled waveguide filter but Q has increased by increasing the cavity height in the integer multiple of half wavelength. Atia and Williams [86] did the other work in the field of low loss filter. They use low loss mode TE_{011} of circular waveguide and demonstrated a four pole quasi-elliptic filter at 12 GHz. The unloaded Q of 16000 achieved at 12 GHz. Within the same line a fully tunable filter at Ka-band has been reported by using TE_{011} mode circular cavity [87]. The unloaded Q of 16000 achieved at 12 GHz. Within the same line a fully tunable filter at Ka-band has been reported by using TE_{011} mode circular cavity [87]. The authors has done a remarkable work was done in the field of low loss filter by introducing the concept of Super Q [88, 89]. They developed filter around 19 GHz and 30 GHz has extremely high Q of better than 25000 at 19 GHz. Here, the higher order TE_{221}mode of a cylindrical cavity resonator used for filter realization. The TE_{221}

mode has 55% higher Q than TE_{011} mode of the cylindrical cavity resonator used for low loss filter. The figure 2.7 shows the size comparison of 8-pole super Q filter with conventional TE_{113} mode filter.

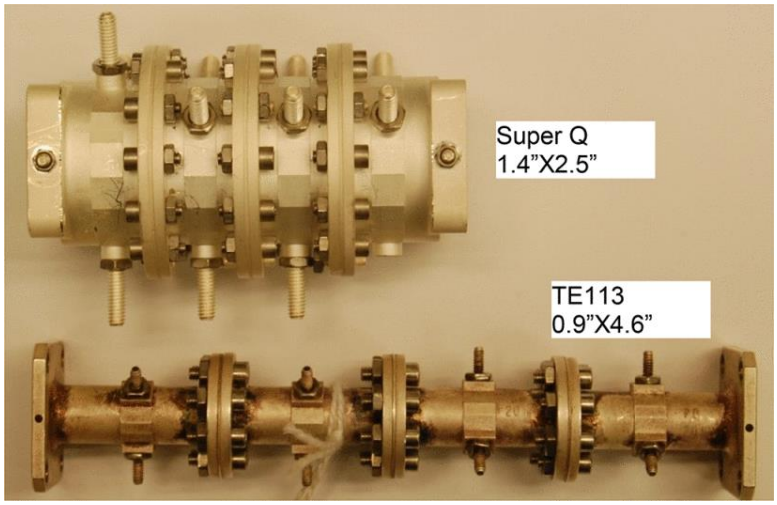

Figure 2.7 *30-GHz eight-pole super Q filter and a TE_{113} version with the same filter function [89].*

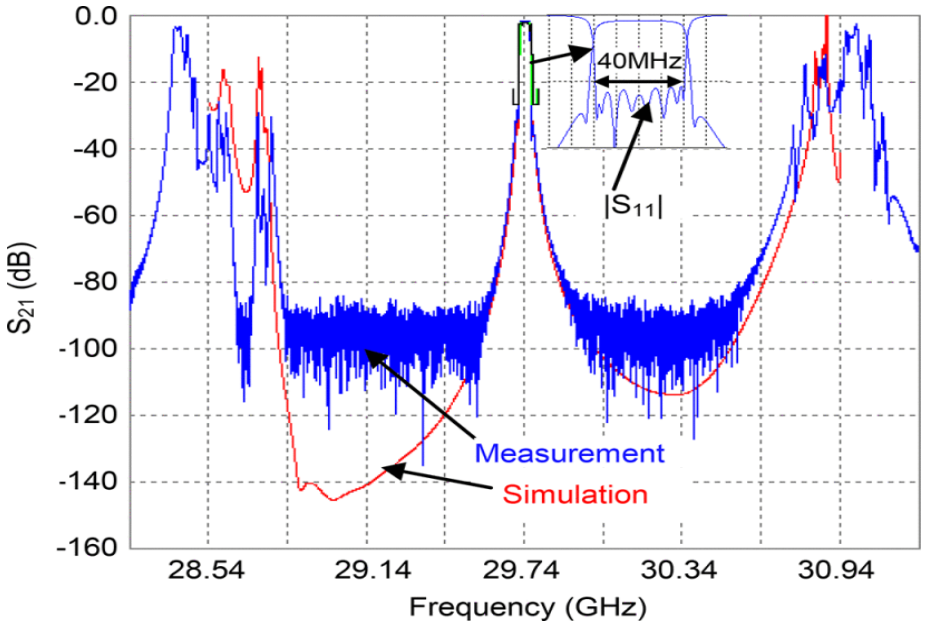

Figure 2.8 *Wideband RF performance of the fabricated eight-pole super Q filter operating at 30 GHz with 40-MHz bandwidth [89].*

The figure 2.8 shows the wideband performance of Super Q filter at 30 GHz. The filter performance is superior and is good for narrowband and channelization applications like multiplexer filters. The spurious-free window is 1.8 GHz, which is not suitable for this filter to be used for designing wideband filters and for Pre-select filters used at the front end of the payload.

2.3. Predistortion

The Q-factor depends on the material selection, resonator type and size. However, to increase the Q, one must often increase the dimensions of the resonator cavities, resulting in a larger and heavier filter. It may not always be practical due to overall design constraints driven primarily by the application. The concept of Predistortion was first proposed by Livingston [90] and later described in more detail by Williams [91] for cross-coupled microwave filters. In Predistortion, during the polynomial synthesis, the transmission poles of the polynomial are moved toward the jω axis by a fixed amount [90, 91] shown in figure 2.9. However, both of these works flatten the loss of the filter over frequency without reducing the size and mass.

They apply the Predistortion technique on the High Q filter, which does not reduce size and mass, but severely deteriorate insertion and return loss. The recent advancement in the technique [92-95] is use adaptive Predistortion method that applies adaptive correction factors to the transmission poles of the filter function polynomial. This technique leads to improvement in insertion loss

and group delay equalization and permits a filter that is implemented in lower Q technology to emulate the performance of a higher Q counterpart. In [92], authors demonstrated predistorted filters made from low Q coaxial resonator that can achieve an equivalent Q of >20000 while providing more than a three-to-one reduction in mass and volume over current C-band single-mode dielectric resonator filters [92,95], yet only introducing an additional 4 dB of insertion loss. The two ways Predistortion used in microwave filters for (a) mass and size reduction by using a low Q resonator and emulate them to behave as a high Q resonator. (b) The RF performance of the existing filter made from a high Q resonator. The other techniques [96-97] similar to predistortion, where the microwave filter is designed with non-uniform Q and demonstrate on microstrip technology. The use of resistive coupling for its implementation is a tedious task to incorporate in the three-dimensional resonator.

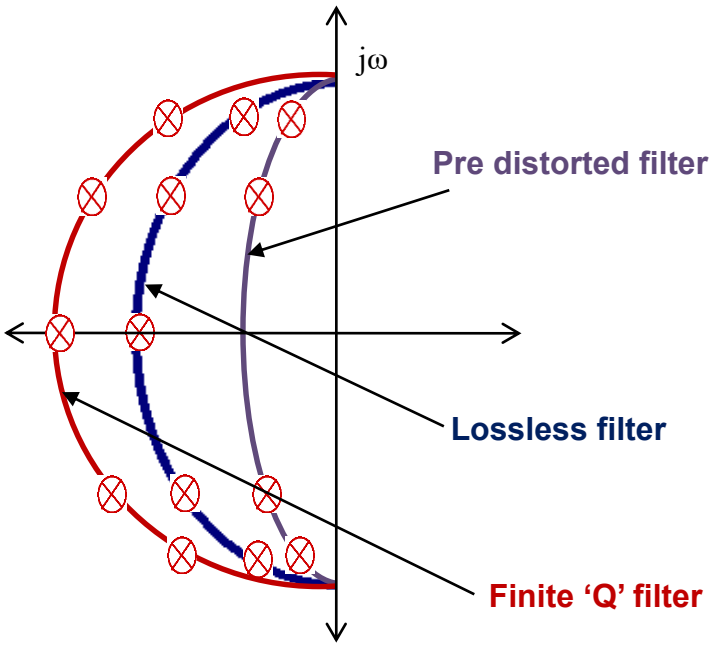

Figure 2.9 *Distribution of poles for Pre-distorted, lossless and finite Q filter.*

The Predistortion technique is suitable to the input multiplexers where insertion loss of filter is not critical, and the return loss is governing by circulators and isolators. Thus, standalone filter return loss is of little importance. Moreover, the filter tuning is cumbersome due to poor return loss.

2.4. Temperature Compensated Filters

The communication payload filters are resonators coupled filters that operate in large temperature excursions (-15^{0}C to 65^{0}C) in the space environment. The efficient use of spectrum with minimal guard band makes filter design more stringent with a low design margin. Moreover, the self-heating of the filter has increased due to the increase of power of the satellite. These payload filters fabricated from the metal and its frequency response drift due to the thermal drift. So, the payload filters compensated over temperature to perform their intended function over the mission life. The temperature compensation approaches employed in the microwave devices based on [98, 99]:

A. Use of material with high thermal stability with respect to dimensions and RF properties.

B. Temperature-controlled environment eliminates the root cause of temperature drift.

C. Designing a device using materials with specific dimensional or property drift, so that net temperature drift is insignificant.

The selection of approach for temperature compensation in filters depends on ease of implementation, simple and high reliability over the mission life.

A. Thermal stability and material science

The easiest way is to use the material with a low coefficient of thermal expansion (CTE) that makes the filter both thermally and dimensionally stable. The early design using Invar for high thermal stability [100]. Invar has a low CTE of 1.6 ppm/^{0}C, which exhibit 93% reduction in temperature drift compare to aluminium with a CTE of 23 ppm/^{0}C. Compare to other conductors like copper and aluminium, Invar is bulky and has poor thermal conductivity. Invar is three times heavier than aluminium and has thermal conductivity 1/20th of aluminium thermal conductivity. The Invar filter trapped heat inside [101, 102] and act as a thermal insulator compared to aluminium. The composite material and graphite fiber epoxy composite (GFEC) used in the development of cavity filters [77-79] instead of Invar, as they are lightweight and exhibit dimensional stability that meets that of Invar. However, they require elaborate quality control and are tough to manufacture than modern Invar waveguides filters.

B. Temperature controlled RF design

The Thermal drift in RF components can also be minimized by subjecting them to control temperature. Research that implements this approach using both active and passive cooling presented here.

In [101], Atia proposed a TE_{113} dual-mode cavity filter that uses a heat exchanger to reject heat more efficiently. The cavity walls are constructed from Invar. Due to the poor thermal conductivity of Invar, Atia proposes that thick copper irises attached to an external heat exchanger, which has

used to conduct heat out of the cavity. The high thermal conductivity of copper, along with the large surface area of the heat exchanger, allows heat to be dissipated more efficiently. A cross-section of the proposed filter shown in figure 2.10.

However, adding a heat exchanger results in an increase in mass and volume over a traditional filter, and it requires a low ambient temperature to provide an effective heat sink.

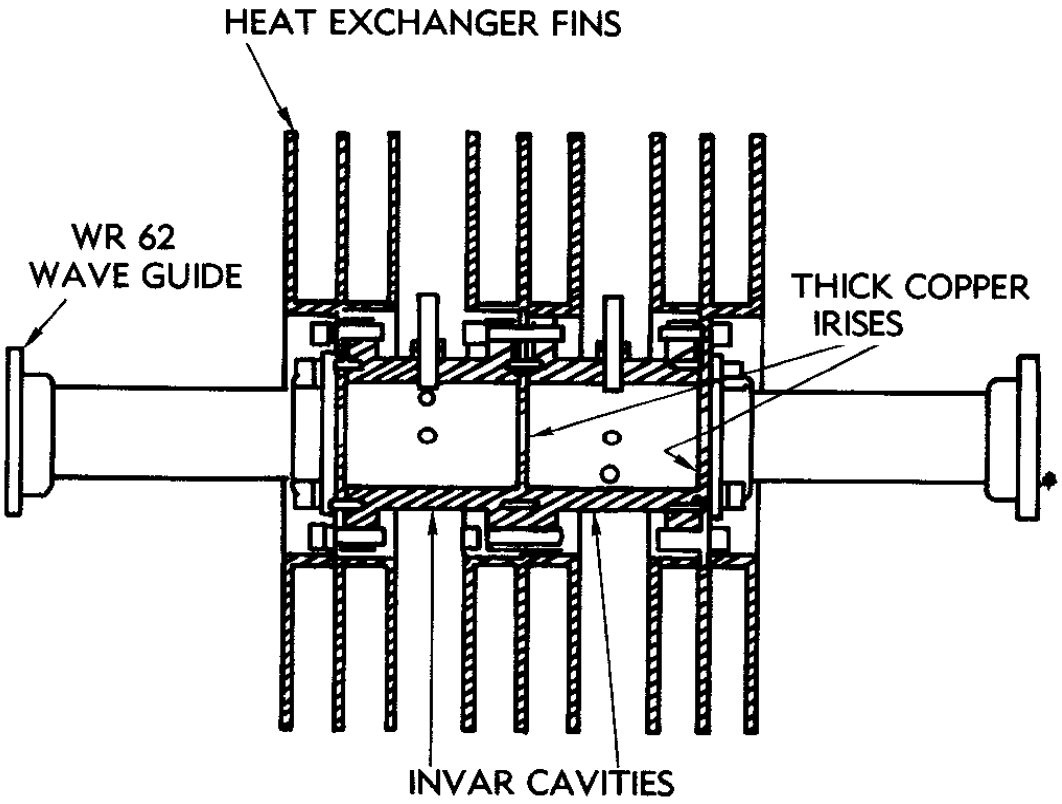

Figure 2.10 *Bandpass filter with heat exchanger [101].*

In [102], Rosowsky and Wolk propose a satellite multiplexer that dissipates heat using heat pipes. This multiplexer uses the Invar waveguide to construct the filter portion of the multiplexer. Heat pipes containing

ammonia are attached to the Invar cavities. As the ammonia is heated, it evaporates and travels to the evaporation zone, near the perimeter of the satellite. Heat dissipated by radiation, the ammonia condenses, and the cycle continues. A cross-section of the waveguide and heat pipe shown in figure 2.11. However, the large contact area is required to dissipate the heat, but the filters are small to provide a sufficient contact area for heat dissipation.

The other work is on HTS [103, 104], which offer ultra-high unloaded Q but require cryocoolers to maintain the temperature of 77K. The reliability issue with the cryocoolers over the satellite mission limits this approach.

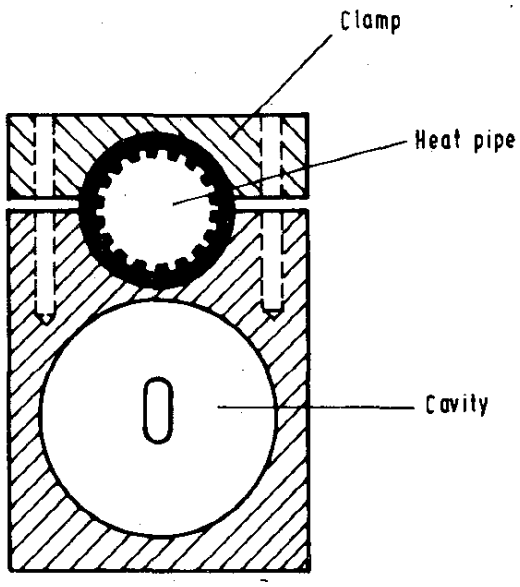

Figure 2.11 *Cross-section of heat-pipe cooled waveguide [102].*

C. Net thermal stability approaches

This approach involves choosing appropriate materials for part of the resonator to reduce the net temperature drift. Combline resonators and filters have been

widely used in communication systems since Matthaie presented the theoretical basis for their design in [105, 106], which are well suited to moderate- and narrow-band applications. Figure 2.12 shows a typical combline resonator. The cavity resonance depends heavily on the capacitance between the tuning screw and the partial resonator rod (coaxial post), and that a negative temperature characteristic for this capacitance will result in a thermally stable resonance [107]. With the use of significantly different CTEs materials for the housing and tuning screw, the temperature coefficient of the capacitance can be substantially negative. However, realizing a temperature compensated resonator using this empirical approach is time-consuming and iterative.

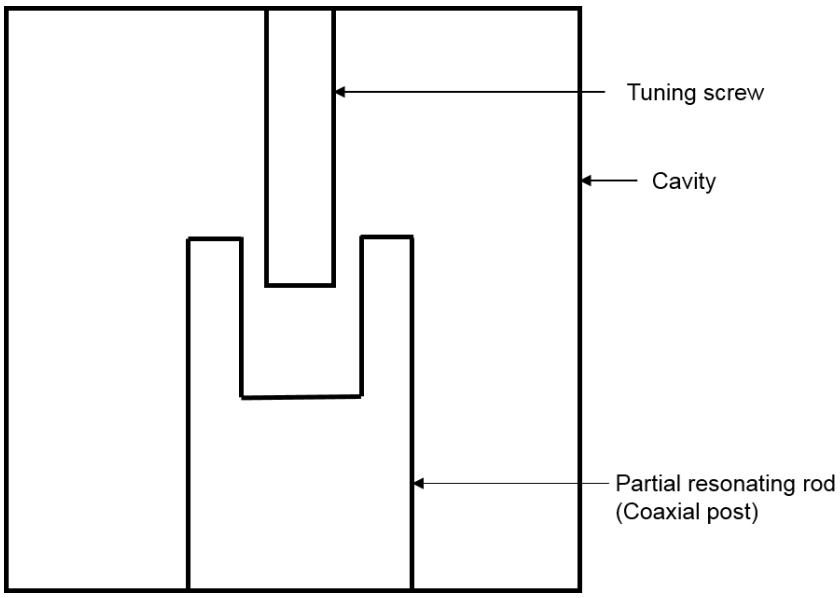

Figure 2.12 *Cross-section of a temperature-compensated combline resonator.*

Zaki later proposed a mode-matching approach incorporating perturbation techniques that allowed for temperature stabilization in simulation [108] works well for applications suitable to combline resonators. However, tuning the resonant frequency of a compensated cavity degrades the compensation and Q,

which complicates the implementation of these resonators in filters. Another common approach to reducing temperature drift is to constrain cavity expansion. The two related designs have proposed [109, 110], which used a control rod made from a low CTE material to restrain the increase of the cavity surfaces shown in figure 2.13 and 2.14.

The other design [109, 1110] shown in figure 2.15 uses a domed wall shaped resonator, where one domed wall of cavity resonator constructed from low CTE material. The edge of the dome is fixed to the cavity by the retaining ring. When the cavity expands, the dome will deflect inward, and this inward deflection compensates for the expansion of the cavity. However, the temperature compensation depends on the CTE of cavity, CTE of the dome, the shape and thickness of the dome, which need to be very thin.

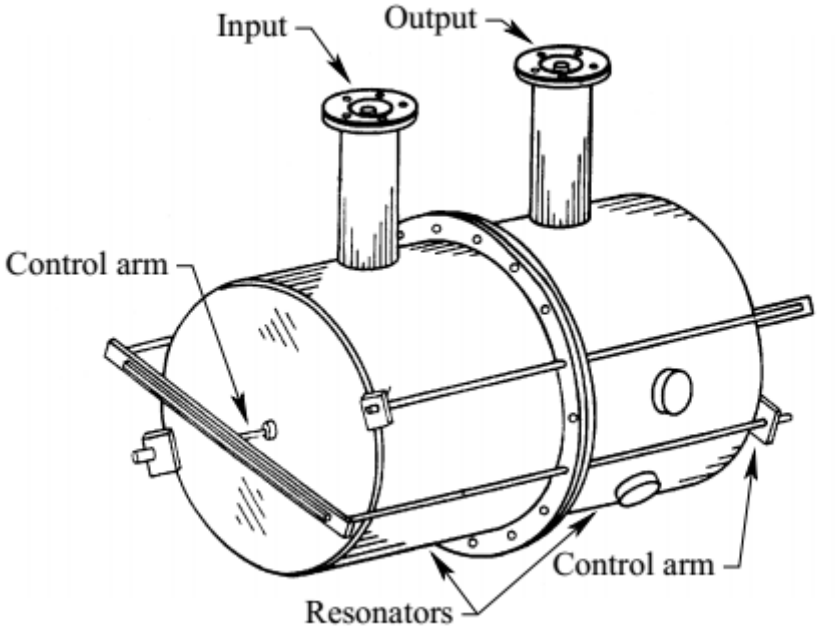

Figure 2.13 *Sketch of constrained expansion temperature compensated cavity filter [109].*

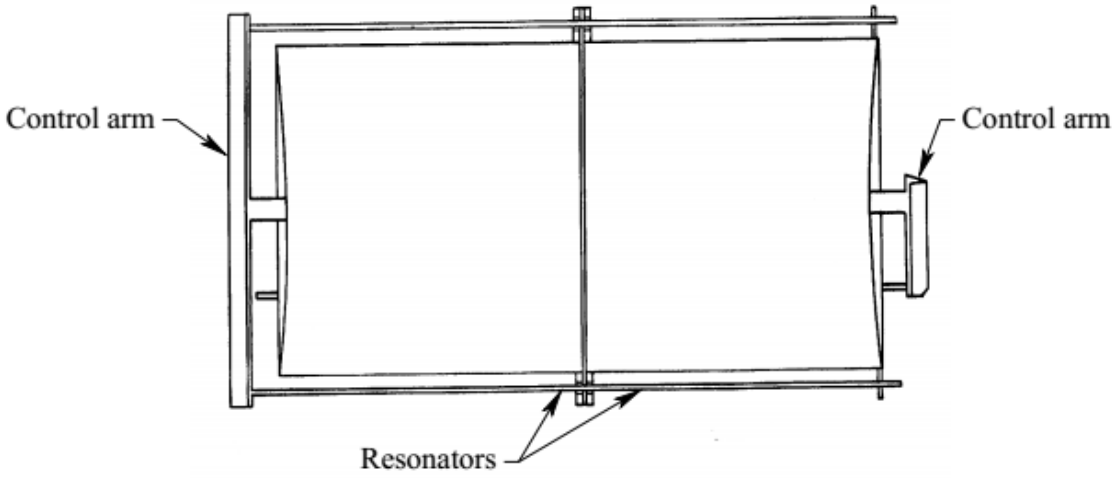

Figure 2.14 *2D view of Sketch of constrained expansion temperature compensated cavity filter [109].*

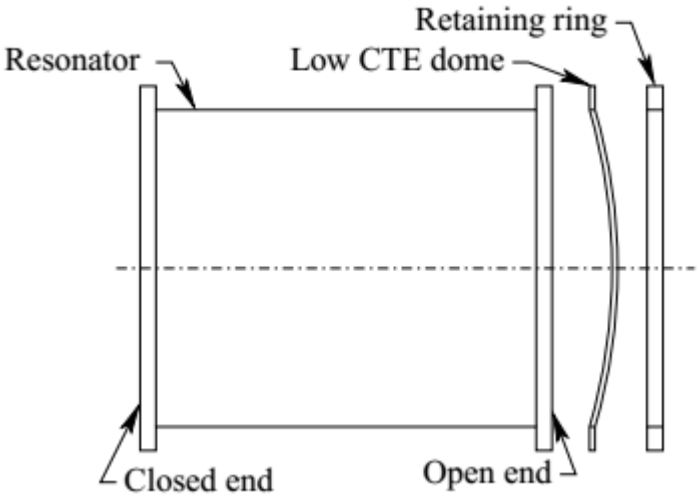

Figure 2.15 *Domed wall temperature compensated resonator [110].*

A patent granted to Lundquist proposed a filter based on differential expansion [111]. In his work, a high CTE metal iris protrudes into the cavity made of substantially low CTE metal shown in figure 2.16. The electrical length of the cavity shortens by the protrusion of the iris. Thus, it compensates for the expansion of the cavity walls. This temperature compensation makes the

resonator complex, increases the complexity of the filter design and affects reliability. Moreover, at Ka-band, the resonator dimensions are small, and this approach is difficult to implement.

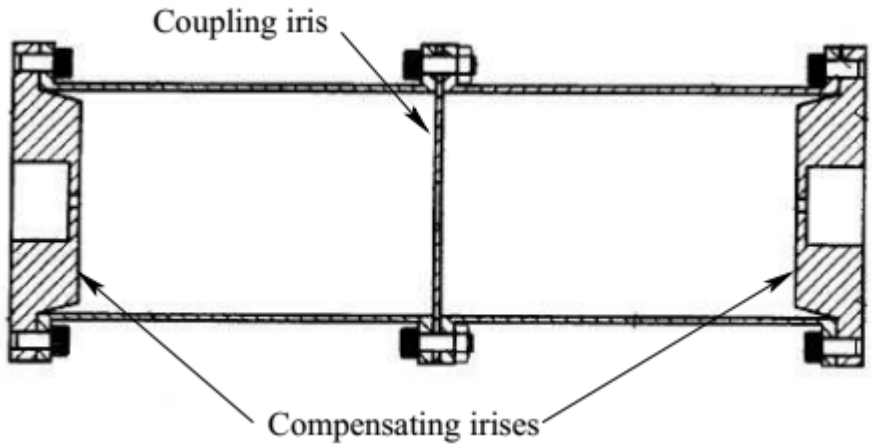

Figure 2.16 *High CTE iris based temperature compensated filter [111].*

Another constrained expansion design was proposed by Fitzpatrick in [112] shown in figure 2.17, and similar work done by authors [113] to compensate for 7-channel high power Ku-band OMUX. The filter uses an external compensator to deflect the end wall of a dual-mode cavity. The low CTE compensator will deflect the end wall inward, decreasing the length of the cavity, and it counteracts the effect of cavity expansion. The amount of compensation will depend on the end-wall thickness, the differential CTE of the control arm and cavity. The compensation can be adjusted by adjusting the tension in the control arm. The tuning range of the compensation is limited, and care must be taken to avoid plastic deformation of the end wall, which lead to hysteresis.

The shaped memory alloys are a class of metal that change their shape when the bias force has applied and retained when the bias force has removed. The

resistive heating is used in SMA to produce a thermally driven actuator. These actuators have utilised to produce temperature compensated filters [114]-[116]. The movement of the tuning rod in the cavity has controlled by the SMA spring. It compensates for the effect of overall cavity expansion. The actuation of shape memory alloys is hysteretic concerning temperature. Moreover, at Ka-band, the dimensions are considerably small, and the dimensional sensitivity is high.

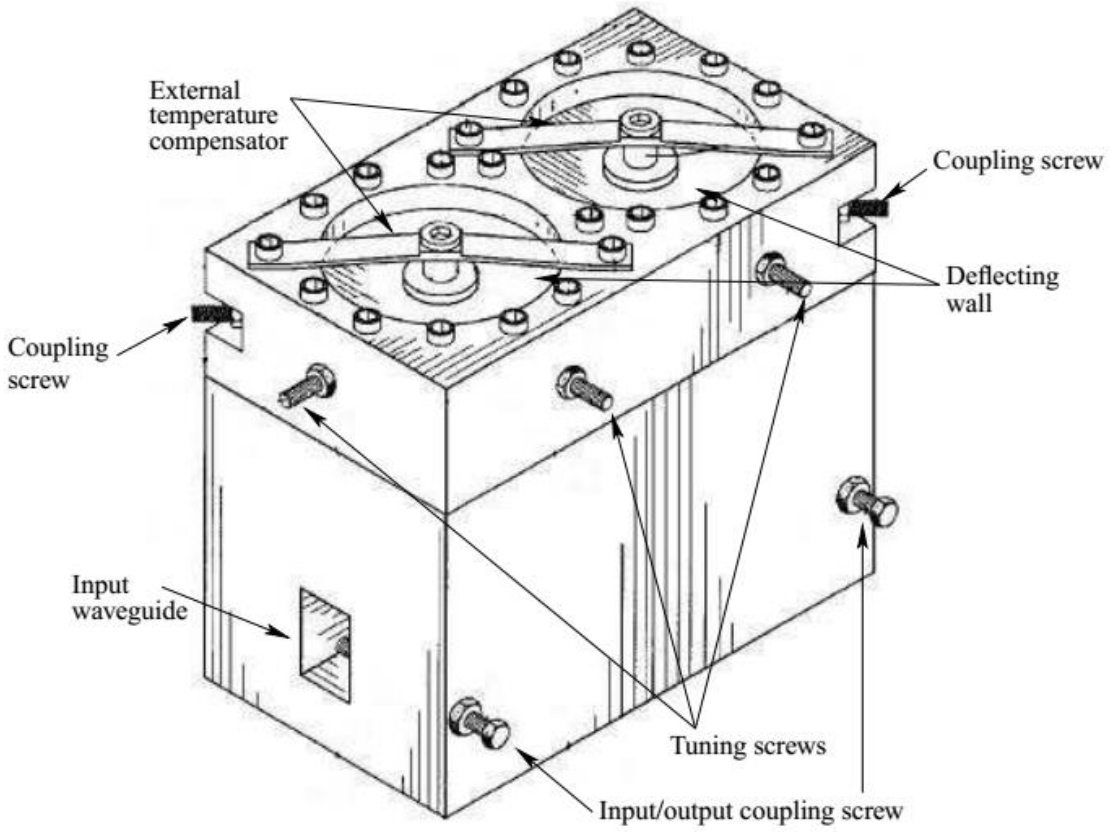

Figure 2.17 *External compensater based temperature compensated filter [112].*

2.5. Summary

The various techniques and technologies used to design filters at the millimeter-wave band, especially Ka-band, have been discussed. All these different

technologies are reviewed from the perspective of their use in the payload filter applications. The focus of most of these technologies is on size miniaturization, weight reduction and performance enhancement. Among these technologies, cavity filters are the most popular due to their high Q and predictable thermal performance. Also, the various techniques to compensate the filter performance over temperature with tolerable frequency drift have reviewed since these filters have to operate in the space environment flawlessly.

Chapter 3

Filter Synthesis

3.1. Introduction

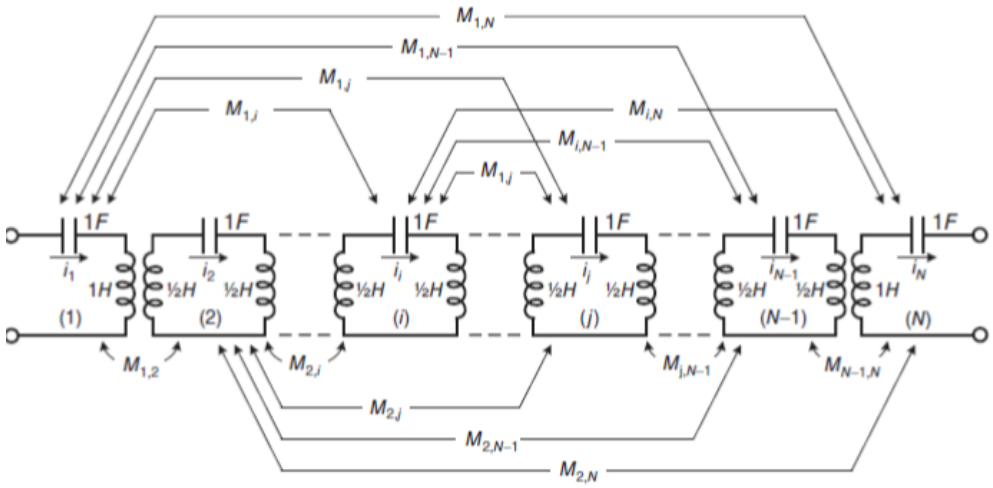

Figure 3.1 *Multi-coupled series-resonator bandpass prototype representation.*

(source courtesy: A.E. Atia)

The filter synthesis involves the characteristic polynomial synthesis, which is used to synthesize the coupling matrix. The concept of the coupling matrix was introduced by Atia and Williams [11, 12]-[117, 118], where they used was a "bandpass prototype" (BPP) circuit model shown in figure 3.1. The circuit is a cascade of lumped-element series resonators intercoupled through transformers; each resonator comprising a capacitor of 1 F in series with the self-inductances of the mainline transformers with a total 1 H within each loop,

which gives a center frequency of 1 rad/s, and the couplings will be normalized to give a bandwidth of 1 rad/s.

Moreover, every loop is theoretically coupled to every other loop through cross-mutual couplings between the mainline transformers. The order of the filter and the position of transmission zeros used to synthesize the polynomial. These characteristic polynomials used to synthesize the coupling matrix via the admittance matrix [119]. The N+2 transversal coupling matrix synthesis and its steps of synthesis are given below:

3.2. Polynomial synthesis

The amplitude squared transfer function that defines any two-port lossless filter network

$$|S_{21}(s)|^2 = \frac{1}{1+\varepsilon^2|K_n(s)|^2} \tag{3.1}$$

where s= σ+ j Ω is the complex frequency variable, $K_n(s)$is the characteristic function which determines an nth order filter response. $K_n(s)$ can be expressed by a ratio of two polynomials

$$K_n(s) = \frac{F_n(s)}{P_n(s)} \tag{3.2}$$

The $F_n(s)$ and $P_n(s)$ together with another polynomial $E_n(s)$ are the so-called characteristic polynomials, which is used to define the S-parameters as shown in

$$S_{11}(s) = \frac{F_n(s)}{E_n(s)} \tag{3.3}$$

$$S_{21}(s) = \frac{P_n(s)/\varepsilon}{E_n(s)} \tag{3.4}$$

where the ripple constant ε for Chebyshev response is defined as below in order to normalize the equal ripple level of S_{21} at $\Omega = \pm 1$

$$\varepsilon = \frac{1}{\sqrt{10^{\frac{RL}{10}}-1}} * \frac{P_n(s)}{F_n(s)}\Big|_{s=j} \tag{3.5}$$

where RL is the passband return loss level in dB

The $P_n(s)/\varepsilon$ is the numerator of $S_{21}(s)$, it determines the transmission zeros of the filter's response. Similarly $F_n(s)$ determines the reflection zeros. The all of the three characteristic polynomials assumed to be normalized, i.e., the coefficient of highest order term is unity.

The characteristic polynomials defined in terms of their roots given by (3.6) and (3.7)

$$P_n(s) = \prod_{i=1}^{n_z}(s - TZ_i) \tag{3.6}$$

$$F_n(s) = \prod_{i=1}^{n}(s - RZ_i) \tag{3.7}$$

Where TZ_i and RZ_i represent the frequency points of the transmission zeros and reflection zeros on the normalised frequency domain, respectively; n_z represent the number of the finite frequency transmission zeros; the number of the reflection zeros is always the same as the order of the filter, which is n in this case.

with $P_n(s)$ and $F_n(s)$ known, as long as $E_n(s)$ is obtained, the S-parameters can

be determined. By using alternating pole method, $E_n(s)$ can be obtained. Since these three characteristic polynomials are not independent from each other, they can be expressed in one equation by applying the conservation of energy law to (3.3) and (3.4):

$$S_{11}(s)S_{11}(s)^* + S_{21}(s)S_{21}(s)^* = 1 \tag{3.8}$$

$$F_n(s)F_n(s)^* + \frac{1}{\varepsilon^2}P_n(s)P_n(s)^* = E_n(s)E_n(s)^* \tag{3.9}$$

where ∗denotes the complex conjugate. Since $P_n(s)$ and $P_n(s)$ are known, by applying polynomial multiplications to the left hand side of (3.9), $E_n(s)E_n(s)^*$ can be obtained. There will be 2n roots of $E_n(s)E_n(s)^*$ on the complex plane; they are symmetrical to the imaginary axis. The roots of $E_n(s)$ is strictly Hurwitz polynomial, which satisfies two conditions:

1. The polynomial is real when s is real
2. The roots have non-positive real parts

Therefore, the roots of $E_n(s)E_n(s)^*$on the left half plane have to belong to $E_n(s)$, while the roots on the right half plane belong to $E_n(s)^*$. Hence, $E_n(s)$ is obtained [117].

3.3. Circuit Synthesis Approach

The [ABCD] matrix representing the network a two-port network with unity source and load terminations given by [120]:

$$[ABCD] = \frac{1}{jP(s)/\varepsilon}\begin{bmatrix} A(s) & B(s) \\ C(s) & D(s) \end{bmatrix}$$

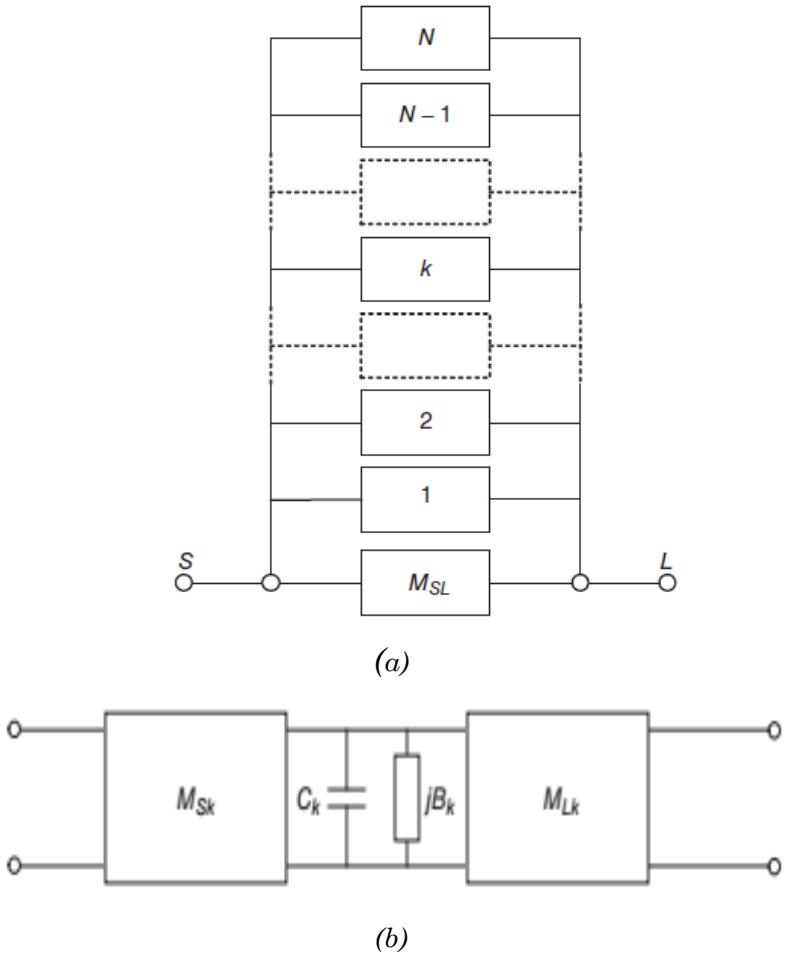

Figure 3.2 *Inter-resonator coupling and its equivalent, (a) N-resonator transversal array including source and load coupling, and (b) Equivalent circuit of K^{th} lowpass resonator in the transversal array.*

where

$$S_{12}(s) = S_{21}(s) = \frac{\frac{P(s)}{\varepsilon}}{E(s)} = \frac{\frac{2P(s)}{\varepsilon}}{A(s)+B(s)+C(s)+D(s)}$$

$$S_{11}(s) = \frac{\frac{F(s)}{\varepsilon_R}}{E(s)} = \frac{A(s)+B(s)-C(s)-D(s)}{A(s)+B(s)+C(s)+D(s)}$$

$$S_{22}(s) = \frac{(-1)^N}{E(s)}\frac{F(s)^*}{\varepsilon_R} = \frac{D(s)+B(s)-C(s)-A(s)}{A(s)+B(s)+C(s)+D(s)} \quad (3.10)$$

Knowing $A(s), B(s), C(s)$ and $D(s)$ polynomial, their coefficients can be expressed in terms of coefficient of $F(s)/\varepsilon_R$ *and* $E(s)$

for N even

$$A(s) = jIm(e_0 + f_0) + Re(e_1 + f_1)s + jIm(e_2 + f_2)s^2 \ldots\ldots + jIm(e_N + f_N)s^N$$
$$B(s) = Re(e_0 + f_0) + jIm(e_1 + f_1)s + Re(e_2 + f_2)s^2 \ldots\ldots + Re(e_N + f_N)s^N$$
$$C(s) = Re(e_0 - f_0) + jIm(e_1 - f_1)s + Re(e_2 - f_2)s^2 \ldots\ldots Re(e_N - f_N)s^N$$
$$D(s) = jIm(e_0 - f_0) + Re(e_1 - f_1)s + jIm(e_2 - f_2)s^2 \ldots\ldots + jIm(e_N - f_N)s^N \quad (3.11a)$$

For N odd

$$A(s) = Re(e_0 + f_0) + jIm(e_1 + f_1)s + Re(e_2 + f_2)s^2 \ldots\ldots + jIm(e_N + f_N)s^N$$
$$B(s) = jIm(e_0 + f_0) + Re(e_1 + f_1)s + jIm(e_2 + f_2)s^2 \ldots\ldots + Re(e_N + f_N)s^N$$
$$C(s) = jIm(e_0 - f_0) + Re(e_1 - f_1)s + jIm(e_2 - f_2)s^2 \ldots\ldots Re(e_N - f_N)s^N$$
$$D(s) = Re(e_0 - f_0) + jIm(e_1 - f_1)s + Re(e_2 - f_2)s^2 \ldots\ldots + jIm(e_N - f_N)s^N \quad (3.11b)$$

Converting ABCD parameter of equation (3.10) in terms of short-circuited admittance parameters and equating them.

$$[Y_N] = \begin{pmatrix} y11(s) & y12(s) \\ y21(s) & y22(s) \end{pmatrix} = \frac{1}{yd(s)} \begin{pmatrix} y11n(s) & y12n(s) \\ y21n(s) & y22n(s) \end{pmatrix}$$
$$= j \begin{pmatrix} 0 & k_\infty \\ k_\infty & 0 \end{pmatrix} + \sum_{k=1}^{N} \frac{1}{(s - jk)} \begin{pmatrix} r_{k11k} & r_{12k} \\ r_{21k} & r_{22k} \end{pmatrix} \quad (3.12)$$

Where y11n(s), y12n(s), y21n(s), and y22n(s) are the numerator polynomials of the rational polynomials y11(s), y12(s), y21(s), and y22(s), respectively, and yd(s) is their common denominator. Knowing the denominator and numerator polynomials for $y21(s)$ and $y22(s)$., their residues r_{21k} and r_{22k},

k =1, 2,…,N may be found with partial fraction expansions and the purely real eigenvalues λ_k of the network found by rooting the denominator polynomial $y_d(s)$, common to both $y21(s)$ and $y22(s)$. The Nth-degree polynomial $yd(s)$ has purely imaginary roots=jλ_k. Expressing the residues in matrix form yields the following equation for the admittance matrix [Y_N] for the overall network [119].

$$y_d(s) = B(s)$$

$$y_{11n}(s) = D(s)$$

$$y_{22n}(s) = A(s)$$

$$y_{21n}(s) = y_{12n}(s) = \frac{-P(s)}{\varepsilon} \tag{3.13}$$

3.3.1. Synthesis of Two port Admittance Matrix[Y_N]

The [ABCD] matrix for the kth low pass resonator:

$$[ABCD]_k = -\begin{bmatrix} \frac{M_{lk}}{M_{sk}} & \frac{(jB_k+sC_k)}{M_{sk}M_{lk}} \\ 0 & \frac{M_{sk}}{M_{lk}} \end{bmatrix} \tag{3.14}$$

which is converted to equivalent short circuit Admittance matrix

$$y_k = \begin{bmatrix} y_{11k}(s) & y_{12k}(s) \\ y_{21k}(s) & y_{22k}(s) \end{bmatrix} = \frac{M_{sk}M_{lk}}{(jB_k+sC_k)} \begin{bmatrix} \frac{M_{sk}}{M_{lk}} & 1 \\ 1 & \frac{M_{lk}}{M_{sk}} \end{bmatrix}$$

$$= \frac{1}{(jB_k+sC_k)} \begin{bmatrix} M_{sk}^2 & M_{sk}M_{lk} \\ M_{sk}M_{lk} & M_{lk}^2 \end{bmatrix} \tag{3.15}$$

The two-port short-circuit admittance parameter matrix [Y_N] for the overall network may also be synthesized directly from the fully canonical transversal network, the general form of which is shown in figure 3.2 .The two-port short-circuit admittance matrix [Y_N] for the parallel-connected transversal array is the sum of the y-parameter matrices for the N individual sections, plus the y-parameter matrix [y_{SL}] for the direct source–load coupling inverter $M_{SL.}$:

$$[Y_N] = [y_{SL}] + [y_k] \tag{3.16}$$

3.3.2. Synthesis of N+2 Transversal matrix

Equate (3.12) and (3.15)

$$M_{Lk}^2 = r_{22k} \tag{3.17}$$

$$M_{Sk}M_{Lk} = r_{21k} \tag{3.18}$$

$$M_{Lk} = \sqrt[2]{r_{22k}} \tag{3.19}$$

$$M_{Sk} = \frac{r_{21k}}{\sqrt[2]{r_{22k}}} \tag{3.20}$$

This M is the transversal coupling matrix which reduced to the desired coupling matrix after applying similarity transformation on the element of M which is to be annihilated [121]-[123] to desired realizable form.

3.4. Example of 4-2-0 filter synthesis

The synthesis of 4-pole cross-coupled filter with two symmetrically located transmission zeros at ±1.9 and 26 dB return loss are as follows:

1) **Polynomial Synthesis through recursion [119].**

$$S_{21(\omega)}S_{21(\omega)}{}^{*}=\frac{1}{\left[1-j\frac{\varepsilon}{\varepsilon_R}kC_N(\omega)\right]\left[1+j\frac{\varepsilon}{\varepsilon_R}kC_N(\omega)\right]} \tag{3.18}$$

where $kC_N(\omega)=\frac{F(\omega)}{P(\omega)}$ and k is a constant. $C_N(\omega)$ is a filtering function of degree N and its poles and zeros are roots of $P(\omega)$ and $F(\omega)$.

$$C_N(\omega)=\cosh[\prod_{n=1}^{N}\cosh^{-1}(x_n(\omega))] \text{ for } |\omega|>1 \tag{3.19}$$

$$C_N(\omega)=\cos[\prod_{n=1}^{N}\cos^{-1}(x_n(\omega))] \text{ for } |\omega|<1 \tag{3.20}$$

$$x_n(\omega)=\frac{\omega-\frac{1}{\omega_n}}{1-\frac{\omega}{\omega_n}} \tag{3.21}$$

Replacing $\cosh^{-1}$ term in equation 3.19 with its identity.

$$C_N(\omega)=cos\,h[\prod_{n=1}^{N}ln(a_n+b_n)] \tag{3.22}$$

Where $a_n=x_n(\omega)$ and $b_n=\sqrt{x_n^2(\omega)-1}$

Rearranging b_n we get $b_n=\frac{\omega'\sqrt{1-\frac{1}{\omega_n{}^2}}}{1-\frac{\omega}{\omega_n}}$ where $\omega'=\sqrt{\omega^2-1}$

The $C_N(\omega)$ finally expressed as

$$C_N(\omega)=\frac{1}{2}\left[\frac{\prod_{n=1}^{N}(c_n+d_n)+\prod_{n=1}^{N}(c_n-d_n)}{\prod_{n=1}^{N}(1-\frac{\omega}{\omega_n})}\right] \tag{3.23}$$

Where $c_n=\omega-\frac{1}{\omega_n}$ and $d_n=\omega'\sqrt{1-\frac{1}{\omega_n{}^2}}$

Now consider numerator of equation 3.23

$$C_N(\omega) = \frac{1}{2}[G_N(\omega) + G_N{}'(\omega)] \quad (3.24)$$

$G_N(\omega) = \prod_{n=1}^{N}(c_n + d_n)$ and $G_N{}'(\omega) = \prod_{n=1}^{N}(c_n - d_n)$

The $G_N(\omega)$ can be expressed as sum of two polynomial of degree N

$$G_N(\omega) = U_N(\omega) + V_N(\omega) \quad (3.26)$$

Thus, $C_N(\omega)$ calculated by recursion

Consider the case of 4-pole filter with two transmission zeros placed at ± 1.9j. The return loss of filter is 26 dB.

Using recursion, we obtain,

$U = 6.8471\omega^4 - 7.1241\omega^2 + 1$

$V = 6.8471\omega^3 - 3.7006\omega$

Normalizing U and V

$U = \omega^4 - 1.0405\omega^2 + 0.1460$

$V = \omega^3 - 0.5405\omega$

The reflection zeros are same as roots of U, which are ±0.9345j and ±0.4090j. The in-band reflection maxima are same as roots of V, which are ±0.7352j

Constructing polynomials from these roots are

$P(s) = s^2 + 3.61$

$$F(s) = s^4 - 1.0405s^2 + 0.1460$$

$$E(s) = s^4 + 2.6617s^3 + 4.5827s^2 + 4.6595s + 2.9140$$

The value of ε evaluated using equation (3.5) as 1.2404.

2) Synthesis of coupling matrix

Consider equation (3.12) for even N

$$y_{21}(s) = \frac{y_{21n}(s)}{y_d(s)} = \left[\frac{P(s)/\varepsilon}{m_1(s)}\right] \text{ and } y_{22}(s) = \frac{y_{22n}(s)}{y_d(s)} = \left[\frac{n_1(s)}{m_1(s)}\right]$$

And for N odd,

$$y_{21}(s) = \frac{y_{21n}(s)}{y_d(s)} = \left[\frac{P(s)/\varepsilon}{n_1(s)}\right] \text{ and } y_{22}(s) = \frac{y_{22n}(s)}{y_d(s)} = \left[\frac{m_1(s)}{n_1(s)}\right]$$

where

$$m_1(s) = Re(e_0 + f_0) + j\,Im(e_1 + f_1)s + Re(e_2 + f_2)s^2 + \cdots$$

$$n_1(s) = j\,Im(e_0 + f_0) + Re(e_1 + f_1)s + j\,Im(e_2 + f_2)s^2 + \cdots \quad (3.27)$$

Here e_i andf_i, $i = 0, 1,2,3, \ldots\ldots, N$ are the complex coefficient of $E(s)$ and $\frac{F(s)}{\varepsilon_R}$.

for 4-2-0 filter case using equation (3.27) $m_1(s)$ and$n_1(s)$, normalized with $m_1(s)$ are

$$m_1(s) = s^4 + 2.8116s^2 + 1.53$$

$$n_1(s) = 1.3308s^3 + 2.3298s$$

$$P(s)/_{\varepsilon} = P_1 = 0.4031js^2 + 1.4522j$$

with the help of partial fraction, we find the residues and poles of $y_{21} = \frac{P_1}{m_1}$ and $y_{22} = \frac{n_1}{m_1}$ listed in the Table 3.1

$$y_{22} = \frac{1.3308s^3 + 2.3298s}{s^4 + 2.8116s^2 + 1.53}$$

Table 3.1 Eigenvalues, residues, and Eigenvectors for 4-2-0 filter

k	Eigenvalues	Residues		Eigenvectors	
	λ_k	r_{22k}	r_{21k}	$T_{Nk} = \sqrt[2]{r_{22k}}$	$T_{1k} = \frac{r_{21k}}{\sqrt[2]{r_{22k}}}$
1	1.4401j	0.1609	0.1609	0.4012	0.4012
2	-1.4401j	0.5045	-0.5045	0.7103	-0.7103
3	0.8590j	0.5045	0.5045	0.7103	0.7103
4	-0.8590j	0.1609	-0.1609	0.4012	-0.4012

The transversal coupling matrix M_t derived from the Table 3.1

$$M_t = \begin{matrix} 0 & 0.4012 & -0.7103 & 0.7103 & -0.4012 & 0 \\ 0.4012 & 1.4401 & 0 & 0 & 0 & 0.4012 \\ -0.7103 & 0 & 0.8590 & 0 & 0 & 0.7103 \\ 0.7103 & 0 & 0 & -0.8590 & 0 & 0.7103 \\ -0.4012 & 0 & 0 & 0 & -1.4401 & 0.4012 \\ 0 & 0.4012 & 0.7103 & 0.7103 & 0.4012 & 0 \end{matrix}$$

3) Reduction of transversal coupling matrix to folded coupling matrix using annihilation and similarity transformation.

A similarity transform (or rotation) on an coupling matrix is carried out by pre- and post-multiplying Mt by an N +2 × N +2 rotation matrix R

and its transpose R^t. The pivot $[i, j]$ $(i \neq j)$ of $\mathbf{R}_r$ means that elements $R_{ii} = R_{jj} = \cos\theta_r$, $R_{ji} = -R_{ij} = \sin\theta_r$ $(i, j \neq 1 \text{ or } N)$, and θ_r is the angle of the rotation. The other principal diagonal entries are 1 and all other off-diagonal entries are zero. The eigenvalues of the matrix after similarity transformation remain intact.

$$M_r = R_r * M_{r-1} * R_r^t \qquad r = 1,2,3,\ldots\ldots,R \tag{3.28}$$

When a similarity transform of pivot $[i, j]$ and angle $\theta_r(\neq 0)$ is applied to a coupling matrix M_{r-1}, the elements in rows i and j and columns i and j of the resultant matrix M_r change in value from the corresponding element values in M_{r-1}. For the kth element in the row or column i or j of M_r, and not on the cross-points of the pivot (i.e., $k \neq i, j$), the value will change according to the formulas:

$$M'_{ik} = c_r M_{ik} - s_r M_{jk} \;\; for\ an\ element\ in\ row\ i$$

$$M'_{jk} = s_r M_{ik} + c_r M_{jk} \;\; for\ an\ element\ in\ row\ j$$

$$M'_{ki} = c_r M_{ki} - s_r M_{kj} \;\; for\ an\ element\ in\ column\ i$$

$$M'_{kj} = s_r M_{ki} + c_r M_{kj} \;\; for\ an\ element\ in\ column\ j \tag{3.29}$$

The angle for equation (3.29) is given by

$$\theta_r = \tan^{-1}\left(\frac{M_{ik}}{M_{jk}}\right) \;\; for\ the\ kth\ element\ in\ row\ i\ (M_{ik})$$

$$\theta_r = -\tan^{-1}\left(\frac{M_{jk}}{M_{ik}}\right) \;\; for\ the\ kth\ element\ in\ row\ j\ (M_{jk})$$

$$\theta_r = \tan^{-1}\left(\frac{M_{ki}}{M_{kj}}\right) \; for\ the\ kth\ element\ in\ column\ i\ (M_{ki})$$

$$\theta_r = -\tan^{-1}\left(\frac{M_{kj}}{M_{ki}}\right) \; for\ the\ kth\ element\ in\ column\ j\ \left(M_{kj}\right) \qquad (3.30)$$

The pivot points and elements to be annihilate using similarity transformation for reducing transversal matrix to folded matrix 'M' given in Table 3.2

Table 3.2 Pivots and angles of the similarity transformation for reduction of transversal matrix to folded

Transform number r	Pivot [i, j]	Elements to be annhilated	place	$\theta_r = tan^{-1}\left(\frac{cM_{kl}}{M_{mn}}\right)$				
				k	l	m	n	c
1	[3,4]	M_{s4}	In row s	s	4	S	3	-1
2	[2,3]	M_{s3}	In row s	s	3	S	2	-1
3	[1,2]	M_{s2}	In row s	s	2	S	1	-1
4	[1,2]	M_{1L}	In column L	1	L	2	L	+1
5	[2,3]	M_{2L}	In column L	2	L	3	L	+1
6	[3,4]	M_{3L}	In column L	3	L	4	L	+1

$$M = \begin{matrix} 0 & 1.1536 & 0 & 0 & 0 & 0 \\ 1.1536 & 0 & 0.9844 & 0 & -0.3029 & 0 \\ 0 & 0.9844 & 0 & 0\ .8840 & 0 & 0 \\ 0 & 0 & 0.8840 & 0 & 0\ .9844 & 0 \\ 0 & -0.3029 & 0 & 0.9844 & 0 & 1.1536 \\ 0 & 0 & 0 & 0 & 1.1536 & 0 \end{matrix}$$

3.5. Summary

This chapter lays the foundation for the successive chapters. The step-by-step method of synthesizing the coupling matrix for a prescribed position of transmission zeros and return loss of the filter has discussed along with an example. The first step is to synthesize the characteristic polynomial from the filter transfer function through recursion. Then the transversal coupling matrix is extracted from the polynomial using short circuit admittance parameters. This transversal coupling matrix contains some unrealizable and undesired coupling. These couplings are annihilated with similarity transform, and the coupling matrix reduces to folded form in which all couplings are realizable into a physical filter structure.

Chapter 4

Non-Radiative Dielectric (NRD) Waveguide Filter

4.1. Introduction

T. Yoneyama first introduces the NRD guide in 1981 [124]. An NRD guide is a transmission line in which a dielectric strip inserted between two parallel metal plates, where the spacing between the plates is smaller than half a wavelength. The two parallel metal plate acts as a parallel plate waveguide operate below cut-off and block the propagation of electromagnetic wave with electric field parallel to the plate. Figure 4.1 shows the basic structure of the NRD guide. The NRD guide gain popularity at millimeter-wave due to its good technical parameters, low manufacturing cost, and good integration with planar microwave technologies (e.g. microstrip and coplanar waveguide). All these properties of the NRD guide have compared with the existing technology at the millimeter-wave shown in Table 4.1. This chapter starts with the discussion of NRD guide modes. Among various modes, the low loss LSM_{01} mode has used for filter fabrication. An E-plane resonator has introduced. This resonator is used for the development of the NRD guide bandpass filter. Later on, the basic

structure of NRD is modified, and the modified NRD guide bandpass filter is designed and developed around 30 GHz.

4.2. Theory of NRD Waveguide

The NRD guide support hybrid modes, i.e., either an electric field or magnetic field component is absent in the direction perpendicular to the air-dielectric interface. These hybrid modes classified into two groups:

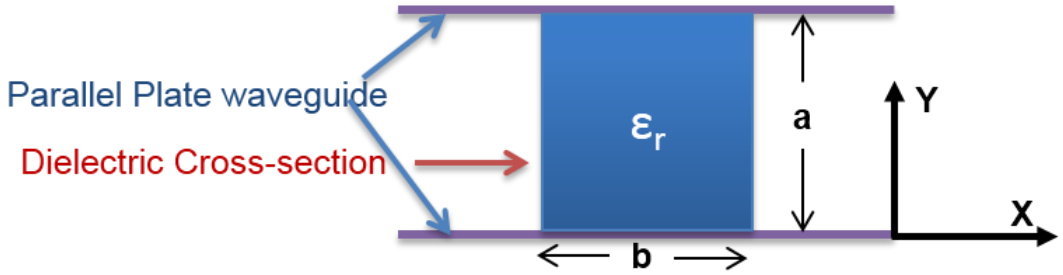

Figure 4.1 *Basic structure of NRD waveguide.*

1. LSE_{mn}: Longitudinal section magnetic modes also referred to as TM^x or E^x modes. The magnetic field component H_x does not exist in this mode.

2. LSM_{mn}: Longitudinal section electric modes also referred to as TE^x or H^x modes. The electric field component E_x does not exist in this mode.

'm' refer to the order of the solution of a transcendental equation in the x direction. Thus, m ranges from 0, 1, 2…'n' is the number of a half wavelength between the metal plates, thus n = 0, 1, 2…

The first two hybrid modes of NRD are LSE_{01} and LSM_{01}. These modes are shown in figure 4.2. LSM_{01} mode preferred for passive devices because of its low

loss.

Table 4.1 Comparison of various technologies at millimeter band

Features	Technology		
	NRD	**Fin-line**	**MMIC**
Loss in the millimeter wave band	Very low	Low	High
Radiation at discontinuities	No	No	Yes
Production cost	Low	Medium	Very High
Production technology	Easy	Medium	Very difficult
Integration with antenna circuits within one technology	Yes	No	Yes

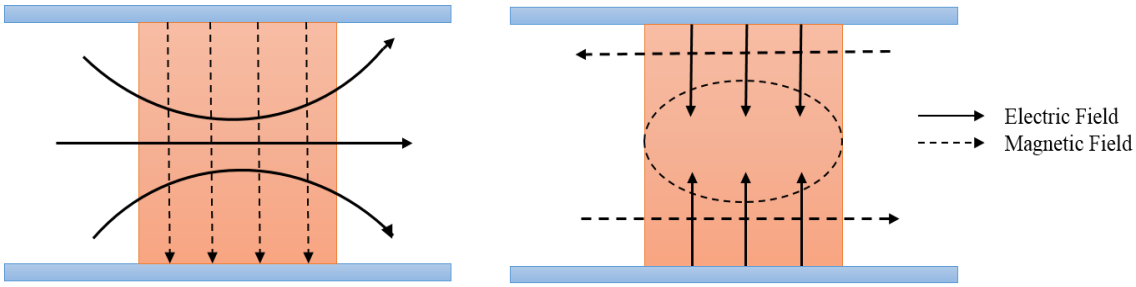

(a) *(b)*

Figure 4.2 *Plots of NRD guide field pattern: (a) LSM_{01} mode, (b) LSE_{01} mode.*

4.3. NRD Guide Bandpass filter

The microwave filters are resonators coupled filters, and its basic element is resonator, which supports various modes. Till now, many papers have published where NRD guide technology used for the realization of bandpass microwave filters. The first bandpass NRD-guide filter had proposed by Yoneyama in 1984 [125]. They were composed of series NRD-guide resonators coupled either by air gaps or by thin dielectric strips. There was

a difficulty in establishing the proper relative positions of resonators. Therefore, the thin dielectric strips were added, which allow one to keep the constant distance between the resonators. Both of these approaches had satisfactory transmission characteristics. Malherbe and Oliver [126] described a similar topology with dielectric resonators coupled by round holes made in the NRD-guide dielectric rod. Another coupling mechanism has proposed by F. Bonne and Ke-Wu [127]. The series of resonators coupled by double strip NRD-guide. The advantage of both presented filter topologies is ease of manufacturing. The significant reduction of filter length has achieved by Ke-Wu et al. [128]. They proposed a filter composed of a cascade of resonators where the coupling between them achieved by the so-called metal windows. It results in a 25 % reduction in length and steeper transmission characteristic in the stop band. Although filters shown [126]-[128] are easy to manufacture and have a shorter length, and higher order modes are excited in the discontinuities which create the filter structure. These modes occur because the discontinuities are not uniform in the vertical direction. Higher order modes can seriously deteriorate the filter response. Due to this fact, the filter design becomes more complicated, and the effect of these modes should consider in the design.

To over these problems, the E-plane resonator based Bandpass filter reported by Yoneyama [129]. An E-plane resonator made from NRD guide by introducing a discontinuity (metal) in the E-field plane. The E-plane resonator supports LSM_{01} mode. E-plane resonator preferred because of its ease of fabrication, better fabrication tolerances, and spurious free

performance. The approach [129] shows better RF performance, but it lacks tunability. The placing of foils suffers two problems: (i) create minor air gaps (ii) Foil dimension tolerances. The lithography process also limits by dimensional tolerances. There is a spurious in the lower side of the passband. Once, this filter fabricated, the center frequency, as well as coupling, cannot be tuned. The current proposed work presents a new approach to design a fully tunable (both center frequency and bandwidth) filter. This approach is less depending on fabrication tolerances as well as provides good RF performance.

4.3.1. E-plane Resonator

Table 4.2 Specifications of the filter

Specifications	Value
Center Frequency (CF)	43.5 GHz
Bandwidth	350 MHz
Rejection @ CF±500 MHz	≤ -20 dB
Return Loss	≥ 17 dB

The filter realized by using an E-plane NRD guide resonator. The E-plane resonator realized in the NRD guide by introducing a metallic discontinuity in the electric field plane. The discontinuity must be symmetric, which eliminate the possibility of spurious mode. Figure 4.3(a) shows the typical E-plane resonator, introducing a discontinuity (metal) in the E-field plane. The E-plane resonator supports LSM_{01} mode. The field pattern of LSM_{01} mode in NRD guide shown in figure

4.3(b). E-plane resonator has preferred because of its ease of fabrication, better fabrication tolerances, and good spurious free performance.

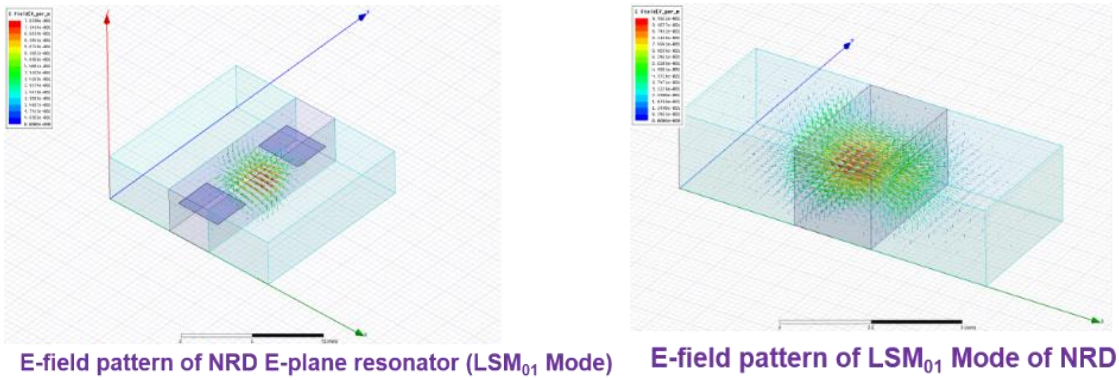

(a) (b)

Figure 4.3 *LSM$_{01}$ mode E-field pattern, (a) E-plane resonator CAD model, and (b) NRD guide CAD Model.*

4.4. Filter Design

After exhaustive EM analysis of E-plane resonator, it has found that instead of using foils, the screw of a suitable dimension can provide tunability in the coupling. So, M2 screw has selected in the design, which can tune both center frequency and coupling. The M2 silver plated screws have used to minimize losses. Eigenmode solver of EM simulator has used for determining the dimension of NRD guide with the condition that the 'a' dimension should be less than half the wavelength of operating frequency. The Teflon of dielectric constant 2.1 considered in the eigenmode simulation, and the NRD dimensions are optimized for a wide spurious free window and best achievable Q-factor. The NRD dimensions are a=3.1 mm and b=3.7 mm, and the parallel plate width is 15 mm. With these NRD guide dimension, the E-plane NRD resonator quality factor is 2500 at 43.5 GHz. The fourth-order chebyshev filter is designed with

E-plane NRD resonators and they are coupled through each other by the dielectric and M2 screws. Figure 4.4(a), (b) and (c) shows the 3D CAD model along with its dimensional parameter in top view and side view, respectively. The simulated response of the filter shown in figure 4.4(d). The design parameters, along with their values used for the EM simulation of figure 4.4, are listed in table 4.3. It is a very good solution at very high frequency, but this design doesn't have a standard input-output waveguide interface, which poses a problem to test this design on the test bench. Moreover, there is a spurious at the lower side of the passband.

Table 4.3 Design parameters and their values for NRD filter of figure 4.4

Design Parameters	Value (mm)	Design Parameters	Value (mm)
a	3.1	g_{01}	1.9
b	2.8	g_{12}	0.765
d	3.0	g_{23}	0.5
R1	8.73	cavx	15.0
R2	7.85	rad	2.0

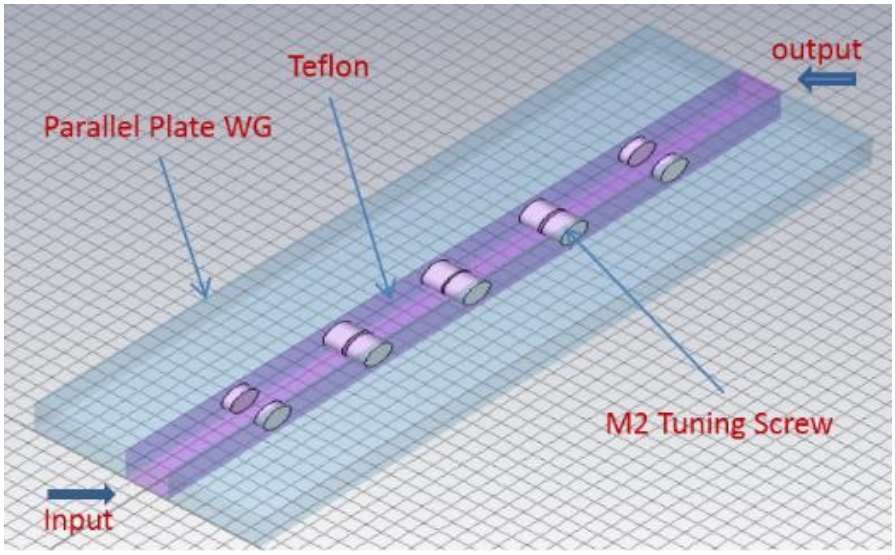

(a)

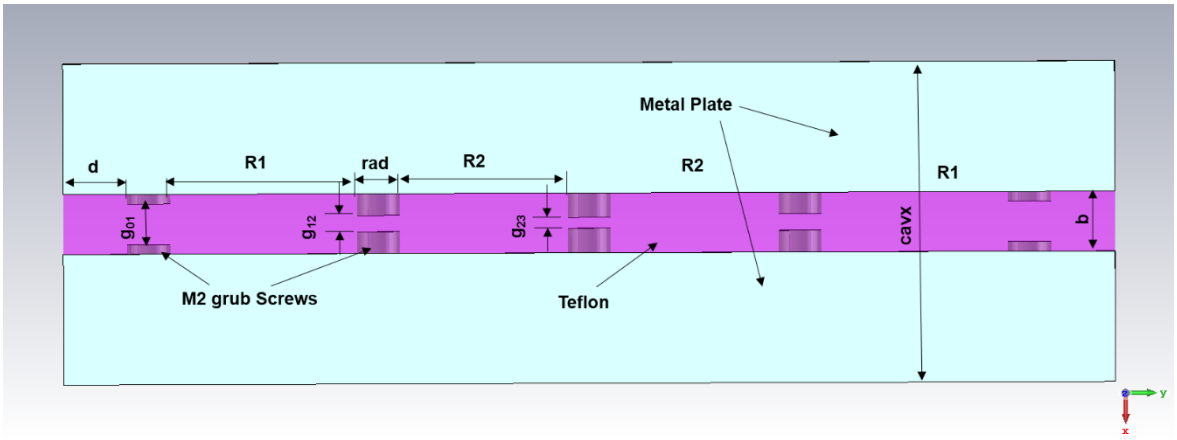

(b)

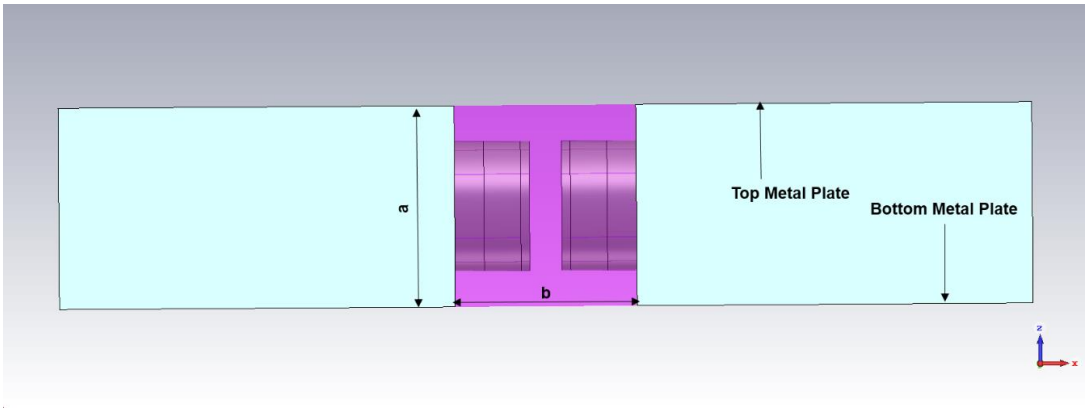

(c)

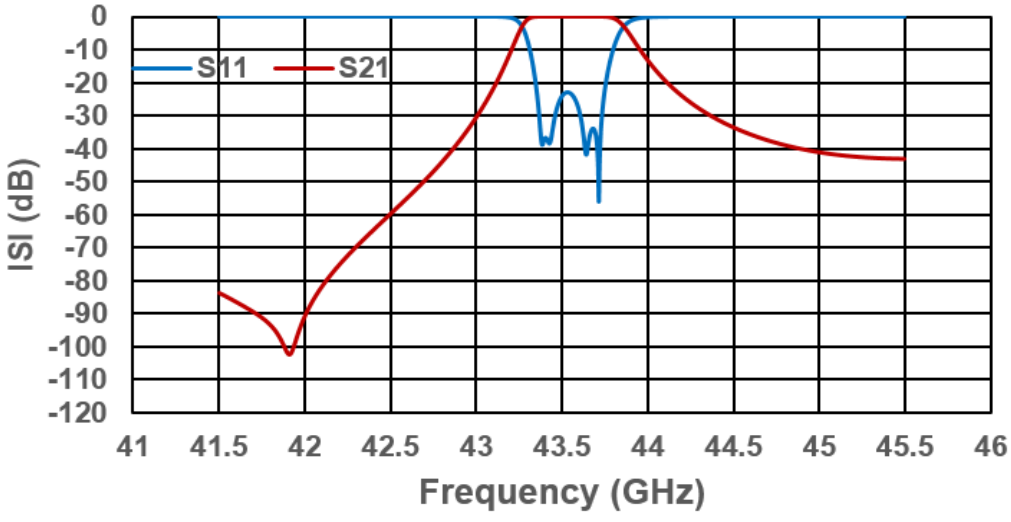

(d)

Figure 4.4 *E-plane NRD guide filter and its simulated response; (a) 3D EM CAD model, (b) Top view of Filter CAD model, (c) Side view of filter CAD model, and (d) Simulated Response.*

The WR22 standard input-output waveguide interfaces are used to overcome the above limitation. This interface is an integrated part of the design. The NRD guide dielectric tapered at input and output interface to match the VSWR of both NRD guide and WR22 interface. This tapering is optimized to realize spurious-free input-output coupling. The modified filter model, along with dimension parameters, are shown in figure 4.5 (a), (b), and (c) as a 3D CAD model, top view and side view, respectively. The value of design parameters shown in figure 4.5 is listed in table 4.4. The simulated response of this approach shown in figure 4.5(d). This approach keeps the RF performance intact, but still, there is a problem of spurious mode, which appears as transmission zero in the lower side of the passband. Moreover, precise drilling of the hole for the M2 screw also poses limitation.

In the EM analysis of the design, it has found that if through-hole has done in the same location, instead of drilling precise holes for M2 screw, the spurious has eliminated from the lower side of the passband. This approach relaxes fabrication tolerances and provides superior RF performance.

Table 4.4 Design parameters and their values for MNRD filter of figure 4.5

Design Parameters	Value (mm)	Design Parameters	Value (mm)
a	3.1	g_{01}	1.83
b	3.7	g_{12}	0.234
d	3.9	g_{23}	0.152
R1	5.528	cavx	15.0
R2	5.235	rad	2.0
L1	5.0	t1	3.0
WR22a	5.69	WR22b	2.845

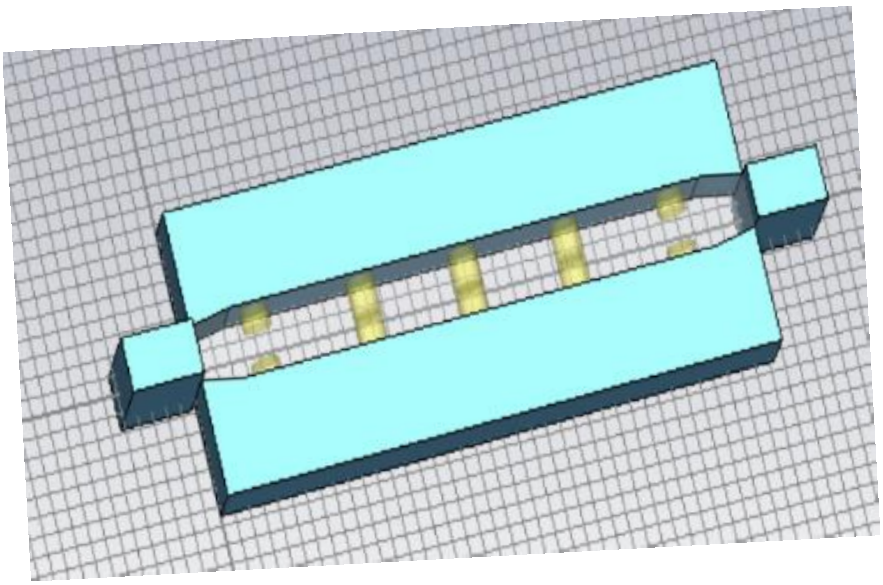

(a)

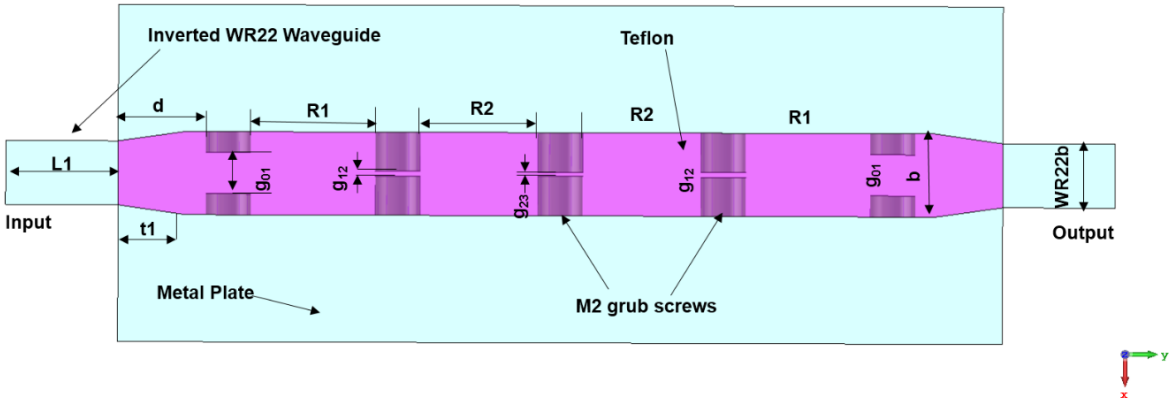
Inverted WR22 Waveguide
Teflon
d
R1
R2
R2
R1
L1
g_{01}
g_{12}
g_{23}
g_{12}
g_{01}
b
WR22b
Input
t1
Output
Metal Plate
M2 grub screws
y
x

(b)

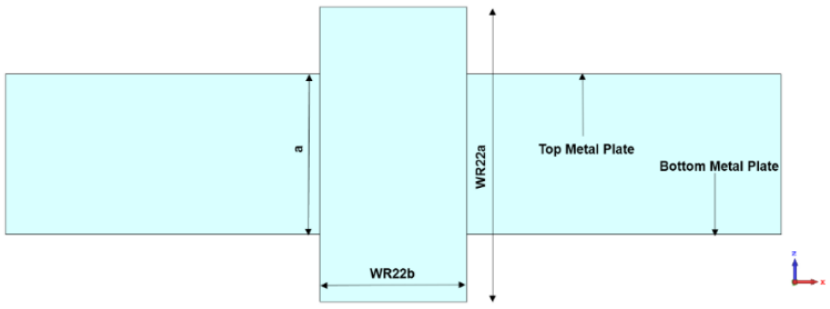
a
WR22a
Top Metal Plate
Bottom Metal Plate
WR22b
z
x

(c)

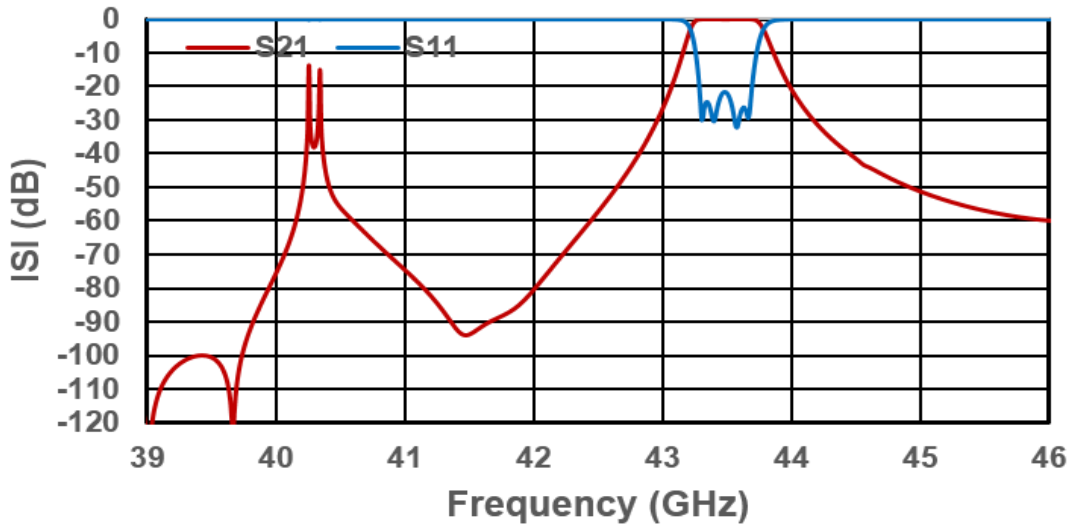

(d)

Figure 4.5 *Modified NRD guide filter; (a) Filter CAD model; (b) Top view of Filter CAD model, (c) Side view of Filter CAD model, and (d) Simulated response.*

Here, the coupling between resonators is through air gap instead of Teflon, which provides coupling in the previous design approaches. The basic structure of NRD is modified, so the final approach is MNRD (modified NRD) E-plane resonator bandpass filter.

Table 4.5 Design parameters and their values for MNRD filter of figure 4.6

Design Parameters	Value (mm)	Design Parameters	Value (mm)
a	3.1	g_{01}	0.991
b	3.7	g_{12}	0.196
d	5	g_{23}	0.152
R1	5.487	cavx	15.0
R2	5.378	rad	2.0
L1	5.0	t1	3.5
WR22a	5.69	WR22b	2.845

The MNRD E-plane resonator bandpass filter model, along with dimension parameters, are shown in figure 4.6 (a), (b), (c), and (d) as a 3D CAD model, top view, side view, and cut-sectional view, respectively. The value of design parameters shown in figure 4.6 is listed in table 4.5. The simulated response of this approach shown in figure 4.6(e). It is difficult to find, commercially available M2 screws of the smaller length required for tuning, instead, the M3 grub screw of any length are available. Hence, M3 grub screws are used for inter-resonator coupling and input-output coupling.

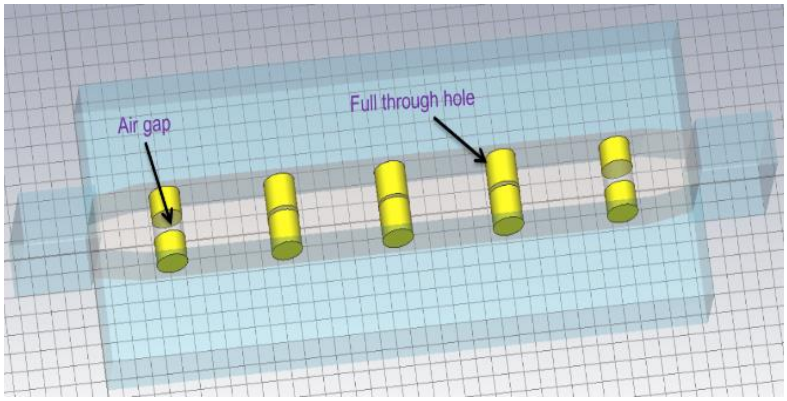

(a)

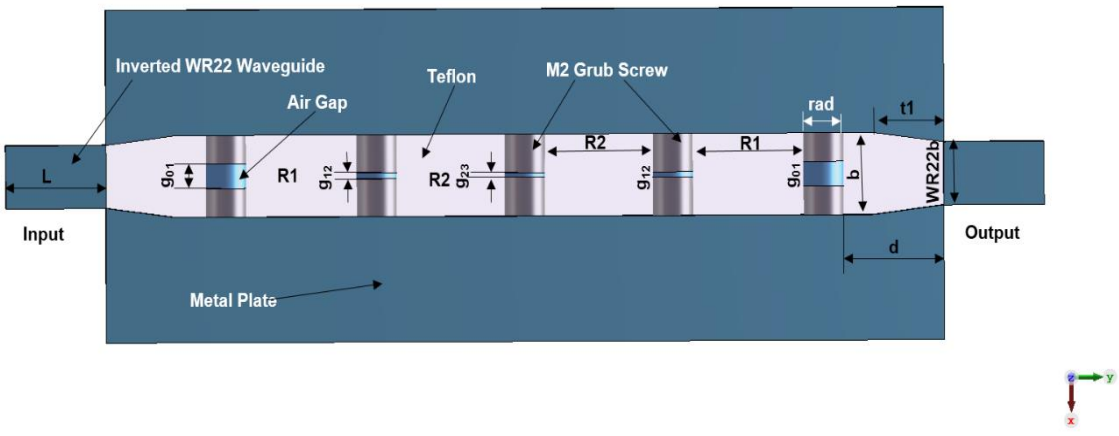

(b)

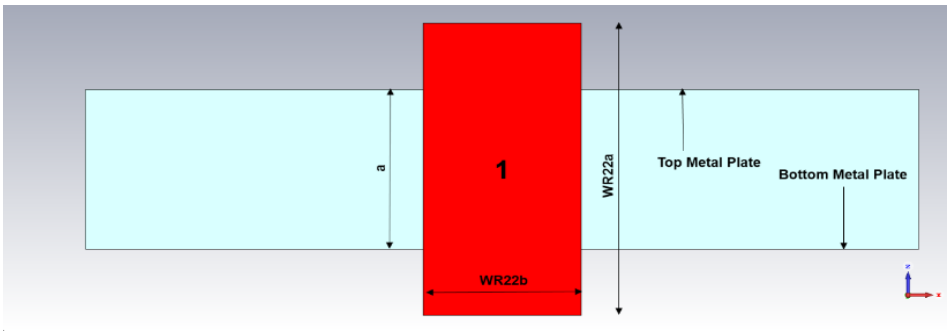

(c)

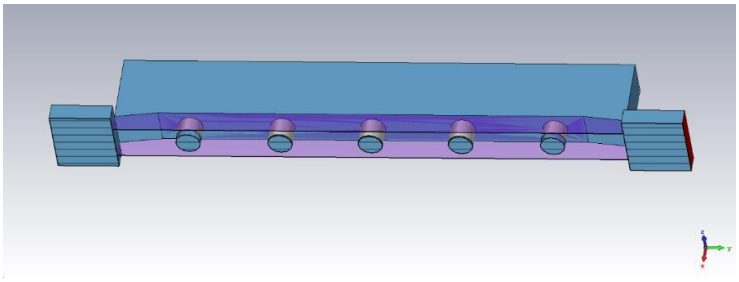

(d)

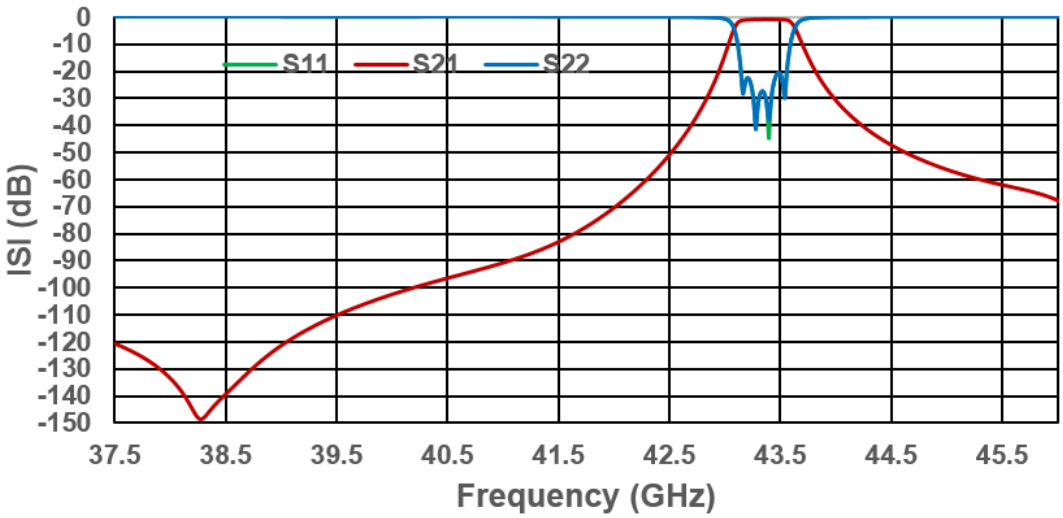

(e)

Figure 4.6 *MNRD guide filter CAD model with through hole for air gap coupling, and its simulated response; (a) MNRD guide filter CAD model, (b) Top view of MNRD filter, (c) Side view of MNRD filter, (d) Cut-sectional view of MNRD filter, and (e) Simulated results of MNRD filter.*

The filter designed at 30 GHz with WR28 waveguide as input-output interface and M3 grub screws for inter-resonator coupling. The design parameters shown in the top view of the filter in figure 4.7 (a), and the fabricated filter shown in figure 4.7(b) and (c). The filter has fabricated by a standard milling process. The two parallel metal plates of the filter are made from Aluminium with a fabrication tolerance of ± 20 microns. The dielectric has made from Teflon with a dielectric constant of 2.1. The fabrication tolerance of ±50 micron has considered for Teflon, and the tapping for the M3 grub screw is done with the M3 tap tool. The four numbers of M2 screws mount on the corners of the plate to assemble the filter. The filter is characterized on the VNA with WR-28 sliding load waveguide calibration kit. The two-port waveguide calibration done on VNA with the help of WR-28 coaxial to waveguide adapter and the calibration kit. After calibration, the VNA shows back to back adapter S_{21} is -0.01 dB and the S_{11} and S_{22} are -60 dB. The filter is tuned by a non-deterministic tuning method where passband return is tuned to get the desired response. The EM simulated and measured response shown in figure 4.8(a) and (b). The penetration of tuning screws perturbs the electric field, so it shifts the response to the lower side has the same behaviour as the TE_{101} mode waveguide filter. The center frequency tuning is shown in figure 4.8(c), where different plots showed the change in center frequency due to a variation in penetration of the tuning screw.

The measured response is shifted and centered around 29.2 GHz. The insertion loss of the filter is 2.3 dB. This major shift in the center frequency is due to the plasticity of Teflon, which is a soft material that causes variation in the design

dimensions during fabrication. The large insertion loss is attributed to unplated Aluminium plate is used instead of silver plated Aluminium. Moreover, the contact related issues between grub screws and tapped hole in the Teflon, between NRD guide Teflon and the parallel metal plates has major contribution in the filter response degraded performance.

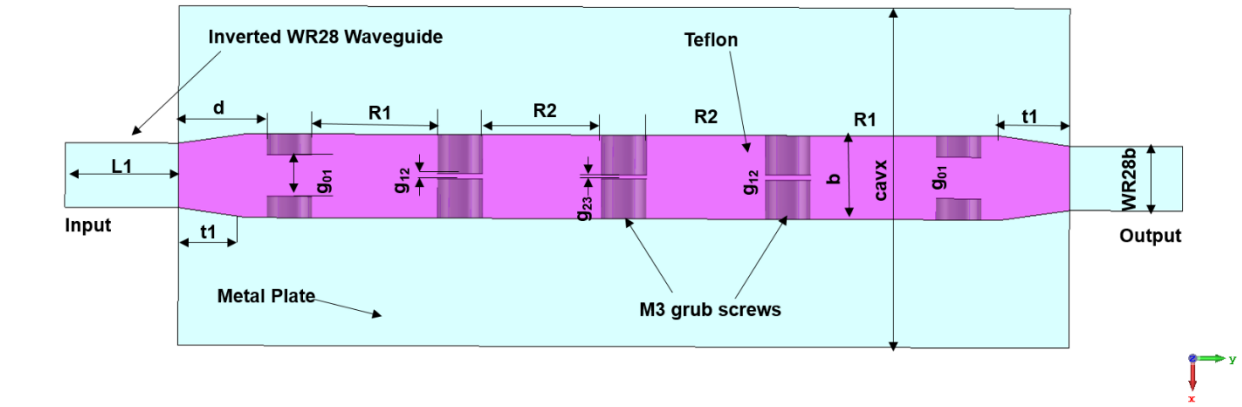

(a)

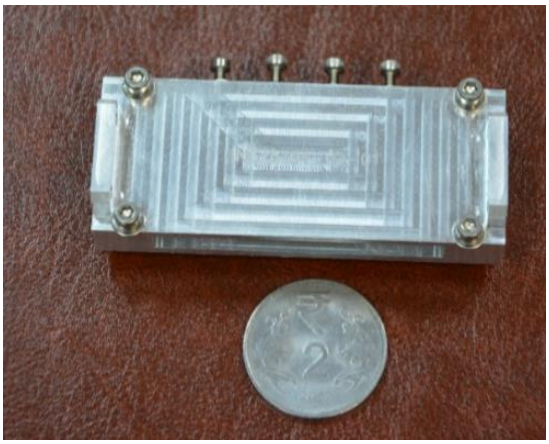

(b)

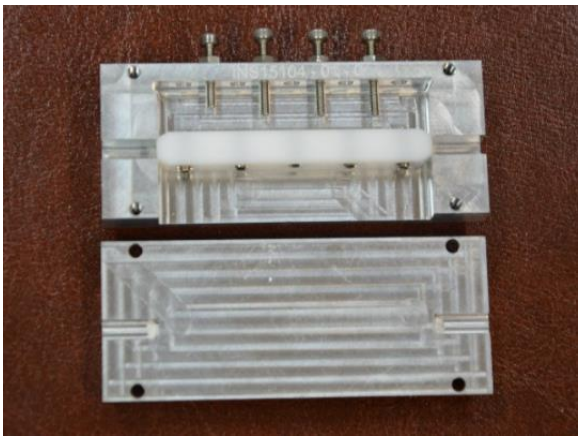

(c)

Figure 4.7 *(a) Top view of MNRD filter at 30 GHz; (b) fabricated MNRD guide filter, and (c) open view of MNRD guide filter.*

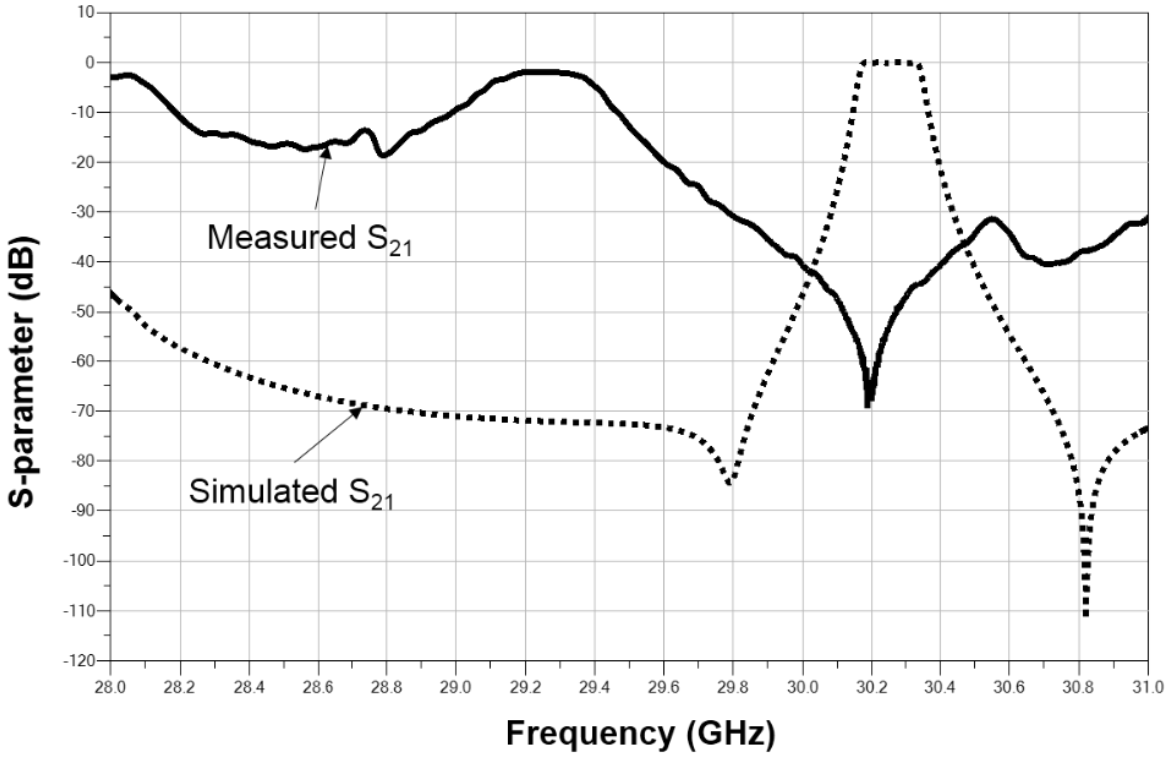

(a)

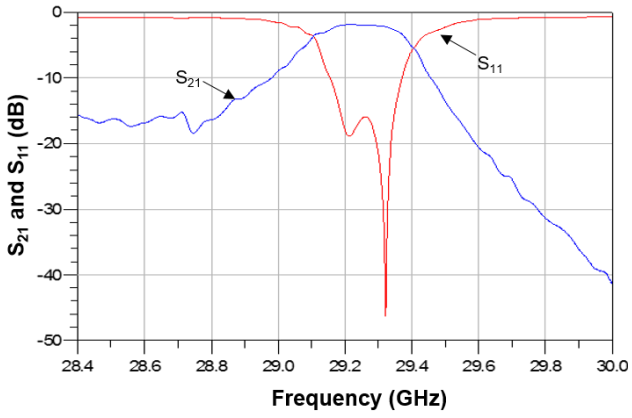

(b)

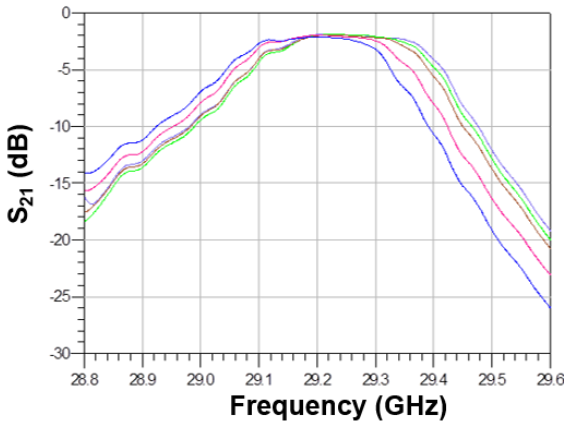

(c)

Figure 4.8 *(a) Simulated and measured response of MNRD guide filter at 30 GHz, (b) Measured response of MNRD guide filter, and (c) Centre frequency tunability due to variation of tuning element penetration.*

Table 4.6 Design parameters and their values for MNRD filter of figure 4.7

Design Parameters	Value (mm)	Design Parameters	Value (mm)
a	3.1	g_{01}	0.836
b	3.2	g_{12}	0.127
d	3.5	g_{23}	0.114
R1	6.84	cavx	15.0
R2	6.91	rad	3.0
L1	10	t1	2.0
WR28a	7.11	WR28b	3.55

4.5. Summary

The design of modified NRD filter design, challenges and measured results are discussed. The novel concept of using grub screw instead of metal foil to realize E-plane resonator bandpass filter. It provides bandwidth tunability, while the center frequency is tuned by perturbing the E-field of the resonator. Initially, the filter design at the center frequency of 43.5 GHz, but due to the non-availability of calibration standard, the filter was designed at 30GHz. There is a large difference between the MNRD filter simulated and measured results due to fabrication uncertainty and the contact related issue. The present configuration of the filter is not suitable to be deployed for payload applications.

Chapter 5

High Q Coaxial Resonator Filter

5.1. Introduction

This chapter provides detailed information about the various higher modes of the coaxial resonator and the application of higher-order mode in the high-performance filter design. The chapter starts with the different higher-order modes of the coaxial resonator and the mode selection criteria for the filter design. After mode selection, the various steps and procedure to design a filter is discussed. The concept of higher-order high Q mode for filter design and realization has validated by taking the example of direct and cross-coupled resonator filters. The cavity filters are the most popular filters at very high frequency. So, an identical configuration rectangular waveguide filter has been designed and realized, and its performance is compared with the higher-order mode coaxial resonator filter (proposed filter). It is mandatory to test the thermal performance of the filter used for the satellite, which gives an idea about the frequency shift of the filter under operating conditions. So, both the proposed and the waveguide filter are subjected to thermal cycling. Apart from these, the high power handling capability of both filters are analyzed. Due to the non-availability of high power test-up, both the filters are analyzed theoretically and validated with commercially available software

5.2. Higher-Order modes of Coaxial Resonator

A metal post of length λ/4 shorted at one end inside a cavity constitutes a coaxial resonator. The shape of the cavity and the post may be cylindrical, cuboidal, and elliptical. It is also called combline resonator or re-entrant cavity, and it supports an infinite number of modes:

1. TEM (Transverse Electromagnetic) Mode: This is the dominant mode of coaxial resonator used for filtering application.

2. Higher-Order modes: TE (Transverse Electric) and TM (Transverse Magnetic) modes.

The dominant mode of the coaxial resonator in each of the shape is Transverse electromagnetic (TEM), where the electric field is radially outward from the post surface to the cavity walls and the magnetic field encircles the volume between the post and the cavity. The electric and magnetic field pattern of TEM mode shown in figure 5.1 There is no component of the electric and magnetic field long Z-axis, i.e., along the length of the coaxial resonator.

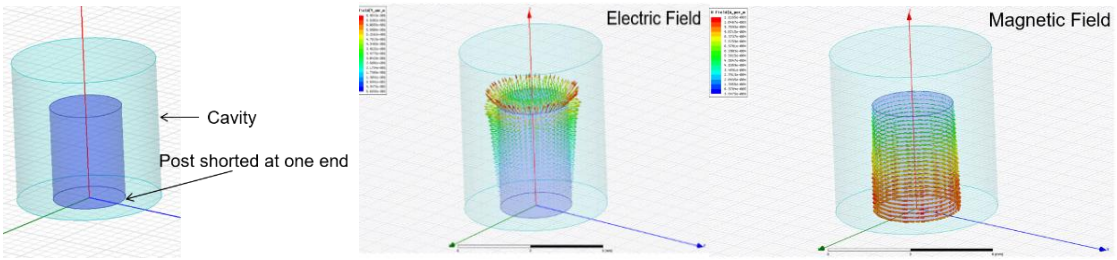

Figure 5.1 *Coaxial resonator and its TEM mode electric and magnetic field pattern.*

The dominant TEM mode preferably used for filtering application from VHF to C-band due to its small size, high Q-factor, wide spurious free-range and predictable thermal behaviour. The resonator Q-factor decreases with an increase in the frequency limit the use of coaxial resonator beyond C-band. The simulated Q-factor of TEM mode coaxial resonator is 2000, which is not enough for the realization of high-performance filters and multiplexers for satellite. There is a need for high Q, wide spurious free-range and a reasonably good size to handle at Ka-band and beyond. The higher-order modes of coaxial resonator have high Q-factor, but apart from high Q TM_{012} mode has wide spurious free-range and a reasonably good size to be used for high-performance filters at Ka-band and beyond.

The cylindrical coaxial cavity structures are used in very high power gyrotron as they permit single-mode operation for larger cavity dimensions. However, the higher-order modes of the coaxial resonator have never used for filter applications. The dimension of the coaxial cavity structure determines the mode and their mode separation. The coaxial resonators' cavity diameter and height are 7.2 mm and 9 mm, respectively, and its post diameter and height are 3 mm and 4 mm, respectively. The first six modes of the coaxial resonator plotted against variation of cavity diameter and the resonant frequency of the resonator is shown in figure 5.2. The eigenmode solver of commercial 3D electromagnetic (EM) simulator is used to find out the resonant frequency and Q-factor. The first mode in the mode chart is dominant TEM mode. The second mode is the dual mode TE_{111}. The fourth mode is TM_{012}, after that dual mode TE_{112}.

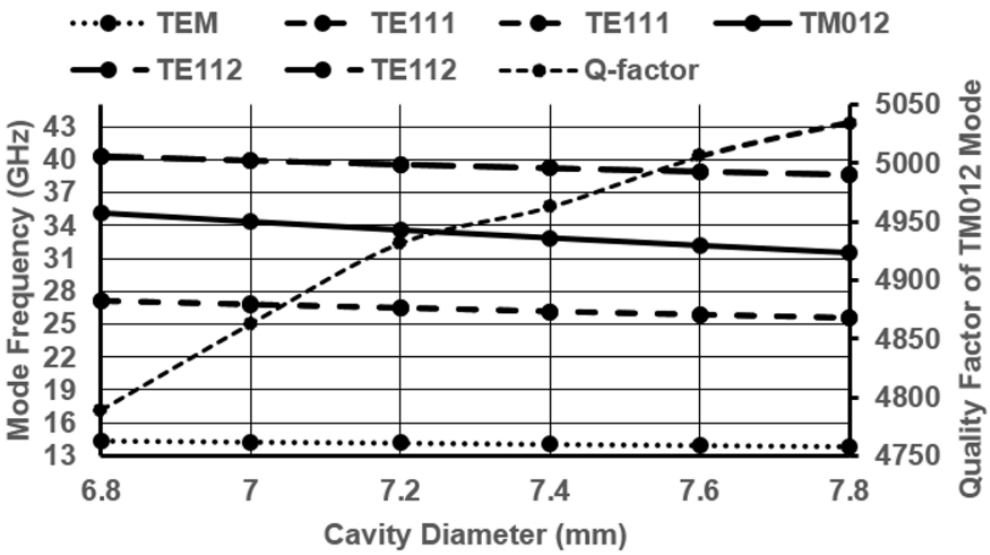

Figure 5.2 *Higher order modes of coaxial resonator.*

5.2.1. Q-factor Measurement

The coaxial resonator supports Transverse Electric (TE) and transverse magnetic TM modes. The higher-order TE and TM modes have high Q-factor. There are two methods to determine the Q-factor and resonant frequency of the modes. The first method is to use the eigenmode solver, which gives the resonant frequency of a lossy resonator. In this method, the loss has considered in terms of conductivity of the metal used for fabrication. The other method is to use the frequency domain solver, and the resonator is exciting by very weak coupling so that it does not load the Q-factor and resonant frequency. In this method, the measurement of peak values gives the resonant frequency. The 3dB bandwidth measured from resonator center frequency and the ratio of the resonator center frequency to 3dB bandwidth gives the Q-factor. This method used to calculate the

Q-factor and resonant frequency practically. Either waveguide or coaxial connector has used for excitation. The 2.92 mm coaxial connector is used for excitation in the frequency domain solver, for estimation of resonant frequency, and Q-factor, as shown in figure 5.3.

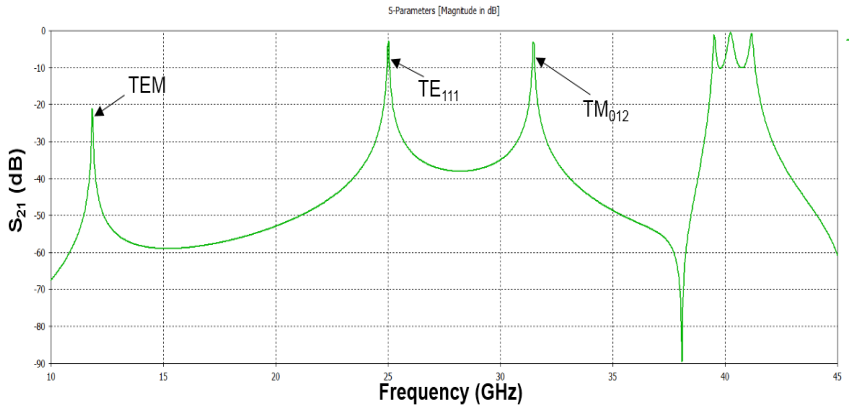

(a)

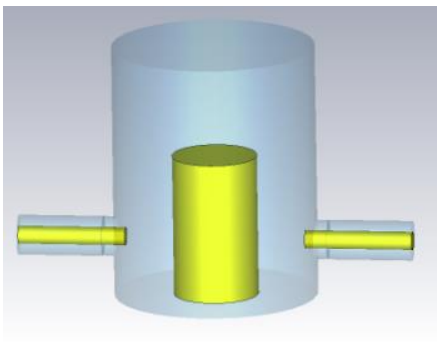

(b)

Figure 5.3 *Resonant frequency and Q-factor of higher order modes of coaxial resonator, (a) Modes of coaxial resonator, and (b) CAD model of cavity for Q-factor measurement.*

The coaxial resonators cavity diameter and height are 7.2 mm and 9 mm, respectively, and its post diameter and height are 3 mm and 4

mm respectively used in figure 5.3 for Q-factor measurement. The 2.92 mm coaxial connectors are at a height of 2 mm from the shorted end of the cavity.

5.3. TM_{012} Mode

The TM_{012} is the fourth mode in the mode chart, and its electric and magnetic field patterns are analogous to the TM_{01} mode of the cavity resonator where there is one variation of the magnetic field along azimuth, two variations along Z-axis, and zero variation along the radial direction. The TM_{012} mode field patterns shown in figure 5.4. The maximum field available near the top of the cavity is sufficient to realize narrow as well as the wide-passband bandpass filter. The simulated quality factor of the single resonator is more than 4800, considering the silver metal boundary. The dimension of the cavity diameter and height is 7.2 mm, and 9 mm, respectively. The post diameter and height are 3 mm, and 4 mm, respectively. The spurious-free window of 7.1 GHz and 6 GHz, below and above the resonant frequency is sufficient to realize wideband filters.

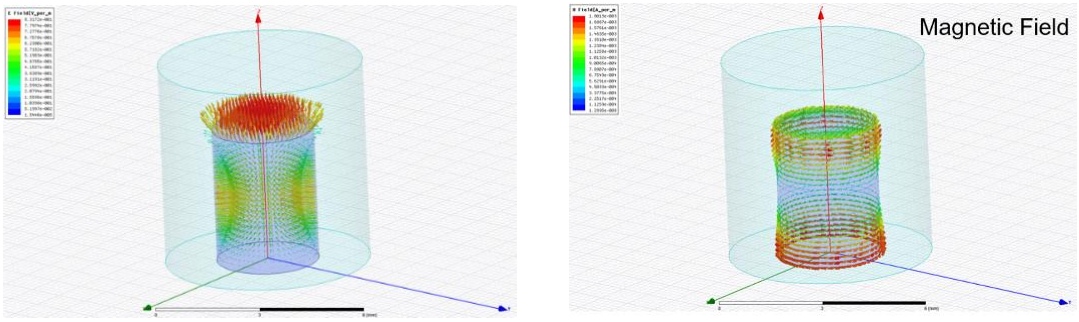

Figure 5.4 *Electric and magnetic field of TM_{012} mode coaxial resonator.*

Similarly, the mode chart is plotted for the first six modes of similar dimension cylindrical cavity as shown in figure 5.5. The dominant mode is dual-modeTE_{111}, and its simulated Q-factor is better than 6500. The next higher mode is TM_{011} has Q better than 6900. Then the next higher modes are TM_{012} and TE_{112}. The spurious-free window between the dominant mode and the next higher mode is 3 GHz, which reduces to 1.5 GHz, as diameter increases from 6.8 mm to 7.8 mm, respectively. The best spurious-free window is 4 GHz at one end and 5 GHz on the other end for TM_{012} mode, but the filter design with this mode have a poor wide stopband due to spurious modes.

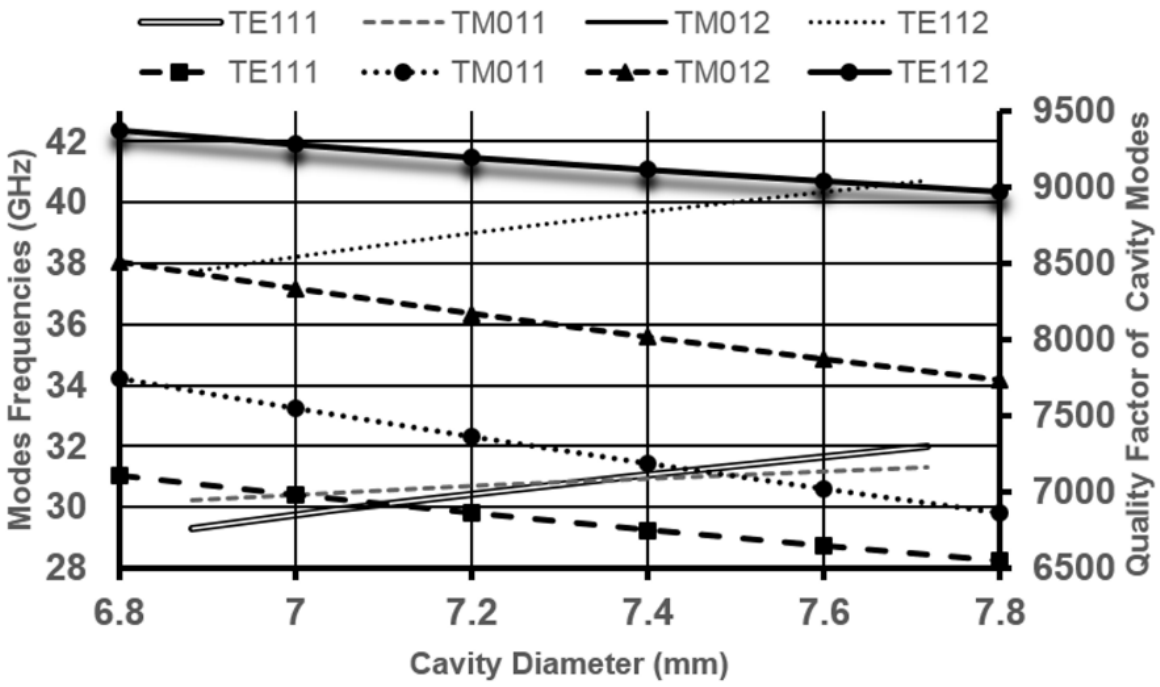

Figure 5.5 *Mode chart of cylindrical cavity resonator.*

5.4. Filter Design

The filter design involves the following steps:

1) ***Synthesis:*** The filtering function is to synthesize for the given specification, which is Chebyshev or Quasi-elliptic. In this, the order of the filter, position of transmission zeros, return loss defined for the synthesis of coupling matrix.

2) ***Validation:*** The coupling values obtained from the coupling matrix are validated on the circuit simulator using parallel resonator and immittance inverter model where the parallel resonator is defined using lumped RLC corresponds to the resonant frequency (Center frequency of the filter), and immittance inverter is realized using a quarter wave transmission line having characteristic admittance equivalent to the coupling values. The feasibility of specifications is validated using this step.

3) ***Virtual experimentation:*** This step determines the resonator dimensions and maps the coupling values into a physical realizable structure. The resonator dimension is realized using an eigenmode solver where the trade-off has done between the resonator size, quality factor and the spurious-free range. The coupling values realized in terms of iris dimension, where an iris placed between the two resonators and vary its dimensions to map the coupling values.

4) ***EM Simulation:*** The N-pole filter model is formed, and all the resonator and irises dimensions obtain from the above steps are mapped into it. These are the initial dimension for the EM simulation. The coupling values mapped into the reflection group delay values. These values are used to simulate and optimize the dimensions to get the desired filter response.

5) ***Fabrication:*** It involves the material selection based on the estimated frequency drift of the filter for the operating temperature range.

The Table 5.1 gives specifications of a typical Ka-band filter of a high throughput satellite. These specifications can be either with direct coupled or cross-coupled filter. The filtering function is synthesized for these specifications and found that a 4-2-0 filter made from the Invar metal, and a 5-2-0 and 7-pole Chebyshev filter made from Aluminium can meet this specification.

Table 5.1 Specification of ka-band pre-select filter

Specification	Values
Frequency Band	30.0-30.5 GHz
Insertion Loss	< 0.5 dB
Bandpass Flatness over BW	< 0.3 dB
Rejection at CF ± 450 MHz	>20 dB
Rejection at 20 GHz	>90 dB
Return Loss	> 20 dB
Input and Output Interface	WR-28

5.4.1. 4-2-0 Filter

In the four pole filter, two transmission zeros placed at ± 1.9i for near band rejection. The 26 dB return loss chosen for filter synthesis. The coaxial resonator dimensions are 7.2 mm, and 9 mm are cavity diameter

and height and 3 mm, and 4 mm post diameter and height.

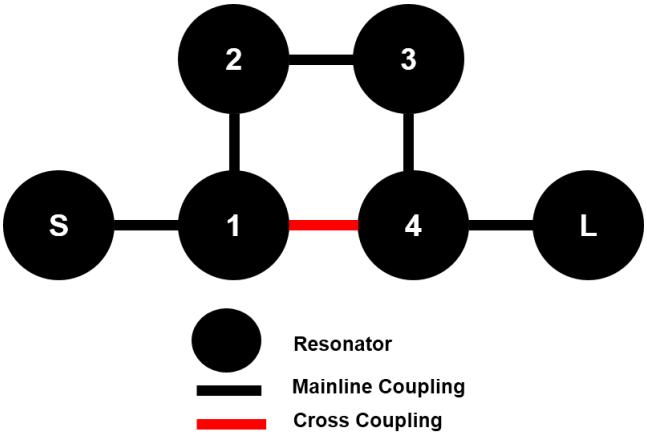

(a)

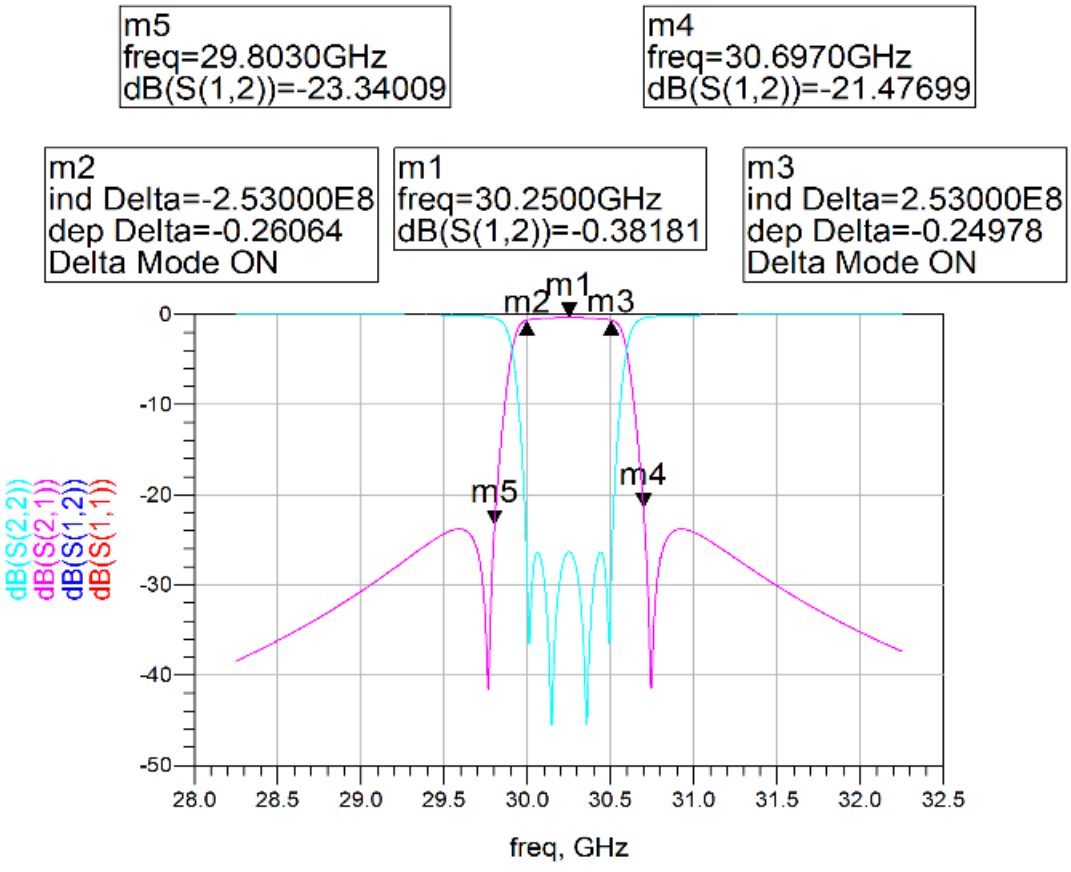

(b)

Figure 5.6 *(a) Schematic, and (b) Circuit simulator response of 4-2-0 filter.*

Table 5.2 Synthesize coupling matrix for 4-2-0 filter

	S	1	2	3	4	L
S	0	1.1536	0	0	0	0
1	1.1536	0	0.9844	0	-0.3029	0
2	0	0.9844	0	0.8840	0	0
3	0	0	0.8840	0	0.9844	0
4	0	-0.3029	0	0.9844	0	1.1536
L	0	0	0	0	1.1536	0

The synthesized coupling matrix for the 4-2-0 filter given in Table 5.2, where the cross-coupling is negative between resonator 1 and resonator 4, and all the mainline couplings are positive. The mainline coupling, i.e., inter-resonator coupling, source to input resonator and load to output resonator shown as the black line in the schematic of figure 5.6(a). The cross-coupling is shown as a red line between resonator 1 and 4 in figure 5.6(a). The cross-coupling is realized using a non-resonating post. The synthesized coupling matrix validated on a circuit simulator, and the circuit simulator response shown in figure 5.6 (b).

The next step is the conversion of these coupling values into the realizable dimension. The design chart is generated using two resonators separated by an iris.

$$\kappa = \frac{f2^2 - f1^2}{f1^2 + f2^2} \tag{5.1}$$

$$f_c = \frac{f1 + f2}{2} \tag{5.2}$$

The coaxial resonator cavity diameter and height is 7.2 mm, and 9 mm, respectively. The post diameter and height are 3 mm, and 4 mm, respectively. These two identical coaxial resonators are separated by an iris of thickness 2 mm and height 3.5 mm from the top of the cavity. Here, iris width is varying, keeping its height fixed. The eigenmode Solver of 3D EM Simulation Software where f_1 and f_2 are the eigenmode frequencies and κ is the coupling value normalized with the filter bandwidth. The average center frequency is f_c. Figure 5.7 shows, the variation of the normalized coupling values due to the variation in the iris width. Non-resonating Metallic post of length 'l' placed between non-adjacent resonators to realize cross-coupling [130].

The post should be normal to the plane of the magnetic field of the resonator. The variation of cross-coupling, with variation in the post length, as shown in figure 5.8.

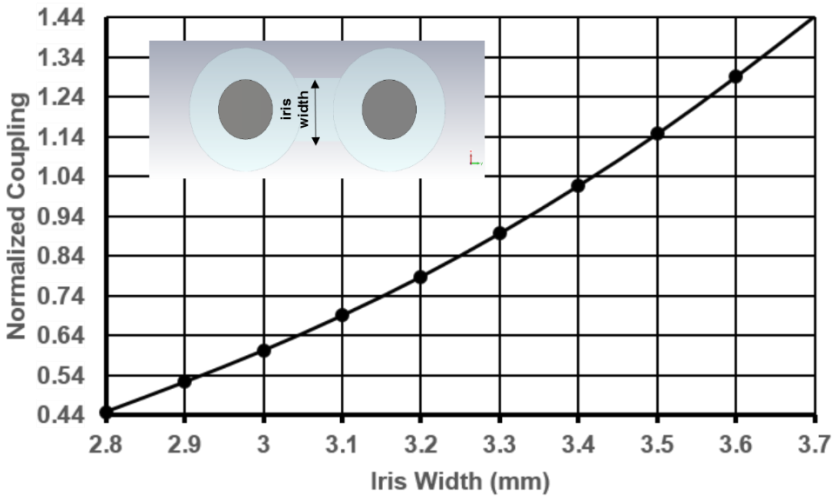

Figure 5.7 *Variation of normalized coupling with iris width.*

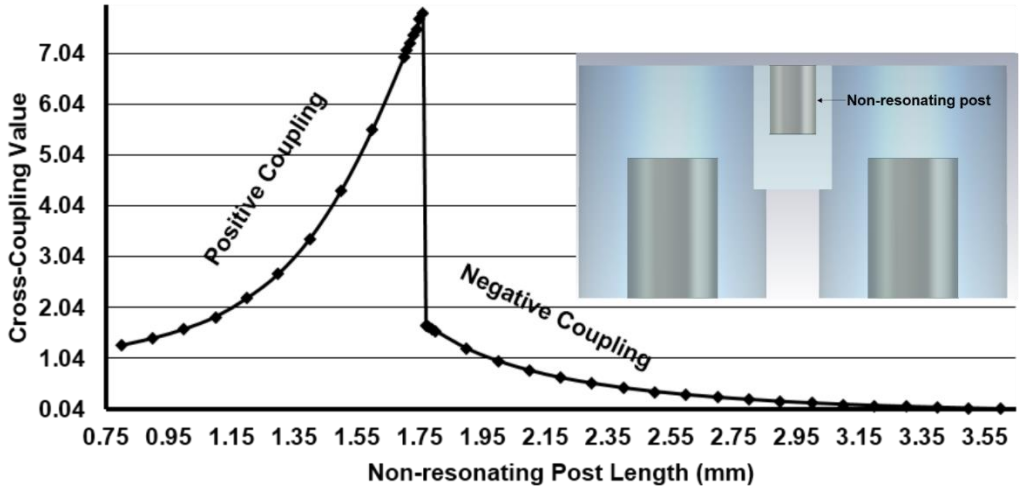

Figure 5.8 *Variation of normalized coupling with the length of non-resonating post.*

The diameter of the non-resonating post shown in figure 5.8 is 1.6 mm, and its height is varying from the top of the cavity. It is placed in an iris of thickness 2 mm and height 3.6 mm. The increase in the length of the post decreases the gap between the post and iris. Initially, the coupling is positive and maximum when the post length is 1.75 mm. Then further increase in length changes the nature of coupling from positive to negative and become zero when the gap is zero.

The EM simulation has done with the dimensions obtained from the above design chart. The design parameters for the 4-2-0 filter are shown in the 3D EM CAD model, its side view, and cut-sectional view in figure 5.9(a), (b), (c) and (d). The values corresponding to the design parameters are listed in Table 5.3. The simulated response of 4-2-0 coaxial resonator filter shown in figure 5.9(e).

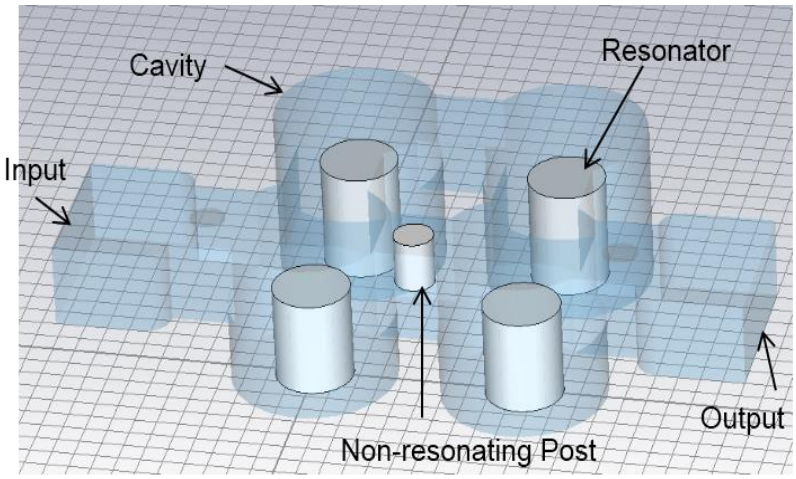
Cavity
Resonator
Input
Output
Non-resonating Post

(a)

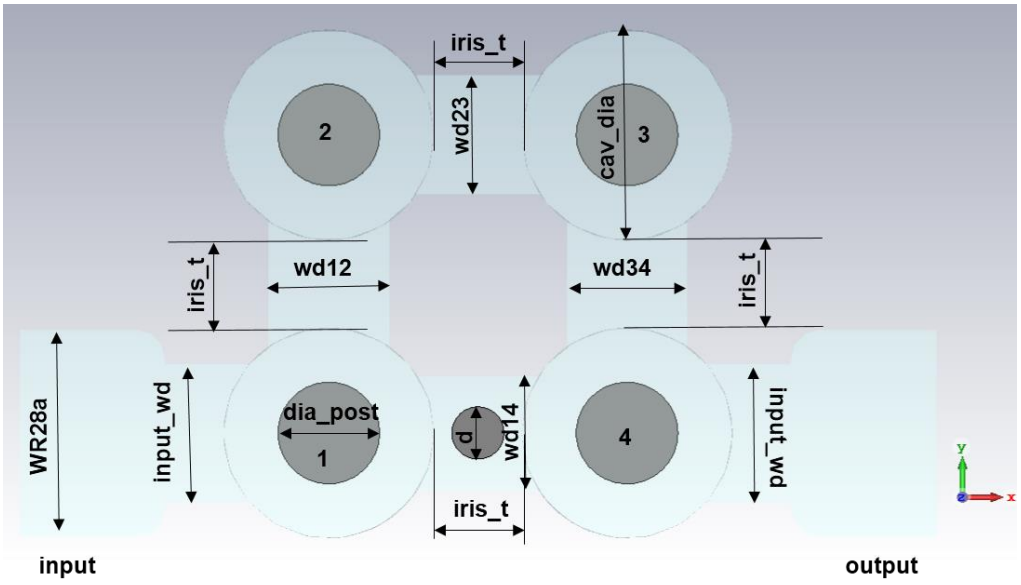
iris_t
wd23
cav_dia
2
3
iris_t
wd12
wd34
iris_t
WR28a
input_wd
dia_post
1
d
wd14
4
input_wd
iris_t
input
output

(b)

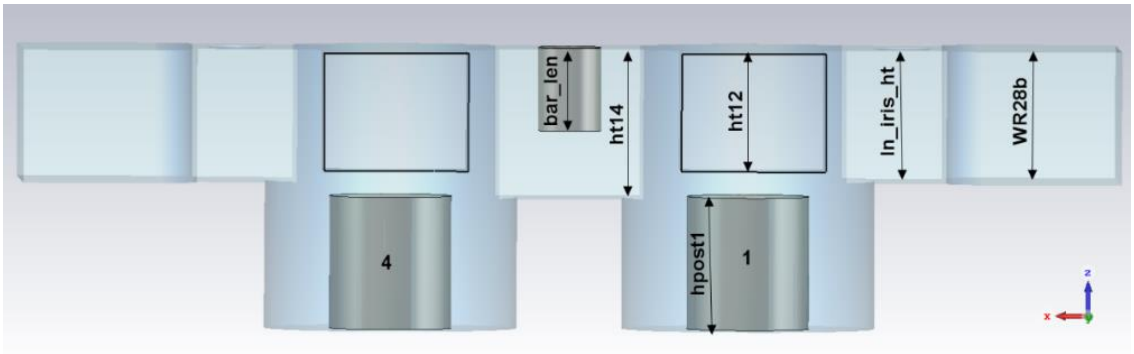
bar_len
ht14
ht12
In_iris_ht
WR28b
4
hpost1
1

(c)

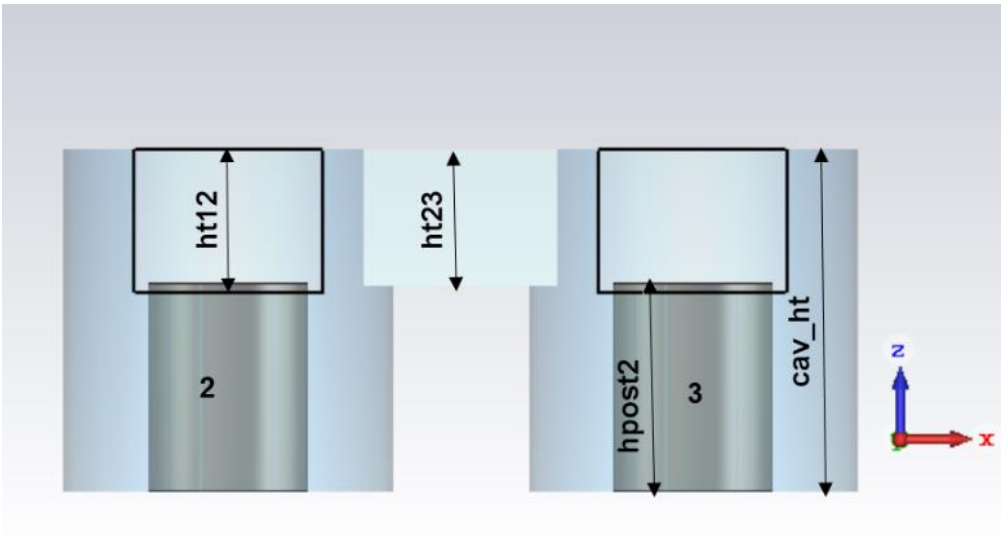

(d)

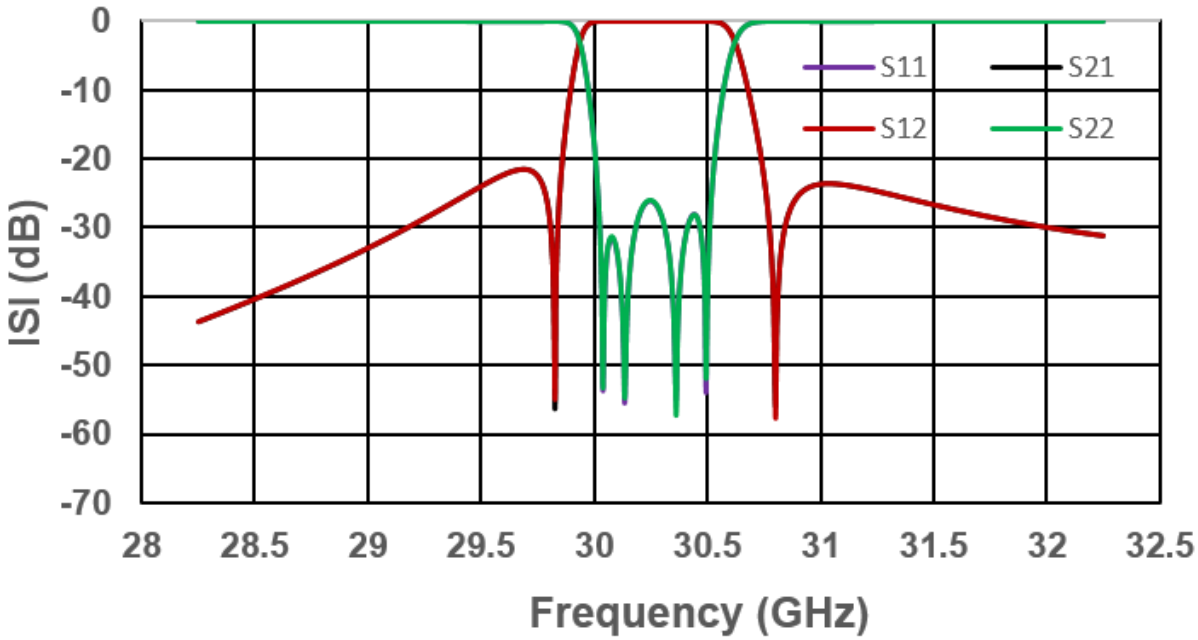

(e)

Figure 5.9 *(a) 3D EM CAD model of4-2-0 coaxial resonator filter, (b) Top view of 4-2-0 coaxial resonator filter, (c) Sectional view shows resonator1 and 4, (d) Sectional view shows resonator2 and 3, and (e) Simulated response of 4-2-0 coaxial resonator filter.*

Table 5.3 Design parameters and their values for 4-2-0 coaxial resonator filter

Design Parameters	Value (mm)	Design Parameters	Value (mm)
hpost1	3.53	input_wd	4.72
hpost2	4.555	wd12	4.14
cav_dia	7.25	wd23	4.1
cav_ht	7.5	wd34	4.14
iris_t	3	wd14	3.9
post_dia	3.5	ht12 and ht34	3.15
wr28a	7.1	ht23	3
wr28b	3.55	ht14	4
d	1.8	bar_len	2.22

The filter fabricated using Invar, and its fabricated hardware and its measured response show in figure 5.10. The measured response shows that the transmission zero on the higher side of the passband is not prominent. The reason is the gap between the self-locking tuning element and the tapped-hole results in improper grounding, which affects the transmission zero shape.

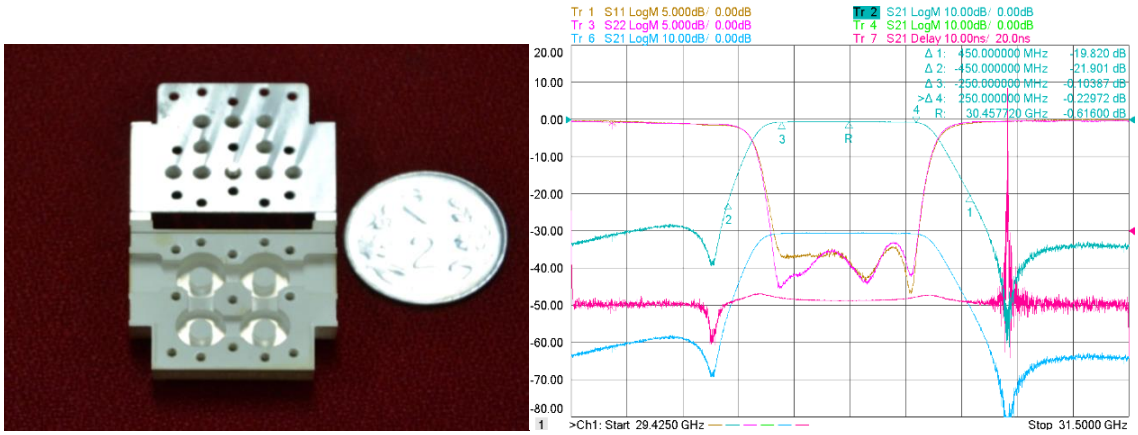

Figure 5.10 *Fabricated 4-2-0 filter and its measured response.*

Initially, it has assumed that the Invar metal is difficult to machine. So, there is a gap between the tuning element and the tapped-hole. Due to this reason, the same filter has fabricated in Aluminium metal, which is

easy and precise to the machine. Figure 5.11 shows the fabricated filter.

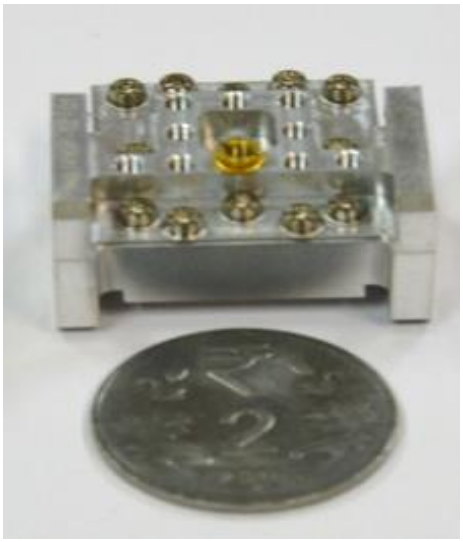

Figure 5.11 *Fabricated 4-2-0 filter in Aluminium metal.*

However, in both cases, there is no change in the response. Hence, the type of tuning element type change from self-locking tuning element to M2 gold plated screw with hexagonal locking nut is used. The two different filters: Direct-coupled seven-pole Chebyshev filter and five-pole cross-coupled filter designed and fabricated to validate the concept of higher-order mode of the coaxial resonator for filtering application.

5.4.2. Direct Coupled 7-pole Chebyshev filter

The 7-pole filter synthesized for the specifications of Table 5.1. The return loss keeps at 26 dB corresponds to a passband ripple of 0.01dB. The synthesized coupling values for input and output coupling (J_{01} and J_{78}) is 1.202, between resonator 1 and resonator 2 (J_{12} and J_{67}) is 0.9493, between resonator 2 and 3 (J_{23} and J_{56}) is 0.6410 and between resonator 3 and 4 (J_{34} and J_{45}) is 0.5918. The filter is inline and symmetric, so the

rest of the inter-resonator coupling is the mirror image of the coupling between resonators 1 to 4. The top and cut-sectional view, along with the design parameters shown in figure 5.12(a) and (b). The resonators are numbered from 1 to 7 in figure 5.12(a). The values for the design parameters of figure 5.12 are listed in Table 5.5. The iris width of all the inter-resonator and input and output irises shown in figure 5.12(a). The EM simulation has done using these coupling values. Figure 5.12(c) shows the filter fabricated from Aluminium and silverplated to minimize loss. The value of design parameters of figure 5.12 are listed in Table 5.4. The simulated and the measured narrow response of the filter shown in figure 5.13 (a) and the measured wideband response in figure 5.13(b). The plot shows group delay on the primary axis with an orange colour trace. The S-parameters shown in the secondary y-axis. The measured return loss is better than 20dB, and the insertion loss is 0.77dB, which is 0.27dB more than the desired specification of Table 5.1. This more insertion loss is attributed to the lack of perfect contact between the top and the bottom filter boxes and self-locking threaded screws for iris tuning.

Table 5.4 Design parameters and their values for 7-pole Chebyshev coaxial resonator filter

Design Parameters	Value (mm)	Design Parameters	Value (mm)
l1	4.103	wd_in	4.88
l2	4.955	wd_12	4.06
l3	5.083	wd_23	3.73
l4	5.103	wd_34	3.66
t	2	d1 and d2	3.5 and 7.1

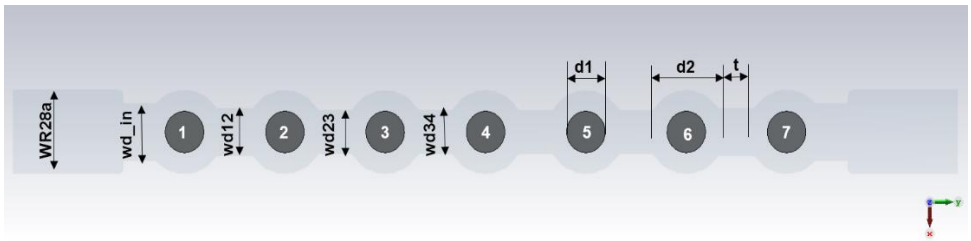

(a)

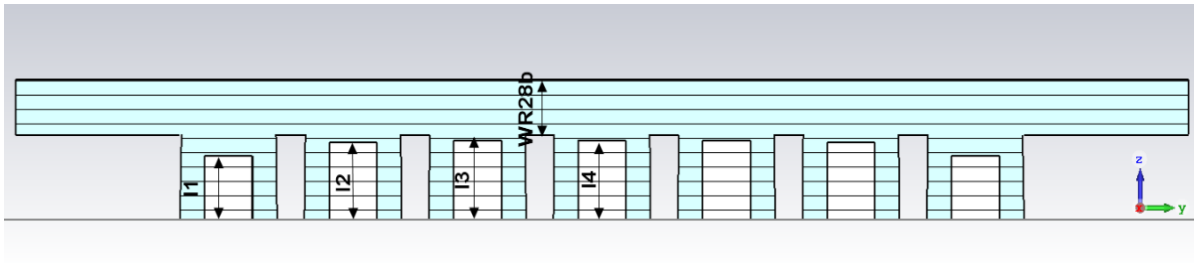

(b)

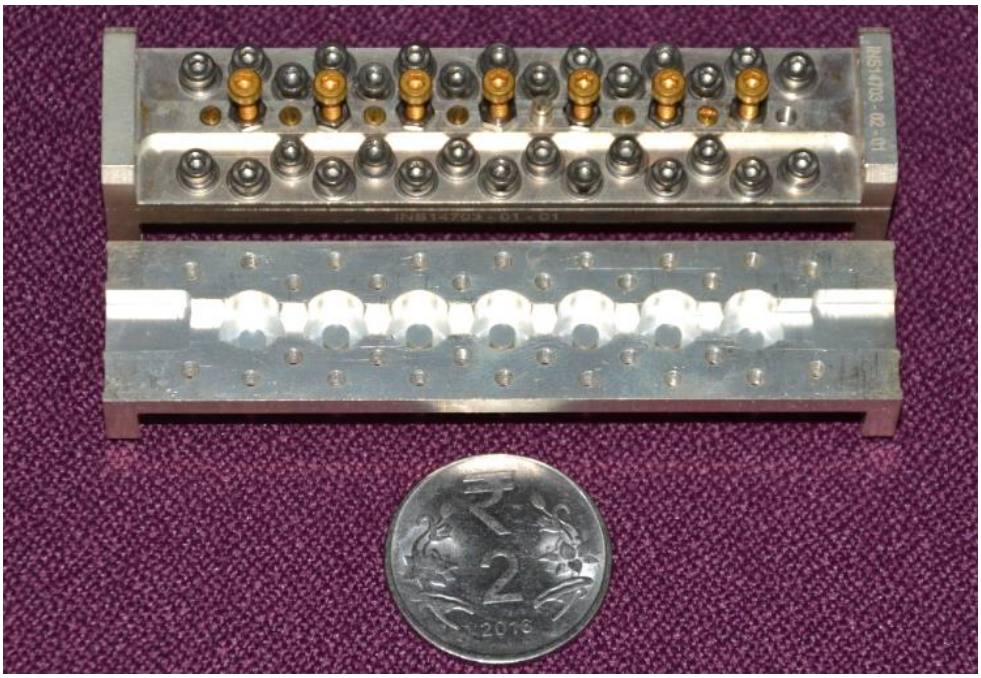

(c)

Figure 5.12 *7-Pole Chebyshev TM_{012} mode coaxial resonator filter, (a) Top view, (b) Cut-sectional view, and (c) Fabricated filter.*

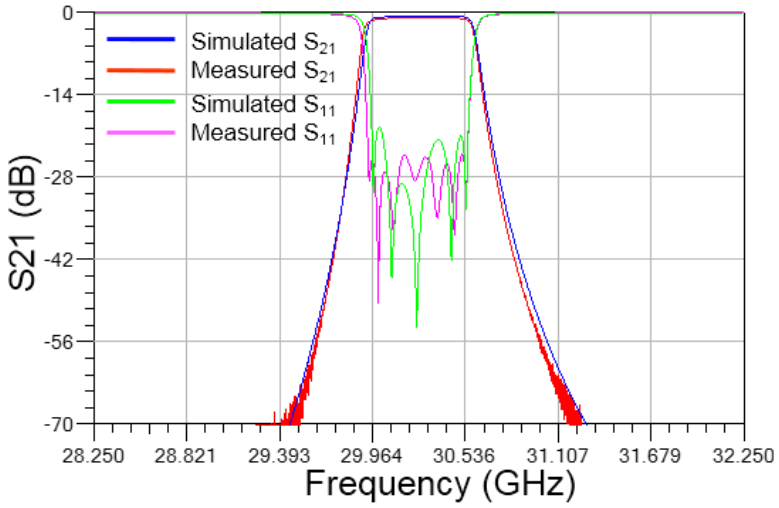

(a)

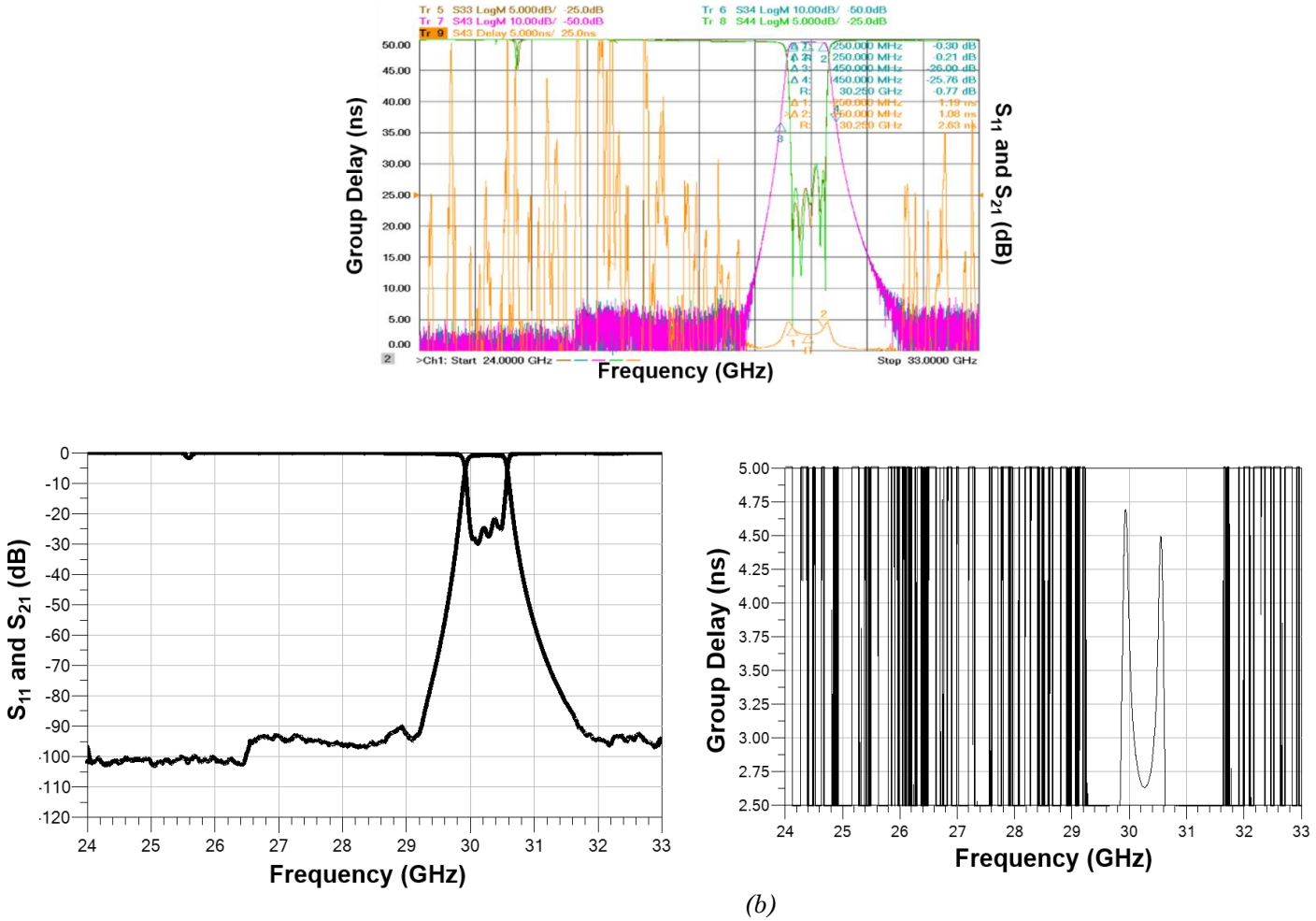

(b)

Figure 5.13 *Simulated and measured response of 7-Pole Chebyshev TM_{012} mode coaxial resonator filter (a) Simulated and measured narrowband response, (b) Measured wideband response: S-parameters and Group delay.*

The specified value of relative group delay is 5 ns while the measured relative group delay over the band is 1.2 ns. The filter is designed to be used as a Pre-select filter and the minimum value of group delay and insertion loss provide extra margin to the system.

5.4.3. 5-2-0 Filter

The filter synthesized for the specifications given in Table 5.1. In synthesis, the order is 5 with two transmission zeros placed at ± 1.45i for near band rejection. The 26 dB return loss chosen for filter synthesis. The synthesized coupling matrix for 5-2-0 filter given in Table 5.5.

Table 5.5 Synthesize coupling matrix for 5-2-0 filter

	S	1	2	3	4	5	L
S	0	1.1226	0	0	0	0	0
1	1.1226	0	0.9029	0	-0.3270	0	0
2	0	0.9029	0	0.8427	0	0	0
3	0	0	0.8427	0	0.5949	0	0
4	0	-0.3270	0	0.5949	0	0.9603	0
5	0	0	0	0	0.9603	0	1.1226
L	0	0	0	0	0	1.1226	0

The layout of the filter given in figure 5.14 where the resonators coupled to each other through irises and the cross-coupling realized with a non-resonating post. The two resonator model separated by iris is used to generate the design chart for the coupling values. The generated design chart map these coupling values into the physical realizable dimensions.

Figure 5.15 shows the variation of iris height with the coupling bandwidth and the variation of the resonant frequency of spurious TE_{112} mode. The increase in the height of iris will result in a decrease of spurious-free range. The variation of coupling bandwidth and TE_{112} spurious mode variation due to variation of iris width shown in figure 5.16.

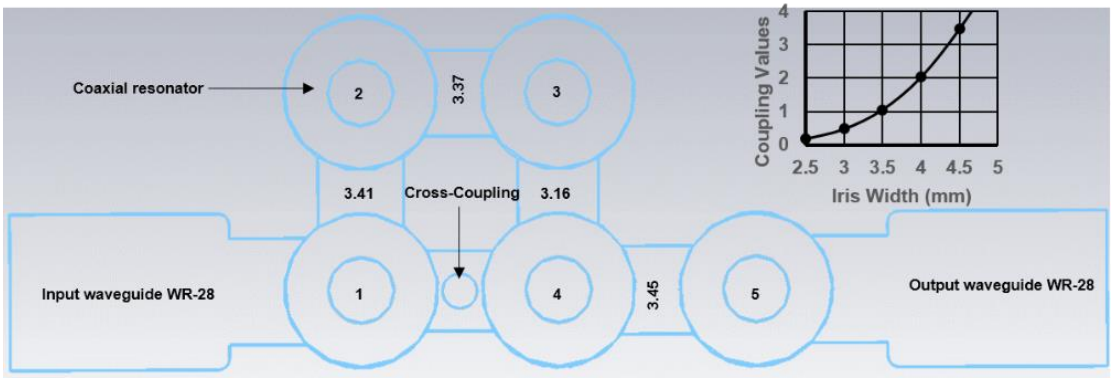

Figure 5.14 *Layout of 5-2-0 filter.*

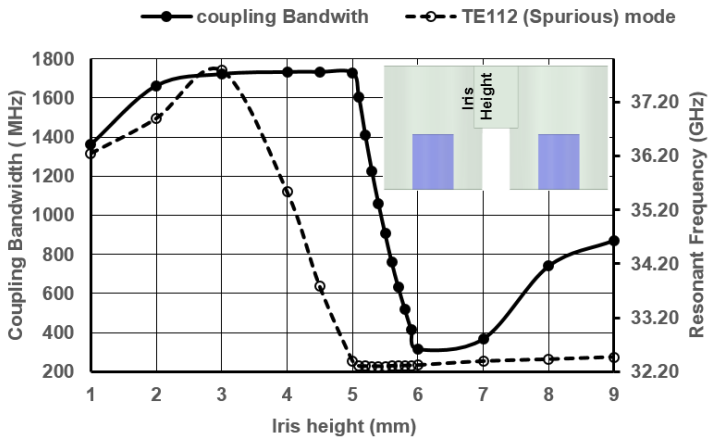

Figure 5.15 *Variation of coupling bandwidth and TE_{112} (spurious) mode resonance frequency with variation in iris height.*

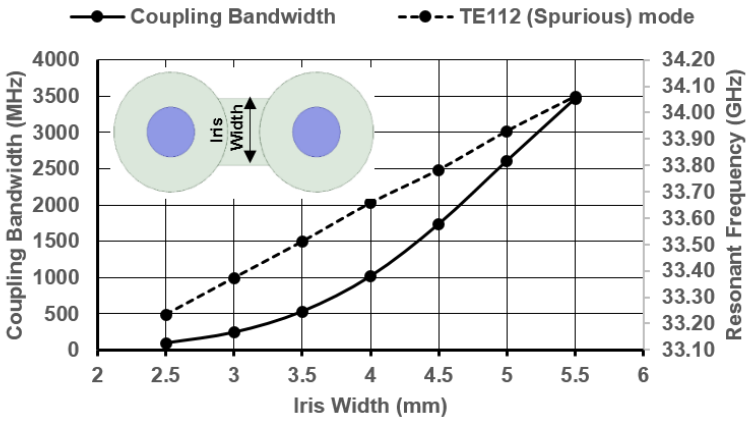

Figure 5.16 *Variation of coupling bandwidth and TE_{112} (spurious) mode resonance frequency with variation in iris width.*

It concludes from figure that the spurious mode is largely affected by iris height variation rather than its width. Moreover, their coupling bandwidth first increase reaches to maximum, then decreases to a minimum, and start increase after that point. This trend is the same, as that observed in the case of TEM mode coaxial resonator. So, it is better to vary iris width to achieve coupling for a fixed iris height. The variation of cross-coupling bandwidth with variation in the length of the non-resonating post shown in figure 5.17.

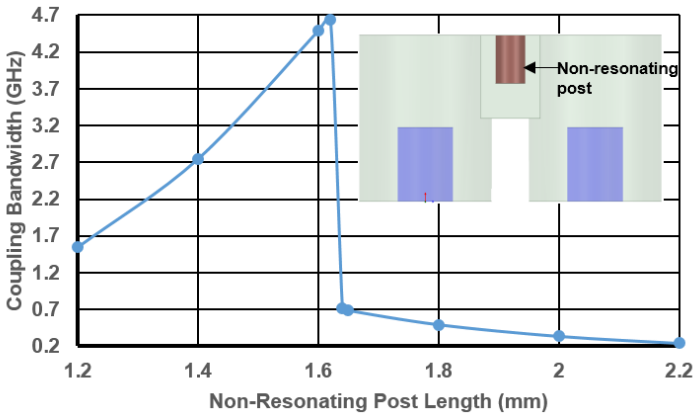

Figure 5.17 *Variation of coupling bandwidth with variation in the length of non-resonating post.*

The coupling first increases and start decreasing after the inflection point. This point distinguishes the nature of cross-coupling, which is positive before the inflection point and becomes negative beyond that point.

Figure 5.18 gives the calculated reflection group delay values for the coupling values of Table 5.3 and is calculated by Either [131] or using circuit simulator The resonator and irises dimensions are varied to match these reflection group delay values. The resonator whose reflection group delay value calculated is activated, and rests are deactivated. This process repeats until all the reflection group delay values match the above-calculated values along with their respective reflection phase. The cross-coupling value has determined from transmission S-parameter response by activating resonators 1, 2 and 5 and deactivating the rest of the resonators. The transmission S-parameter S_{21} matched for the above-calculated value from the circuit simulator. The EM simulation is done using the dimension obtained from the reflection group delay values and optimized for the required

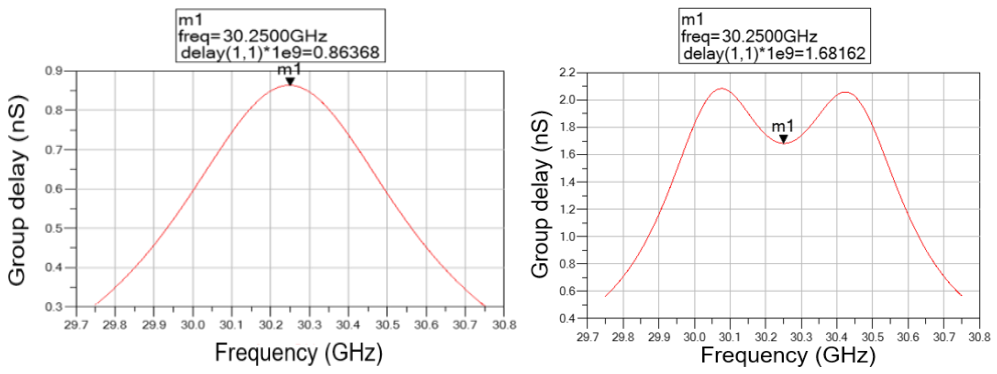

(a) *(b)*

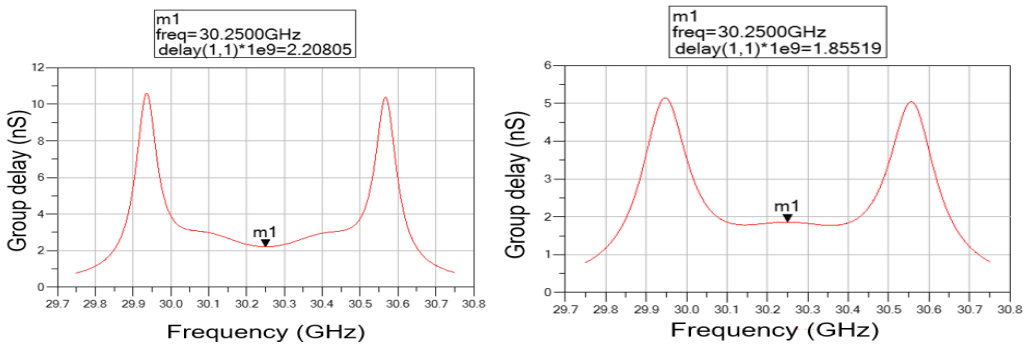

(c) *(d)*

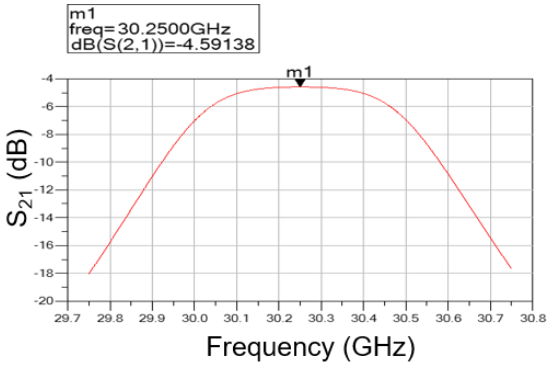

(e)

Figure 5.18 *(a) Reflection group delay for input resonator, (b) Reflection group delay for input and 2nd resonator, (c) Reflection group delay for input, 2nd and 3rd resonator, (d) Reflection group delay for input, 2nd, 3rd and 4th resonator, and (e) Cross-coupling estimation by transmission measurement.*

response using parametric optimization of the filter dimensions [132]. Figure 5.19 (a)and (b) shows top view and sectional view, respectively along with the design parameters. Figure 5.19(c) shows the fabricated hardware of TM_{012} mode 5-2-0 coaxial resonator filter. The value for design parameters of figure 5.19 are listed in Table 5.6. The EM simulated response and the measured wideband response of the filter shown in figure 5.20.

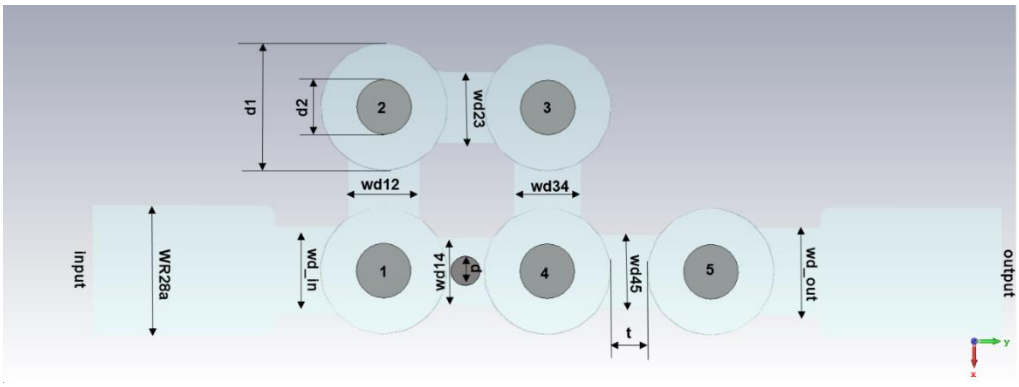

(a)

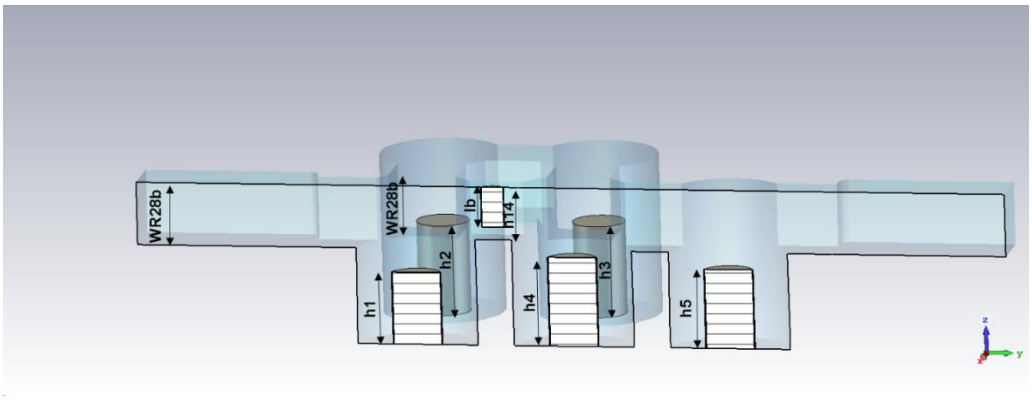

(b)

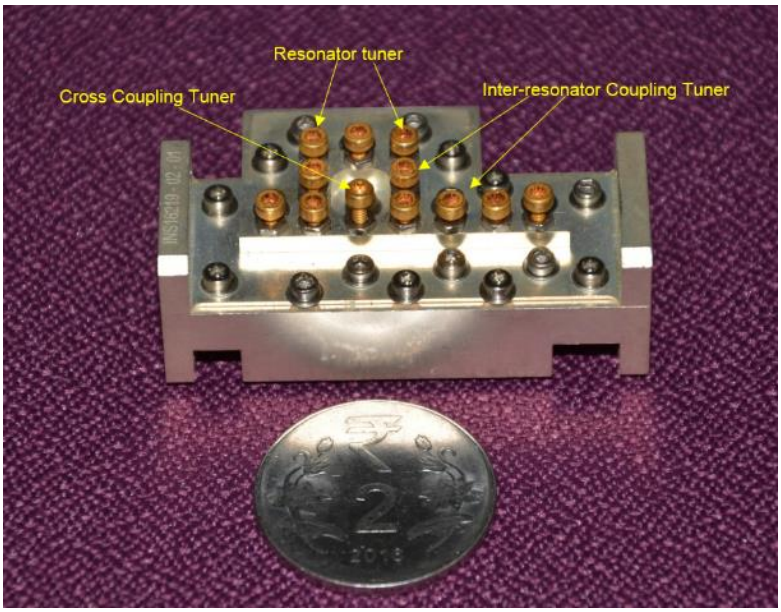

(c)

Figure 5.19 *TM_{012} mode 5-2-0 coaxial resonator filters, (a) Top view, (b) Sectional view, and (c) Fabricated filter.*

Table 5.6 Design parameters and their values for 5-2-0 coaxial resonator filter

Design Parameters	Value (mm)	Design Parameters	Value (mm)
h1	4.1	d	4.72
h2	5.105	wd12	3.9
h3	5.175	wd23	3.915
h4	5.06	wd34	3.655
h5	4.495	wd45	4.015
lb	2.28	wd14	3.65
h14	3	wd_in	4.84
wr28b	3.55	wd_out	4.875
wr28a	7.1	d1 and d2	3 and 7
cav_ht	9	t	2

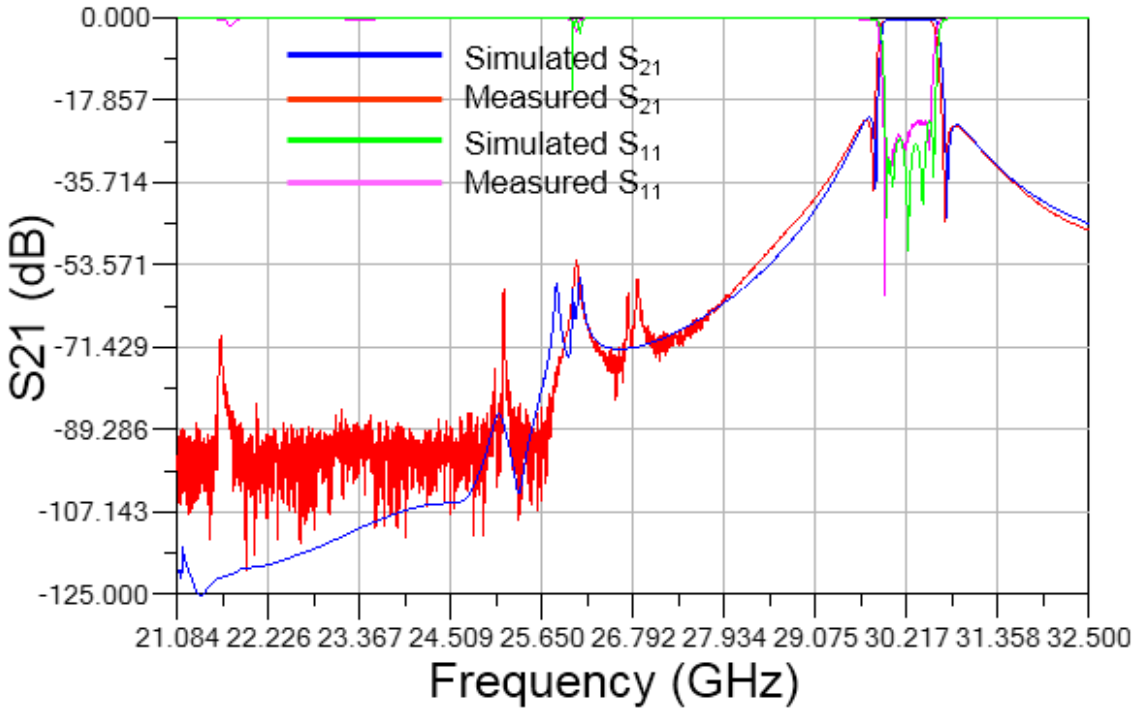

Figure 5.20 *Simulated and measured response of 5-2-0 coaxial resonator filter.*

5.5. Compact waveguide filter

The rectangular waveguide dominant TE_{101} mode resonator has a high-quality factor, very wide spurious free range and predictable thermal performance preferred for the realization of low loss cross-coupled filters at millimeter wave band. Moreover, the waveguide filters have ease of fabrication and very good integration with other subsystems in the transponder chain.

The cross-couplings are either positive or negative in nature and generated by destructive interference between the direct mainline path and the cross-coupled non-adjacent resonator path [133]. The various approaches shown till now in the folded waveguide filters to realize the cross-coupling [134]-[137]. The circular aperture is made in the H-plane of the folded waveguide resonator to generate the cross-coupling [134], but there is difficulty to tune the cross-coupling, and it is sensitive to fabrication tolerance which matters a lot at the millimeter wave band. The other popular approach is to use an overmoded cavity to generate transmission zeros [135, 136]. The advantage of this approach is that the filter can handle very high power, but large size overmoded cavity increases the size of the filter and is suitable for narrowband cases. The use of a combination of TM_{110} mode with non-resonating TE_{10} mode [136, 137] to realize cross-coupling which make filter compact, but at the expense of poor isolation in the lower stopband. This approach is good for realizing input filter but not suitable to realize Pre-select filters which require very high isolation at the transmit band. In ultra-compact cross-coupled waveguide filter, a metal strip is inserted in E-Plane of waveguide [138] to generate transmission zeros.

This approach is sensitive to fabrication tolerance as the strip is thin and its dimensions fixed. Moreover, there is a large imbalance between the side lobes, which make response asymmetric. The other methods are to use a combination of inductive and capacitive irises [139, 140]. The capacitive irises increase the overall filter size and are better suited for very wideband filter due to the aperture of capacitive iris. In this report, the filter is designed using TE_{101} mode waveguide resonator, and the non-resonating post is used to realize cross-coupling [130]. The length of the post governs the nature of coupling. This post is tunable, which relaxes fabrication tolerances and use of post doesn't add any additional cavity to the filter and hence makes the filter compact. Moreover, this filter can handle moderate power due to the concentration of electric field in the gap between non-resonating post and iris.

5.5.1. Filter Design

The filter has designed for the specifications given in Table 5.1. The synthesized coupling matrix has shown in Table 5.5, where negative cross-coupling is between resonator 1 and 4. It found that the resonator Q-factor of 2800 is sufficient to meet all the specifications. The TE_{101} mode WR-28 rectangular waveguide resonators used for the filter realization. The simulated Q of the resonator is 4800 considering silver boundary conditions.

The inter-resonator coupling is realized using inductive irises and the variation in the coupling value due to variation in the coupling iris for

fixed iris depth of 3.5 mm shown in figure 5.21. The inter-resonator coupling increases as the iris width aperture between the cavities increases.

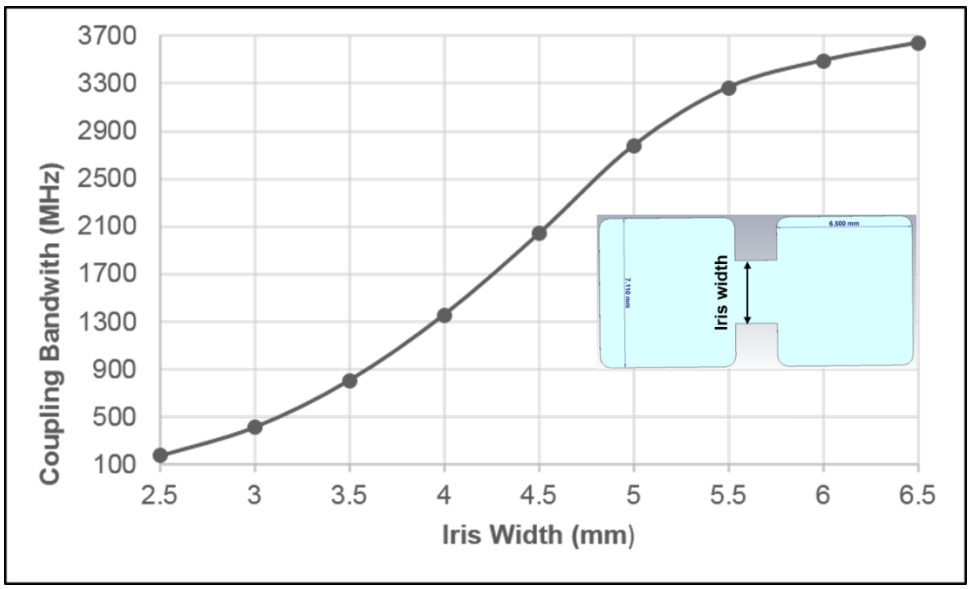

Figure 5.21 *Variation of coupling bandwidth with variation in iris width aperture.*

The non-resonant post depth variation for fixed iris width aperture of 4 mm and iris depth of 3 mm shown in figure 5.22. The coupling increases as the penetration of post increases to a maximum value and then it starts decreases drastically after the point of inflexion, which distinguishes the nature of coupling as this post, can realize both positive and negative coupling. The inflexion point is at 2.16 mm, as shown in figure 5.22 and after inflexion point the post realizes negative coupling. The post is placed normal to the magnetic field plane for realizing cross-coupling. This behaviour of cross-coupling in TE_{101} waveguide resonator is the same as that in TM_{012} mode coaxial

resonator because the orientation of the magnetic field is in the same plane for these resonators. The EM simulation has done for 5-2-0 waveguide filter. The filter is fabricated with the Aluminium metal and is silver plated to minimize loss. The filter is tuned using M2 stainless steel screws with hexagonal locking nut. Figure 5.23 shows the fabricated filter. Its simulated and measured response shown in figure 5.24. The simulated and measured response is in close agreement. The measured insertion loss is 0.45 dB, which is high for the Q more than 2800. The unplated screw used for tuning contributed to this, and their penetration is more, which further increases insertion loss and affect bandpass flatness. The measured results tabulated in Table 5.1.

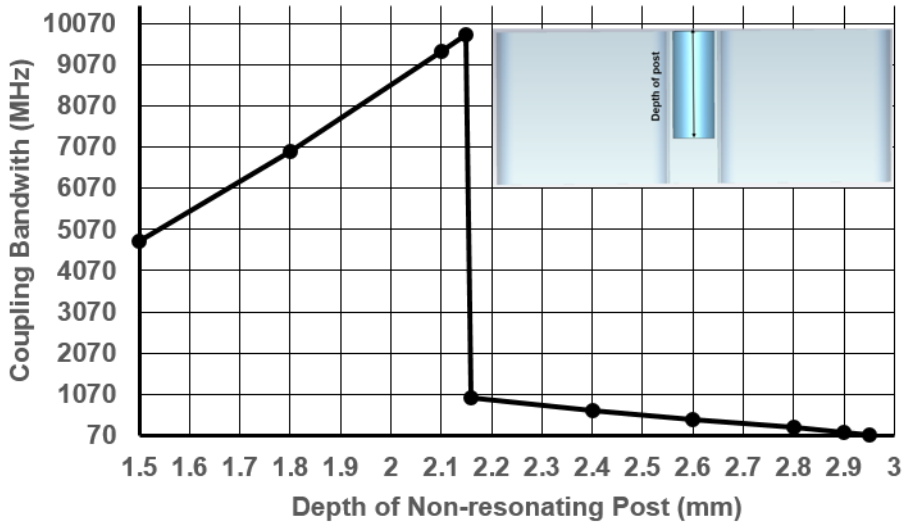

Figure 5.22 *Variation of coupling bandwidth with variation in iris width aperture.*

The measured wideband response of the filter shown figure 5.24(b) and there is no spurious observed in the far band rejection. (stopband)

contrary to the TM_{012} mode coaxial resonator filter where the signature of TE_{111} mode observed in the far stopband. It is due to the dominant TE_{101} mode of the rectangular waveguide resonator used in the design. However, the far band rejection on upper side of passband degrades due to presence of higher order modes of waveguide.

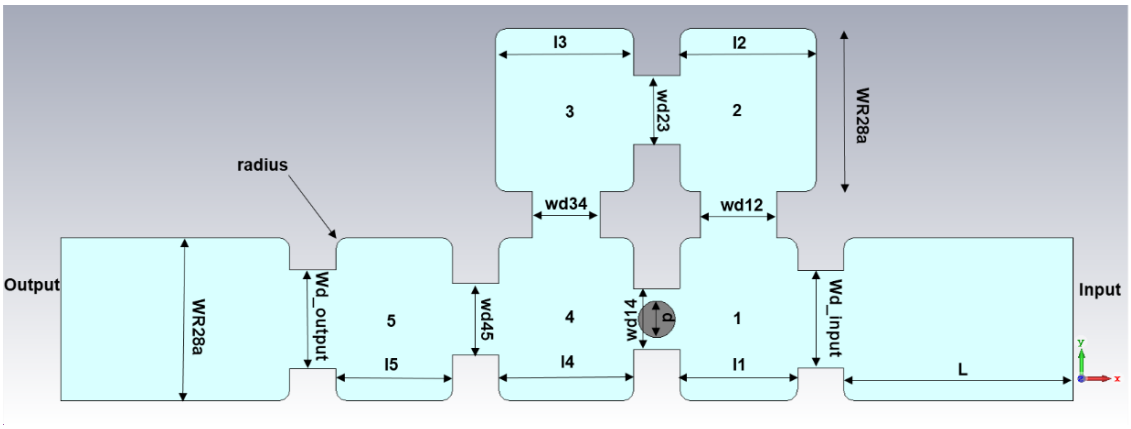

(a)

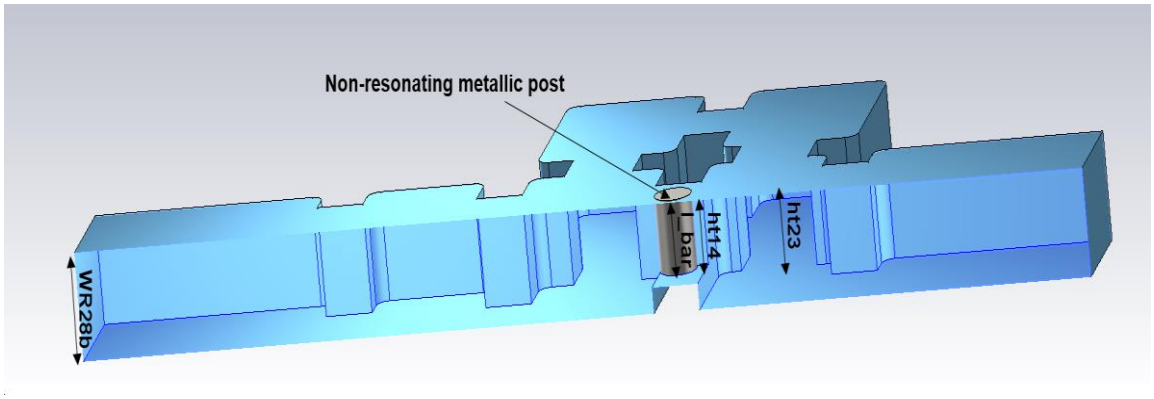

(b)

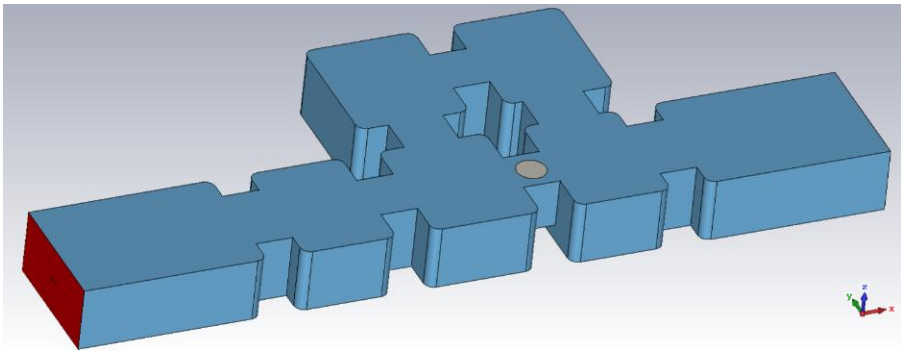

(c)

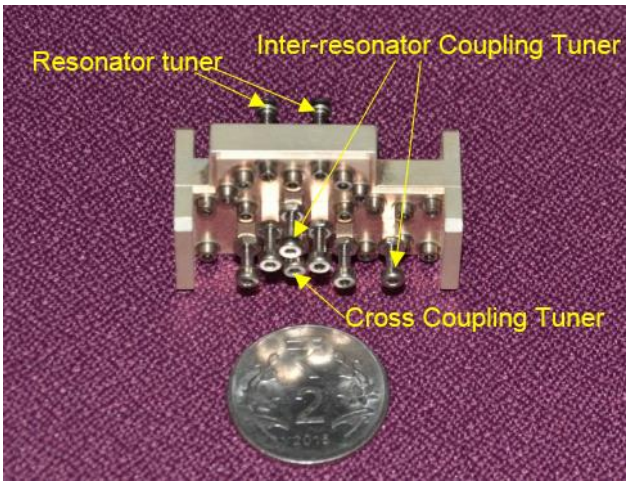

(d)

Figure 5.23 (a) Top *view of 5-2-0 waveguide filter, (b) Sectional View of 5-2-0 waveguide filter, (c) 3D EM CAD model of 5-2-0 waveguide filter, and (d) Fabricated 5-2-0 waveguide filter.*

Table 5.7 Design parameters and their values for 5-2-0 waveguide filter

Design Parameters	Value (mm)	Design Parameters	Value (mm)
L	10.0	wd_input	4.27
L1	5.095	wd12	3.095
L2	5.89	wd23	2.975
L3	6.04	wd34	2.978
L4	5.952	wd45	3.31
L5	5.136	wd14	2.65
wr28a	7.1	wd_output	4.29
wr28b and ht23	3.55	ht14	2.7
d	1.6	l_bar	2.45

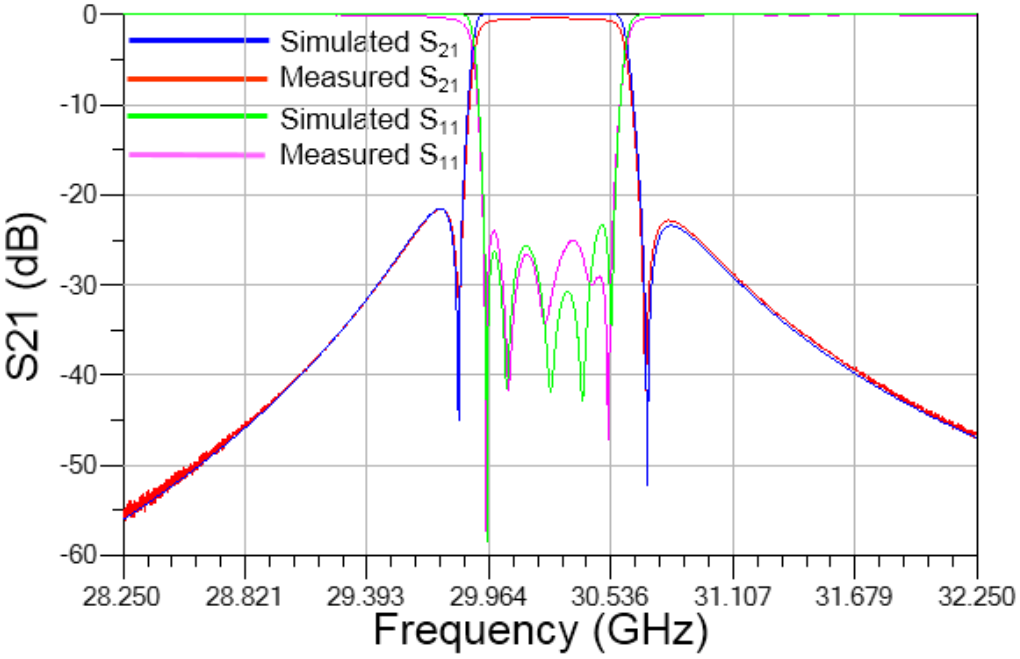

(a)

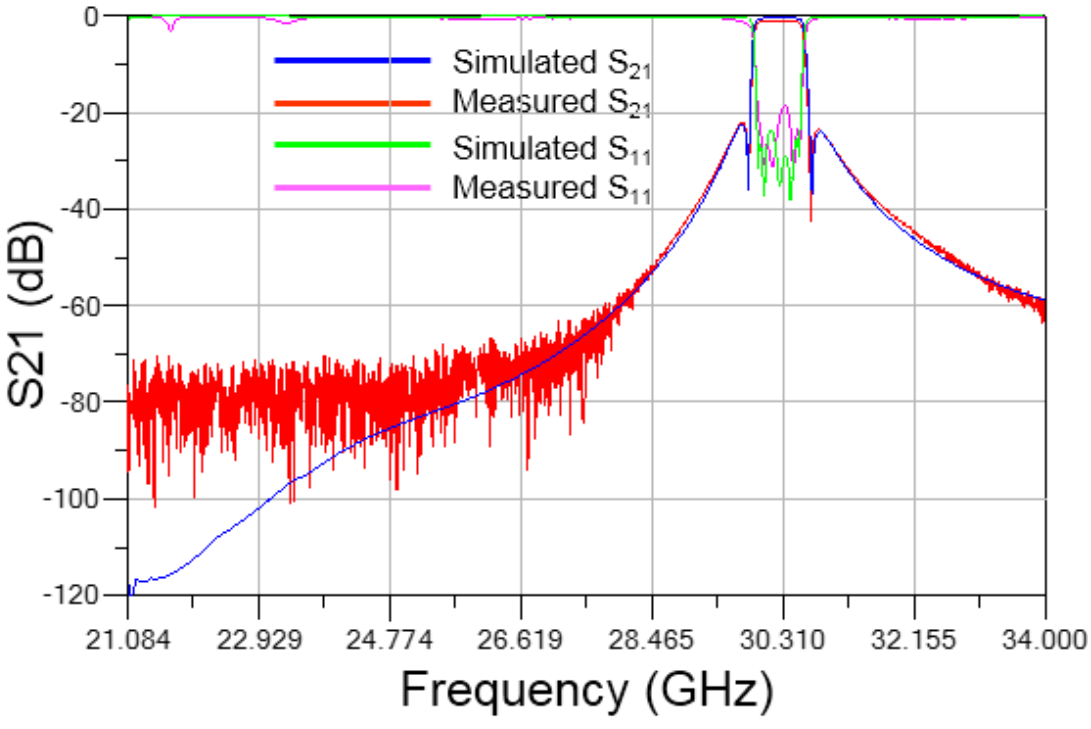

(b)

Figure 5.24 *Simulated and measured response of 5-2-0 waveguide filter, (a) Narrowband, and (b) Wideband.*

5.6. High Power Analysis

The modern satellite uses high-transmitted power to boost their capabilities and meets the growing demands of the users. They employ high-performance microwave filters, which subjected to high RF power. These filters should have a smaller footprint and mass, which pose difficulty in design high power filters due to the confinement of high power in a small volume. The various high power phenomena must consider while designing a filter for high power operations. These phenomena are a multipaction breakdown, ionization breakdown, and passive intermodulation (PIM) interference. All of these phenomena severely degrade the RF performance of the component [119, 142].

1. Multipaction is a high power RF vacuum breakdown phenomenon where there is a resonant growth of free electron space charge due to secondary electron emission [141, 142]. It takes place under vacuum conditions when the mean free path of the electrons is larger than the gap between the walls guiding the flow of the RF power. The primary electrons accelerated by the RF fields impact a surface and release a larger number of secondary electrons, which again accelerated by the RF fields and impacts again, releasing even more electrons results in an avalanche.

    a) Vacuum condition

    b) Applied RF voltage

    c) Frequency of operation in conjunction with geometry of RF components (f x d product)

d) Surface conditions

2. Ionization breakdown is a gas breakdown phenomenon, which occurs when high power RF flows under high pressure in the device. The low-intensity electrons density increases in an avalanche-like manner result in gas ionization forming conducting plasma. The ground-based and some space-bound components are more prone to ionization breakdown as these are tested on the ground at full power at ambient and under vacuum condition. Both the multipaction and ionization breakdown are different types of high power RF failure mode.

3. PIM is largely a workmanship-related issue, and it cannot be predicted accurately for high power microwave filters. The PIM can be improved by design and take care of materials types during fabrication. The ionization breakdown and PIM are beyond the scope of the work [119, 142].

5.6.1. Multipaction Analysis

The high power handling capability of filters is established by the multipaction margin, which is usually 6 dB for the filters used in space applications. The design analysis for multipaction involved [143]:

1) Field Analysis: The analysis of the electric field within the whole filter is performed either by commercially available software or by using the custom-made code.

2) Secondary Emission Yield data (SEY): When an electron of sufficient energy impacts on the surface of a material (primary electron) it can produce the emission of more electrons; this physical process is called secondary electron emission (SEE). The secondary electron emission coefficient or yield (SEY) of a material surface, usually symbolized as σ, is the ratio of the number of emitted electrons to the number of incident electrons of defined incident energy and angle, in field-free conditions and under vacuum conditions. SEE is the material dependent property, which depends on the material type, surface finish, coating or treatment on the material which determine multipaction threshold.

3) Critical regions identification: These regions are either stand-alone or a combination of high voltage region, critical gaps, frequency and secondary emission properties of the material.

5.6.2. Multipaction Margin

The multipaction margin is calculated and validated by design or by the multipaction test set up [143]. The design margin provides good accuracy when there is a limitation of the test setup. The steps to calculate multipaction margin are:

Step1: Critical region identification where the critical gaps in the design identified by field analysis. These are the locations where electric field intensity is maximum. These may or may not be the minimum gap.

Step2: Calculate the threshold voltage (V_{th}) with available Voltage breakdown curves [144] - [146]. The threshold voltage for silver plated parallel plate geometry is given by [144, 147]

$$V_{th} = 63 * f * d \tag{5.3}$$

where, f is the frequency in GHz and d is the critical gap in mm.

Step3: Calculate normalized voltage (V_n). Evaluate the line integral of electric field in the commercial EM solvers for 1W power and is scaled for operating power. The operating power corresponds to voltage (V).

$$V_n = \oint E.dl \tag{5.4}$$

where E is the electric field in V/m.

Step4: The multipaction margin 'M' in dB is given by

$$M = 20 * \log\left(V/V_{th}\right) \tag{5.5}$$

The other method is to use the commercially available tools like SPARK 3D ®, PIC solver or custom made codes.

The high power analysis is carried out with the SPARK 3D ® [147] for the 5-2-0 coaxial resonator and 5-2-0 waveguide filter and observed that the peak power handling capacity of the proposed coaxial resonator filter is 45.525 kW as compared to the waveguide filter which is 11.75 kW only shown in figure 5.25, and figure 5.26 respectively.

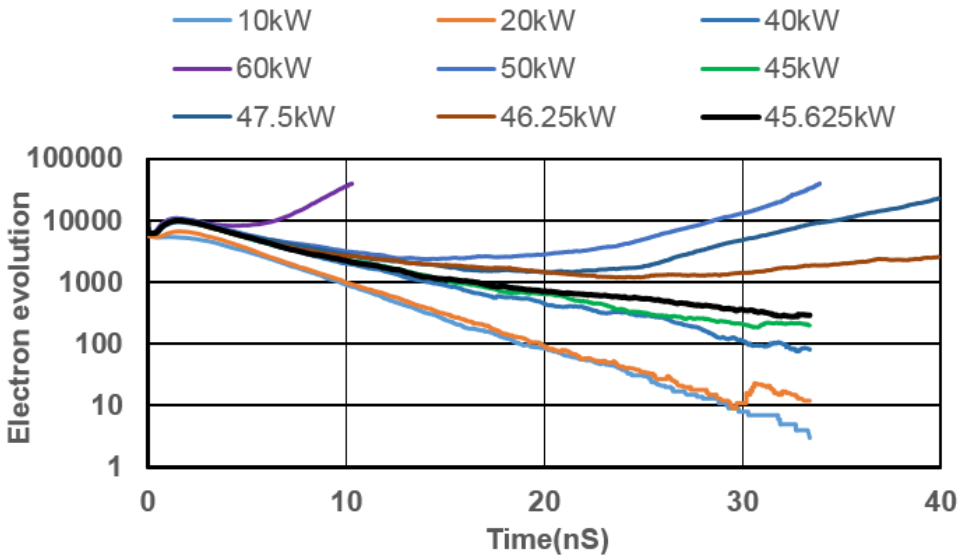

Figure 5.25 *Multipaction analysis of the proposed 5-2-0 coaxial resonator filter.*

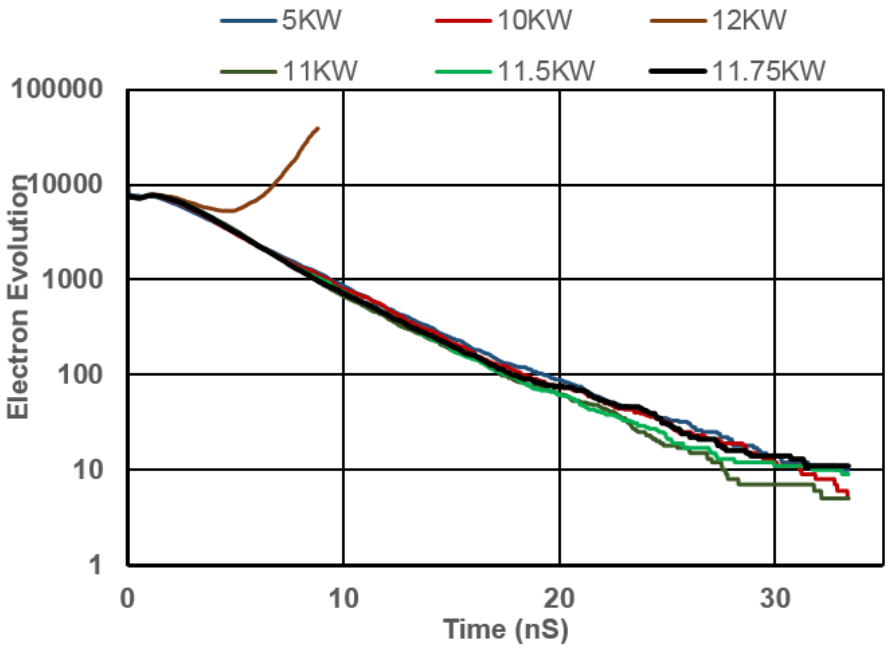

Figure 5.26 *Multipaction analysis of the 5-2-0 waveguide filter.*

The critical gap between the coaxial resonator post and the top cover is close to the parallel plate geometry, and the multipaction margin has calculated for the same. The critical gap is 3.825 mm, and the calculated threshold voltage is 7289 V using (5.3). The normalized voltage 143.02 V,

which is 15000.8 V for 11.38 kW power. Hence, the calculated multipaction margin 6.26 dB corresponds to 45.525 kW threshold power, which validates the result of SPARK 3D ® with the design margin. The gap between the non-resonant post and iris between resonator-1 and 4 is minimum for both the filters. In the case of the proposed filter, critical gap is between the coaxial resonator post-2, 3 and its top cover. This gap is fifteen times more than the minimum. However, in the case of the waveguide filter, the minimum and critical gap are the same. So, the proposed filter power handling capability is four times more than the waveguide filter. Moreover, the non-resonating post used for cross-coupling realization limits the power handling capability of the waveguide filter. The waveguide filter realized by this approach can handle moderate power. The average power handling of the waveguide filter is 6 dB below the multipaction threshold. So, the proposed filter and the waveguide filter can handle 11.38 kW and 2.93 kW average power.

5.7. Performance Comparison

The 5-2-0 TE_{101} mode waveguide filter and 5-2-0 TM_{012} mode coaxial resonator filter tests over the temperature range of -20^0C to 65^0C with 2 hours stabilization at each extreme. The coaxial to WR-28 waveguide adapters used for thermal cycling and the cycling done in the thermal cycling chamber. The 2.92 mm coaxial calibration is done at DUT end using electronic calibration kit, and the filter is connected to the VNA cables using coaxial to WR-28 waveguide adapters. The identical set up used for both the filters. Both the filters

fabricated with the Aluminium metal having 24 ppm/^{0}C as the coefficient of thermal expansion. The frequency drift of the filter calculated by an approximate relation given by

$$\delta f = \alpha \times f_0 \times \delta T \tag{5.6}$$

where, δf is the frequency drift over the temperature, f_0 is the center frequency, δT is the temperature gradient in ^{0}C, and α is the coefficient of thermal expansion for the metal in ppm/^{0}C. The calculated one side frequency drift is 29.04 MHz for the filter operating in the temperature range of 25^{0}C to 65^{0}C.

The measured wideband response of both the filter at ambient shown in figure 5.27. It has found that the coaxial resonator filter has better far band rejection on the lower side of passband as compared to the identical configuration waveguide filter.

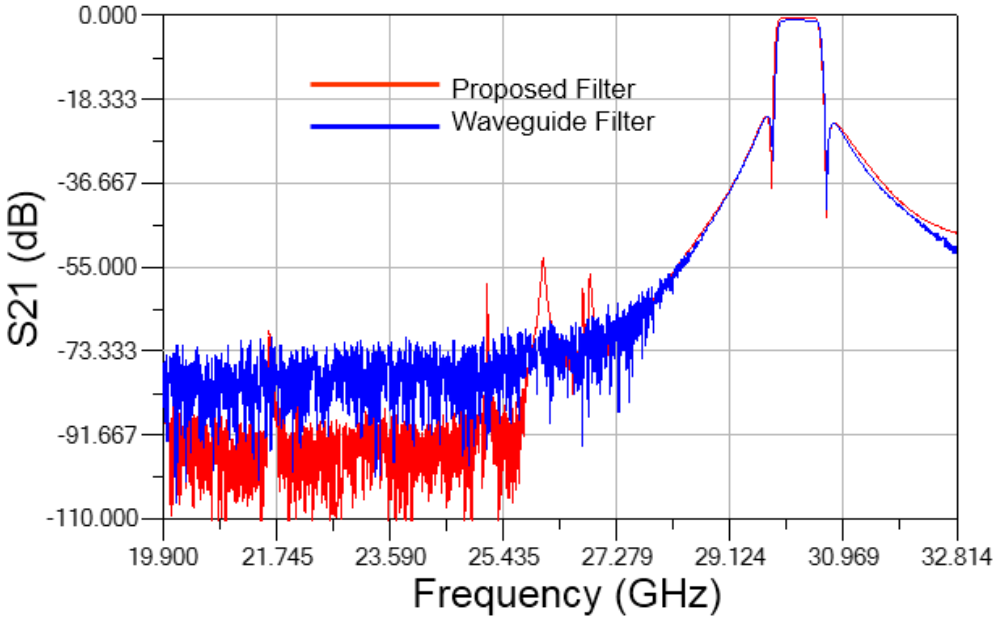

Figure 5.27 *Wideband performance of the proposed coaxial resonator filter and the waveguide filter.*

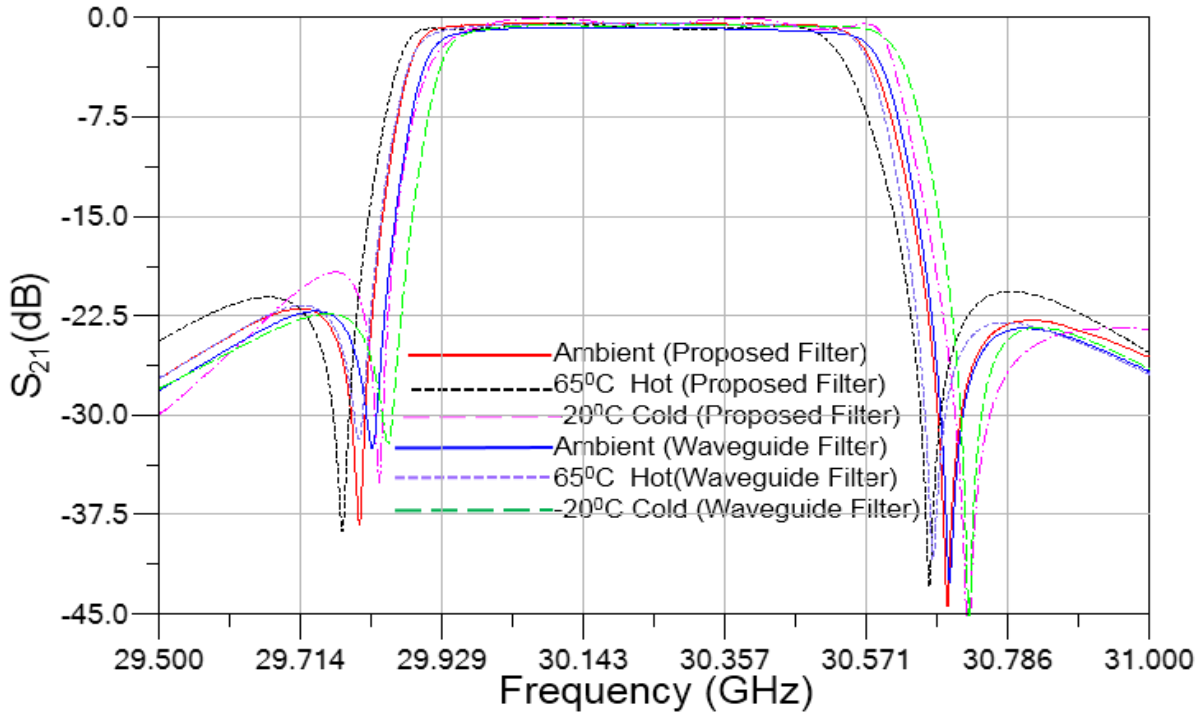

Figure 5.28 *Thermal performance of the proposed 5-2-0 coaxial resonator filter and 5-2-0 waveguide filter.*

These filters have a stable thermal performance, which meets all specification, but the frequency drift of the proposed filter is less than the waveguide filter. Hence, it offers better design margin than the waveguide filter. The measured response of both the filters over the temperature shown in the figure 5.28. The coaxial resonator based filter and waveguide filter shows the same trend during thermal cycling. The response shifts lower in hot (shown as small dotted line) and higher in cold (shown as large dotted line) compared to response at ambient (shown as a solid line), but shift the coaxial resonator based filter is less as compared to the waveguide filter. The performance comparison of both the filters has tabulated in Table 5.8. The comparison of both the fabricated filters shown in figure 5.29.

Table 5.8 Performance comparison of proposed filter, waveguide filter and state of art (SuperQ) filter

Specification	Values	Proposed Coaxial Filter	Waveguide Filter	State of art (Super Q filter)
Center Frequency (CF)	30.25 GHz	30.25 GHz	30.25 GHz	20.0 GHz
Bandwidth (BW)	500 MHz	500 MHz	500 MHz	32.0 MHz
Insertion Loss	< 0.5 dB	0.35 dB	0.45 dB	0.51 dB
Bandpass Flatness over BW	< 0.3 dB	0.18 dB	0.25 dB	No data
Rejection at CF± 450 MHz	>20 dB	38.46 dB	29 dB	>22 dB at CF± 40 MHz
Rejection at 20 GHz	>90 dB	>90 dB	85 dB	No data
Return Loss	>20 dB	> 25 dB	>24 dB	> 23 dB
Input and Output Interface	WR-28	WR-28	WR-28	WR-42
Frequency drift		27 MHz (22.31 ppm/^{0}C)	29 MHz (24 ppm/^{0}C)	2ppm/^{0}C
Mass		34 grams	26 grams	No data
Foot Print		1451 mm^2	1199 mm^2	No data
Power Handling Capability		11.38 KW	2.93 KW	180 W

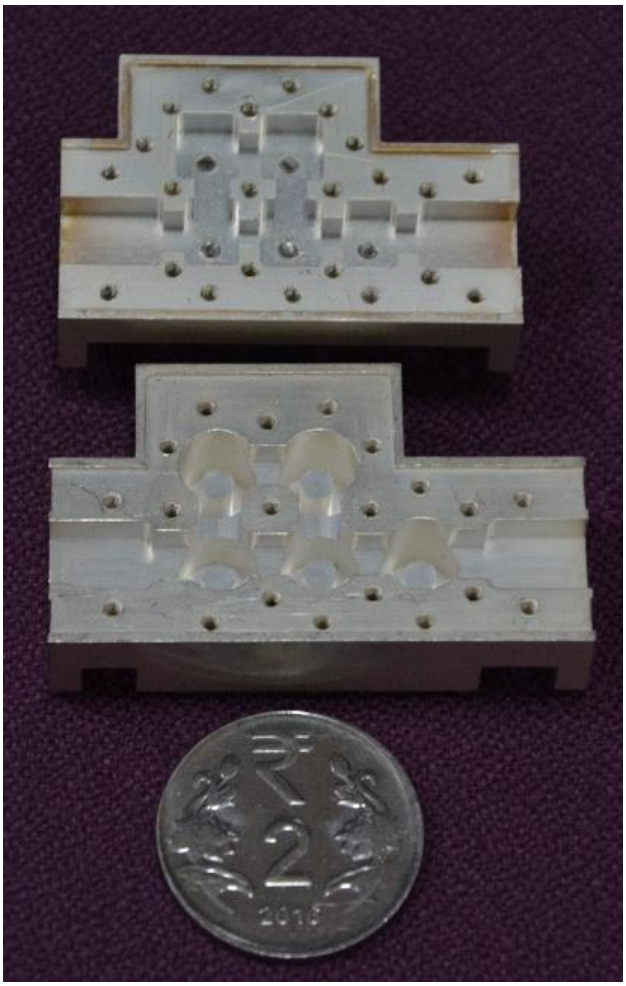

Figure 5.29 *Size comparison of the proposed filter and the waveguide filter.*

The super Q filter reported in [89] is the state of art for high Q high performance filters at Ka-band. This is a very narrowband filter of bandwidth 32 MHz at center frequency of 20 GHz. The filter is fabricated from Invar has very low frequency drift of 2 ppm/^{0}C.The Q is more than 20000 at 20 GHz and is suitable for design of narrowband channel filters due to its inferior spurious free window. The measured available reported specifications of this filter is tabulated in Table 5.8 along with the proposed high Q coaxial resonator filter and the waveguide filter developed at 30 GHz.

5.8. Summary

In this chapter, a novel concept of design a high-performance filter at millimeter wave band with high order mode of the coaxial resonator is discussed in detail. Each aspect of the filter is discussed starting from the synthesis, resonator parameters determination, generation of design charts, EM simulation and the measured results. The concept validated with the design of a 7-pole Chebyshev and cross-coupled filter. The analysis of the high power handling capability of the coaxial resonator and an identical configuration waveguide filter has done. The high power handling analysis is validated by SPARK 3D. The high power measurement test does not perform on the filter due to the non-availability of the set-up. The TM_{012} mode coaxial resonator-based filter shows very good performance and is a potential candidate for deploying satellite filters.

Chapter 6

Temperature Compensated Filters

6.1. Introduction

The material used for the fabrication of the high-performance high-Q three-dimensional filter is metals. The silver plating is done on metal to increases its quality factor. It results in improving the in-band performance parameters of the filter. The frequency drift of the filter depends on the coefficient of thermal expansion (CTE) of the material used to fabricate the filter. Hence, different metal has different CTE, and they have contributed differently to the frequency drift of the filter over the temperature [98, 99, 108].

The other constraint on the payload filter is the mass of the filter. The different metal has different density results in different mass for a given filter topology. The thermal performance of the payload filters is a trade-off between CTE and the density of the metal. Moreover, the ease of fabrication, machining process and the availability of the metal are other factors considered while selecting material for filter fabrication. Aluminium and Invar are the two metal preferred for the fabrication of payload filters. Aluminium has a lightweight and good

thermal conductivity, while Invar has the best CTE among all the metals. The density of Invar is approximately three times the density of Aluminium. Aluminium mostly used in payload filters, but when the filter specification are stringent or the frequency drift is critical, then Invar is used for filter fabrication.

An exhaustive sensitivity analysis of a single coaxial resonator has done. The single resonator closely models the complete filter, and its sensitivity analysis provides a very close estimate of frequency drift due to variation in the CTE of resonator metal and its dimensions. This analysis is an analytical tool used to compensate for the frequency drift of the filter.

This chapter starts with the development of an analytical method of sensitivity analysis of a single resonator for temperature compensation. Then it is implemented on the 5-2-0 TM_{012} mode coaxial resonator filter discussed in the previous chapter.

6.2. Sensitivity Analysis

The sensitivity analysis of the resonator carried out using an eigenmode solver, where the single coaxial resonator has taken into account, which consists of a metallic post inside the cavity. The sensitive dimensions of the filter have taken as a parameter for sensitivity analysis. These parameters are coaxial resonators' cavity height, cavity diameter, post height and diameter. These parameters varied in the small steps where the range took wider than the

variation in the length (Δl) over temperature. The steps so selected will have a minimal impact on convergence error.

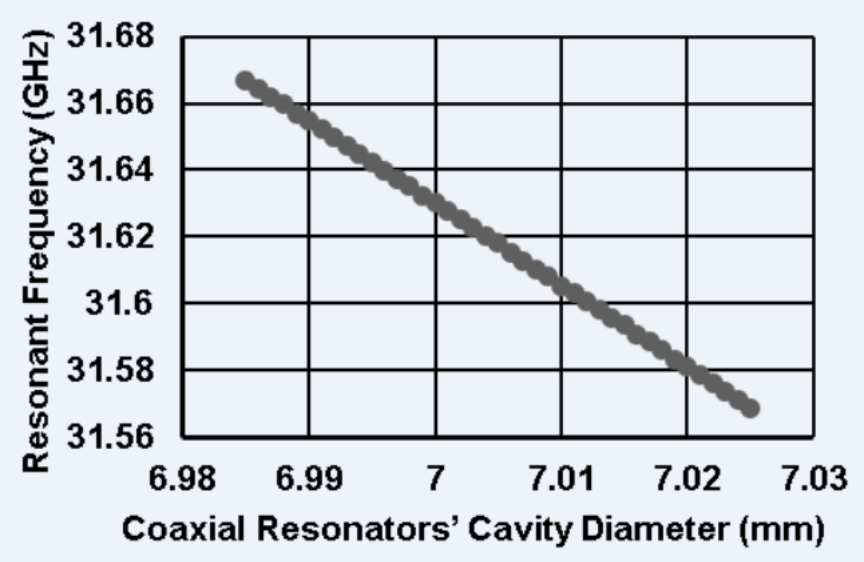

Figure 6.1 *Variation of coaxial resonators resonant frequency vs cavity diameter for TM_{012} mode.*

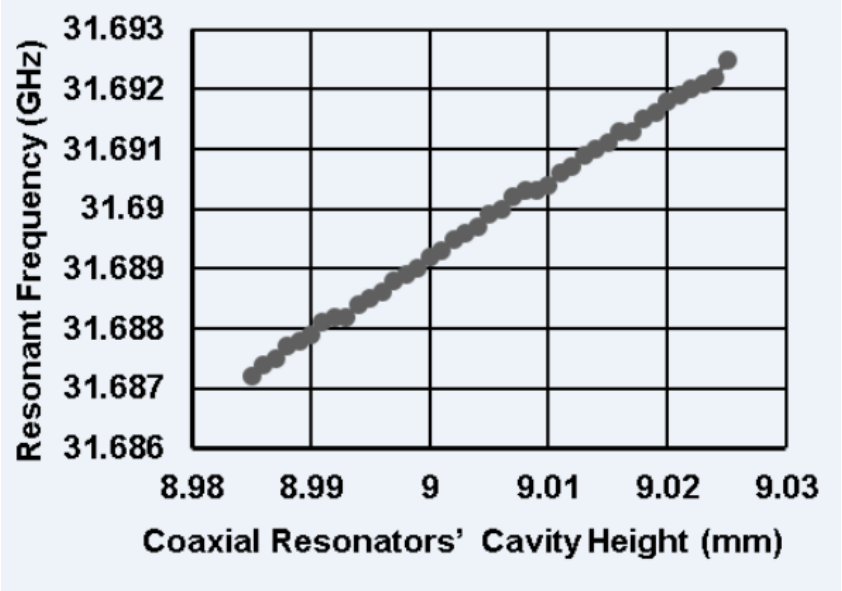

Figure 6.2 *Variation of coaxial resonators resonant frequency vs cavity height for TM_{012} mode.*

The resonant frequency variation due to variations in resonator parameters plotted in figure 6.1, 6.2, 6.3 and 6.4.

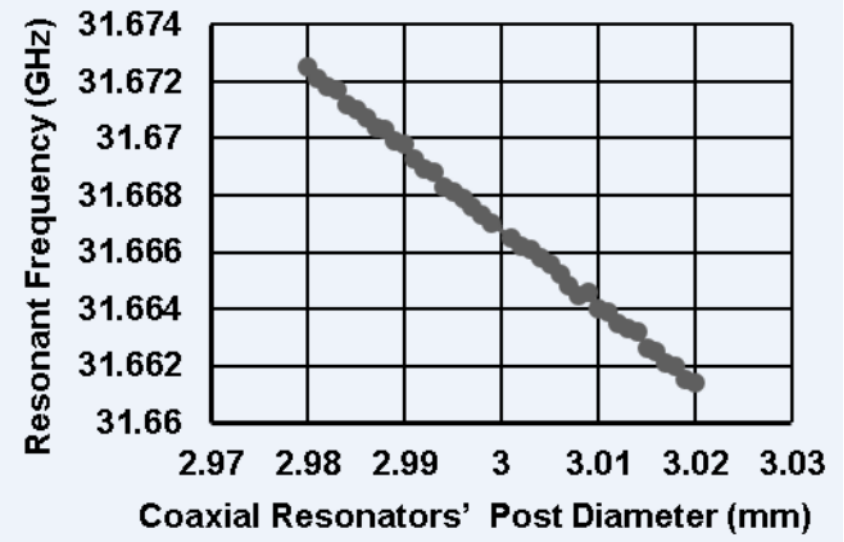

Figure 6.3 *Variation of coaxial resonators resonant frequency vs post diameter for TM_{012} mode.*

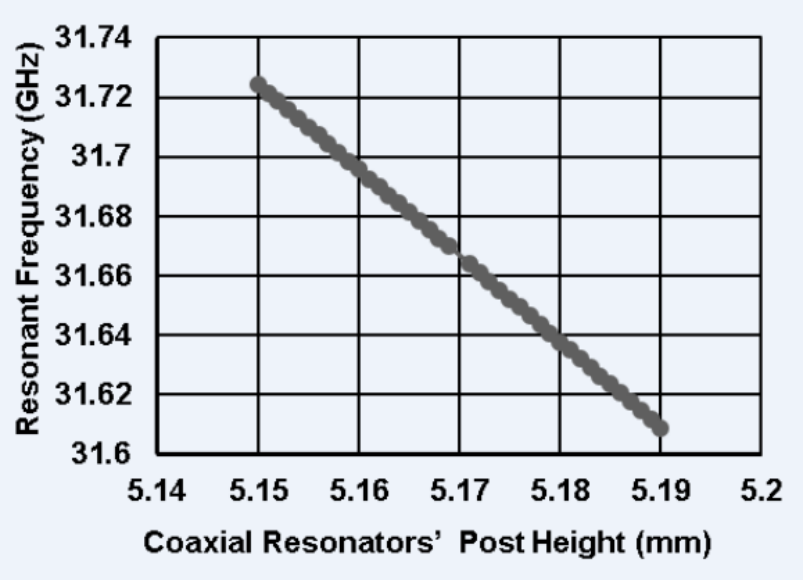

Figure 6.4 *Variation of coaxial resonators resonant frequency vs post height for TM_{012} mode.*

The plots are almost linear for all the parameter, but the slope is different for different parameters. This slope is the sensitivity of the parameter, which plays a dominant role in the temperature compensation of the filter.

The resonator dimensions taken for analysis are 7 mm, 9 mm, 3 mm and 5.17 mm for cavity diameter, cavity height, post diameter and post height respectively. The change in the length (Δl) due to temperature gradient (Δt) is given by

$$\Delta l = \alpha * l * \Delta t \tag{6.1}$$

where, α is the temperature coefficient of thermal expansion (CTE) in ppm/^{0}C, l is the dimension in mm and Δt is the temperature gradient in ^{0}C. The Δt is 40^{0}C for the operation from ambient (25^{0}C) to hot (65^{0}C).

6.3. Temperature Compensation

The frequency drift (Δf) for each parameter is given by

$$\Delta f = S * \Delta l \tag{6.2}$$

where, S is the sensitivity of parameter given by slope of the plot measured in GHz/mm.

The PPM is given by

$$\text{PPM}=\frac{\Delta f_{total}}{fc*\Delta t} \tag{6.3}$$

Table for the temperature compensation is deduced from the plot for the 5-2-0 filter dimension developed at 30.25 GHz in the previous chapter.

The frequency drift is calculated for each parameter considering that the complete filter fabricated from Aluminium metal with a CTE of 24 ppm/^{0}C. The cavity diameter, post diameter and post height lower shift the filter response by 16.4 MHz, 0.794 MHz and 14.26 MHz, respectively. The cavity height higher shifts the filter response by 1.11 MHz. The frequency drift of the filter is 30 MHz, which is close to 27 MHz when the filter tested over the temperature.

It has found from plots that the cavity diameter and post height contributed maximum towards the frequency drift of the filter. The only parameter, which shows reverse behaviour and can balance their effect, is the cavity height. However, its contribution is very small, which can be increased by reducing the cavity height and bring it close to zero. As a result, there will be a large degradation in the quality factor of the coaxial resonator, which will affect the filter in-band RF performance. Moreover, the smaller spurious-free window affects the wideband performance of the filter. It limits the reduction of cavity height for compensation. The increase in the height of the post will also have the same effect, and other dimensions need to be modified to achieve the same resonant frequency. Usually, for the temperature compensation, a composite coaxial post is used, which made of two metals having different CTE. The composition of the metal and their length so selected that it can compensate the filter response over temperature. The combination of Aluminium with CTE of

24 ppm/^{0}C and Invar with CTE of 1.3 ppm/^{0}C is used, which gives the advantage of superior filter performance without increasing its mass.

The minimum frequency drift of 1.57 MHz achieved, for TM_{012} mode coaxial resonator, if the whole filter has fabricated from the Invar metal. However, it will increase the overall filter mass three times. The other approach is to use a composite coaxial post, which does not solve the purpose, as the sensitivity of post dimensions are negative and cavity height is positive.

Table 6.1 calculates the frequency drift for the uncompensated filter completely fabricated from Aluminium. The optimum compensation achieved if the post made of Invar instead of Aluminium. The frequency drift for the post made of Invar and cavity made of Aluminium has calculated in Table 6.2.

Table 6.1 Frequency drift calculation for resonator made from Aluminium

	Cavity Diameter	**Cavity Height**	**Post Diameter**	**Post Height**
Nominal Value (mm)	7	9	3	5.17
Material	Aluminium	Aluminium	Aluminium	Aluminium
CTE (ppm/^{0}C)	24	24	24	24
S (GHz/mm)	-2.4514	0.1287	-0.2758	-2.8848
Δl (mm)	0.00672	0.00864	0.00288	0.004944
Δf (GHz)	-0.016473	0.001112	-0.000794	-0.01426
Δf_{total} (GHz)	-0.0304182			
PPM	-25.2			

It has found that the frequency drift contributed due to post diameter and height is 43 kHz and 0.776 MHz, respectively, for the post made of Invar. The post height reduces drift by 14 MHz when post material changes from Aluminium to

Invar. Therefore, the total drift of the filter reduced to 16.18 MHz compared to 30 MHz when the post made of Invar instead of Aluminium. It gives more margin in design with nearly the same mass as that of a filter fabricated with Aluminium.

Table 6.2 Frequency drift calculation of resonator post made of Invar

	Cavity Diameter	**Cavity Height**	**Post Diameter**	**Post Height**
Nominal Value (mm)	7	9	3	5.17
Material	Aluminium	Aluminium	Invar	Invar
CTE (ppm/^{0}C)	24	24	1.3	1.3
S (GHz/mm)	-2.4514	0.1287	-0.2758	-2.8848
Δl (mm)	0.00672	0.00864	0.000156	0.000269
Δf (GHz)	-0.016473	0.001112	-4.3e-5	-0.000776
Δftotal (GHz)	-0.01618			
PPM	-13.4			

The filter housing made of Aluminium and post made of Invar may contribute to the practical problem of RF grounding due to unevenness between the surface of the cavity and the post. It may lead to the degradation of the RF response of the filter. So, the fabrication is quite challenging in the case of temperature compensated filter at very high frequency. Hence, a 100-micron grove made in each cavity where the post rest.

6.4. Results and performance comparison

Figure 6.5 shows the open view of the fabricated filter designed for the specification of Table 5.1, where two Invar post removed and shown separately. The Invar post rests inside each cavity and mounts with M2 stainless steel

socket head screws. The M1.6 gold plated socket head stainless steel screws used for tuning. The uncompensated filter made from Aluminium shown in figure 5.19. The filter is tuned at 30.24 GHz to care for the vacuum shift. The open view of the filter shown in figure 6.6.

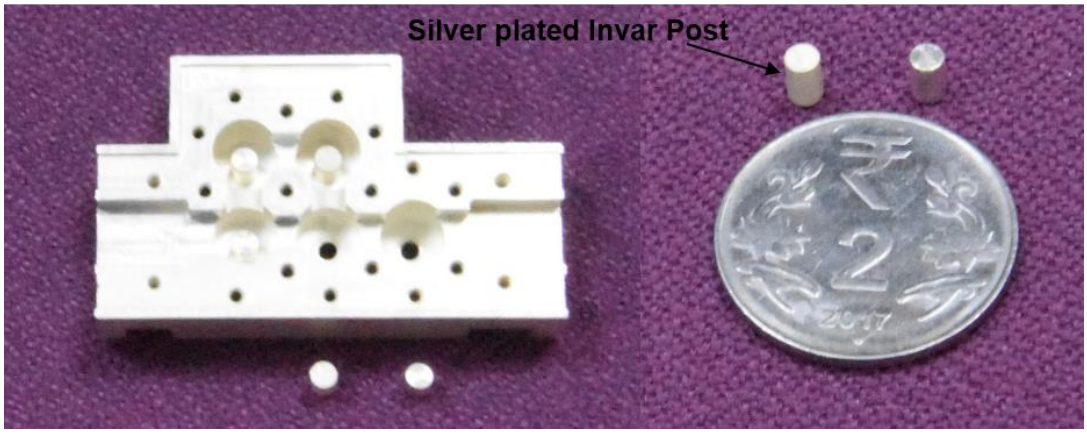

Figure 6.5 *Open view of temperature compensated filter (post removed).*

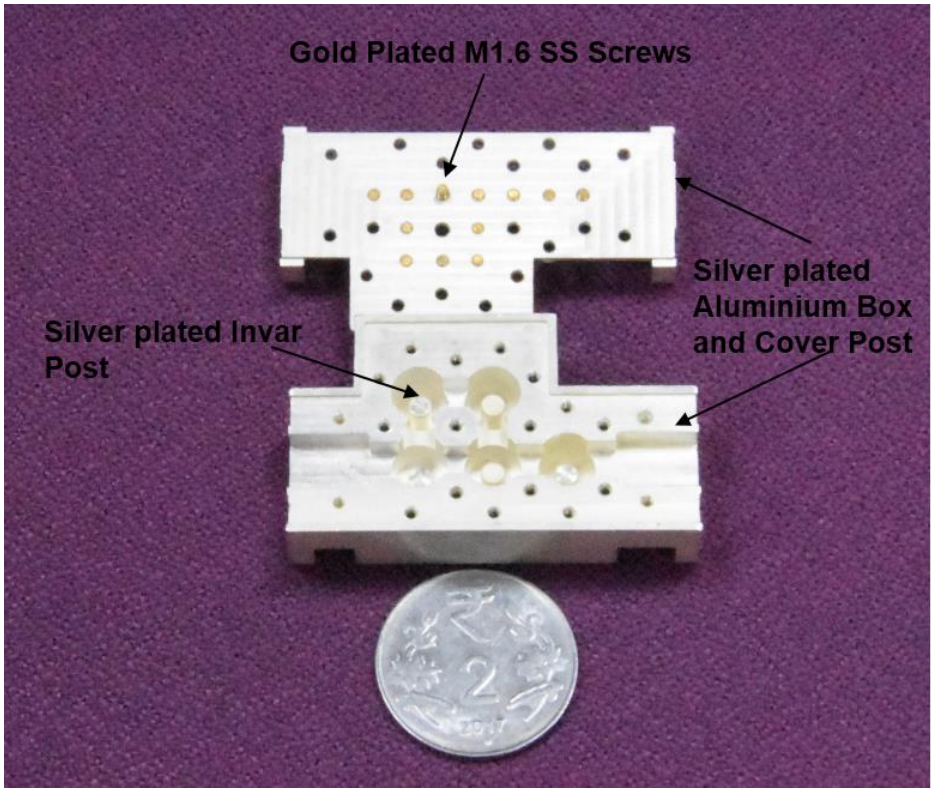

Figure 6.6 *Open view of temperature compensated filter (assembled view).*

The WR-28 waveguide calibration done on VNA and the filter connected to the waveguide adapter. The filter along, with the adapter, placed in the temperature-cycling chamber where the temperature varies from -15^{0}C to 65^{0}C. The two hours of temperature stabilization done at each hot and cold extreme. In hot, the filter response shifts lower, and in the cold, it shifts higher. The measured response of the temperature compensated TM_{012} mode coaxial resonator filter shown in figure 6.7.

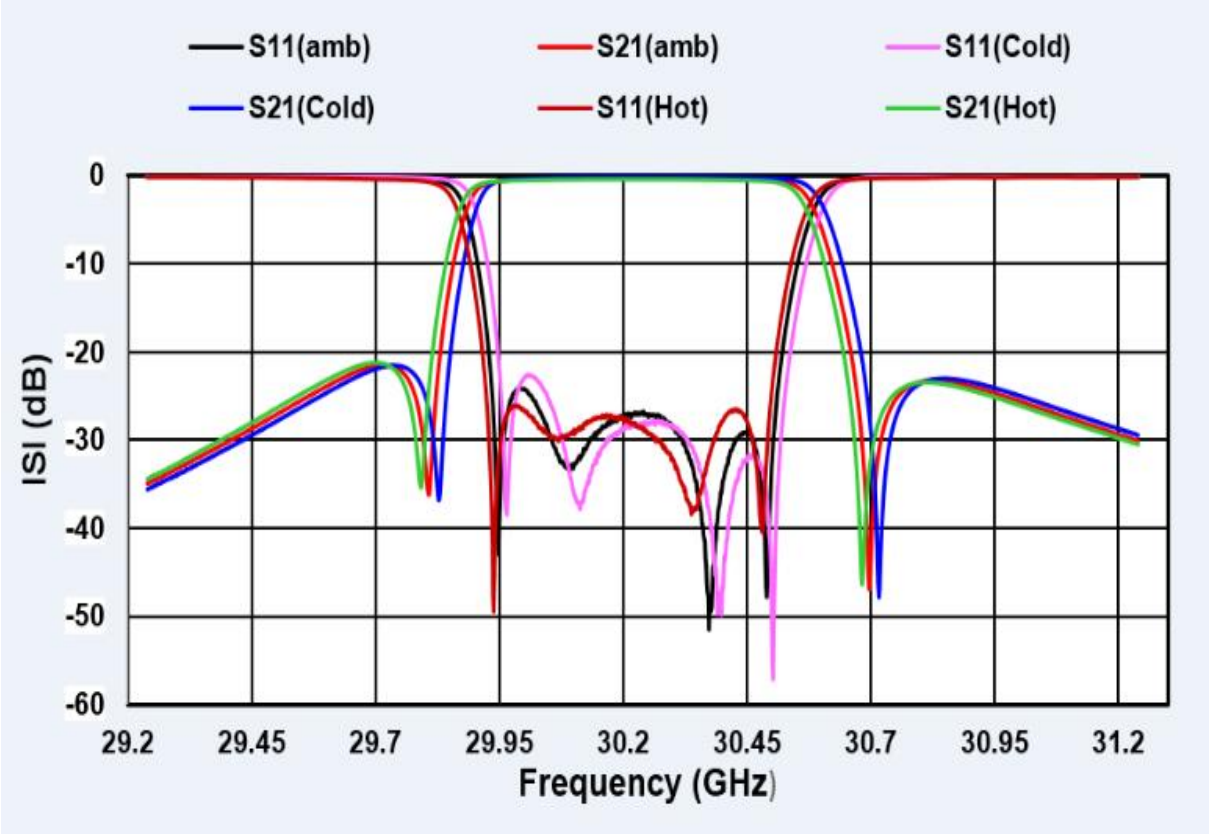

Figure 6.7 *Measured response of temperature compensated filter over the temperature.*

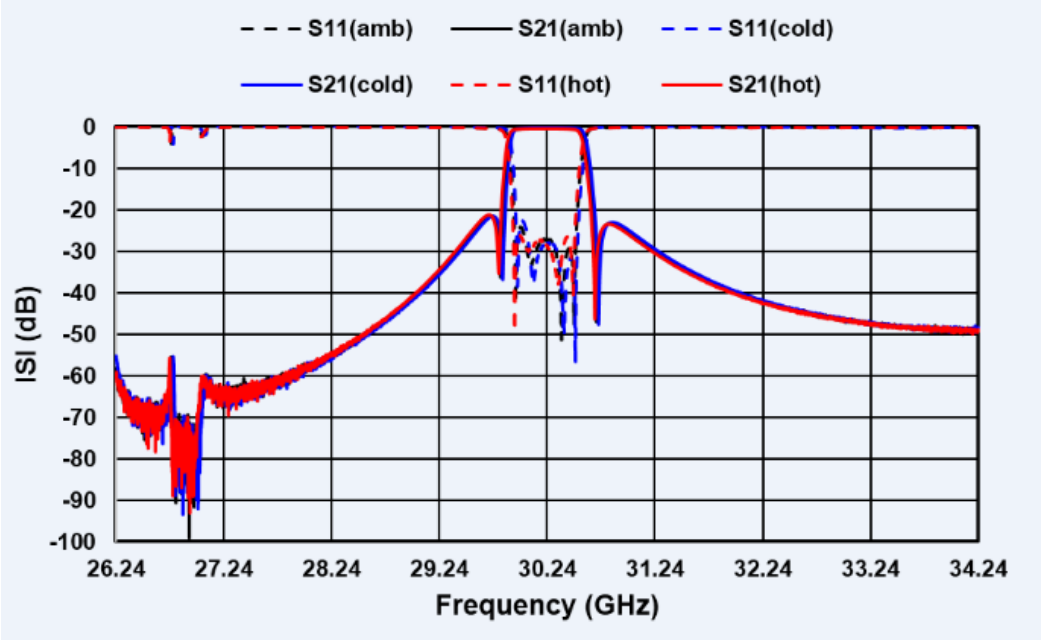

Figure 6.8 *Measured wideband response of temperature compensated filter over the temperature.*

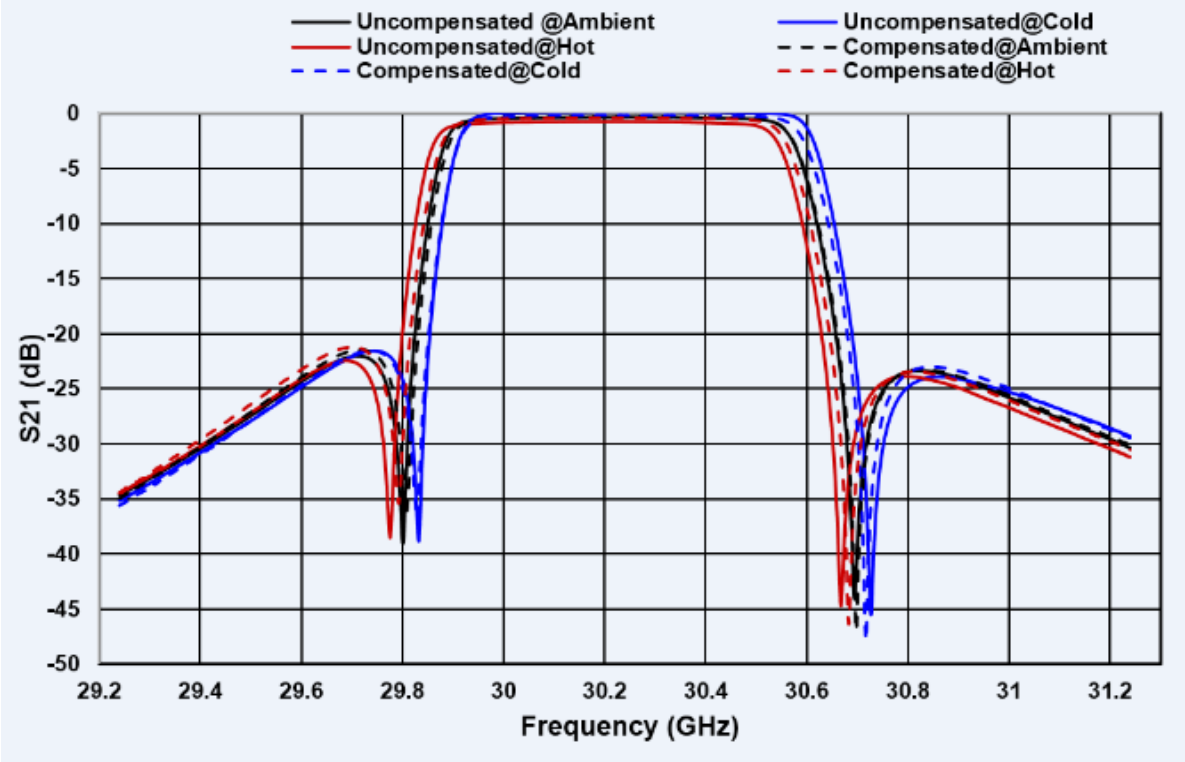

Figure 6.9 *Performance comparison of temperature compensated and uncompensated 5-2-0 filter.*

The measured wideband response of the same filter over temperature shown in figure 6.8. The lower side of the passband shows the TE_{111} mode spurious is below 50 dB, and it does not affect the filter performance.

Moreover, there is no variation and impact of spurious over the temperature. The rejection decreased far higher side of the passband due to the presence of other higher modes of the coaxial resonator. Figure 6.9 shows the performance comparison of compensated and uncompensated filter over the temperature under the same conditions.

Table 6.3 Performance comparison of temperature compensated and uncompensated 5-2-0 filter

Specification	Values	Uncompensated Filter	Compensated Filter
Centre Frequency (CF)	30.25 GHz	30.25 GHz	30.25 GHz
Bandwidth (BW)	500 MHz	500 MHz	500 MHz
Insertion Loss	< 0.5 dB	0.35 dB	0.33 dB
Bandpass Flatness over BW	< 0.3 dB	0.27 dB*	0.20 dB*
Rejection at CF± 450 MHz	>20 dB	20.5 dB**	23 dB**
Rejection at 20 GHz	>90 dB	>90 dB	>90 dB
Return Loss	>20 dB	>25	>25 dB
Input and Output Interface	WR-28	WR-28	WR-28
Frequency drift		27 MHz (22.31 ppm/^{0}C)	18 MHz (14.87 ppm/^{0}C)
Mass		34 grams	37.5 grams

*worst case of flatness in hot

**worst case of rejection in cold

The compensated filter has a frequency drift of 18 MHz, while for the uncompensated filter, it is 27 MHz. The frequency drift in both the filters is

more in cold compared to hot. .The temperature-compensated TM_{012} mode coaxial resonator filter has 9 MHz less frequency drift than the uncompensated filter of identical configuration. The RF performance of temperature compensated filter is at par compared to uncompensated filter with an insignificant increase in the mass.

6.5. Summary

The analytical method of temperature compensation has developed using sensitivity analysis. The single resonator parameters are varied for analysis, and the contribution from each parameter has calculated. The temperature-compensated 5-2-0 TM_{012} mode coaxial resonator filter has developed using this analysis. It has the post made of Invar and the filter box made of Aluminium. The frequency drift of 5-2-0 temperature-compensated has reduced by 9 MHz compared to identical uncompensated filter.

Chapter 7

Conclusions and Future Scope

7.1. Conclusion

The thesis presents two novel types of high Q high performance filters and their realization technologies for used in Ka-band high throughput satellite (HTS). These filters have very good in-band and out-of-band performance, and they require Q better than 2000 with wide spurious free range for their realization. The first is a modified non-radiative dielectric waveguide (MNRD) E-plane resonator bandpass filter where the basic structure of NRD is modified, and the resonators realized with metallic discontinuity introduced in the E-plane of NRD. The filter used the mechanical tuning where tuning screws used to tune the center frequency and bandwidth. The fabricated filter has an insertion loss of 2.3 dB at 29.2 GHz and tunable center frequency. This high loss attribute to the improper contact between dielectric slab, and unplated stainless steel grub screws and improper grounding between unplated parallel metal plates, and dielectric.

The second is the higher-order mode coaxial resonator bandpass filter where higher-order TM_{012} mode of the coaxial resonator used for the first time for filter realization. It is the fourth mode of the coaxial resonator for the given geometry has ultra-wide spurious free range and very high Q require for the realization

of high-performance Ka-band HTS filter. The high Q attributed to the large volume to surface area ratio, which inherently provides the advantage of feasible size handling at Ka-band. The direct-coupled seven pole Chebyshev filter and cross-coupled filters 5-2-0, and 4-2-0 filters are designed and fabricated, which validates the concept of higher-order modes of the coaxial resonator for filter application, meeting all the specifications of a typical Ka-band pre-select filter. To compare the performance of the coaxial filter with the existing waveguide technology, an identical configuration compact waveguide filter is designed and fabricated. The non-resonating post used for the realization of cross-coupling makes the waveguide filter compact, without being the addition of large-sized cavity for cross-coupling realization. The coaxial and waveguide 5-2-0 filters have tested over the temperature range of -15^0C to 65^0C, but the frequency drift of coaxial resonator filter is 2 MHz less than the waveguide filter, and it offers more design margin. The high power analysis of both these filters has done and found that the coaxial resonator filter can handle four times more power than its corresponding waveguide filter. The performance of both the filters has been compared and found that the performance of the coaxial resonator filter is superior having less frequency drift, high Q, better passband and stopband performance, and very high power handling capability.

The frequency drift of conventional cavity resonator filters used in satellite communication depends on the CTE of material used for their fabrication. So, there is a trade-off between mass and RF performance of the filter where the low CTE Invar metal gives minimum frequency drift at the expense of mass.

But, in the case of the coaxial resonator filter, the temperature compensation can be modified by employing a combination of low and high CTE metal with a minimal increase in the filter mass. The analytical tool of sensitivity analysis used for temperature compensation where a single resonator very closely modelled the complete filter. The high Q temperature compensated coaxial resonator filter has demonstrated, whose frequency drift is 18 MHz for the temperature range of -15^0C to 65^0C, which is 9 MHz less than the uncompensated filter of identical configuration. The RF performance of the compensated filter is superior compared to the uncompensated filter without any significant increase in the filter weight. It offers more design margin without increasing any design complexity. This approach maintains the Q and has same spurious free performance as that of uncompensated filter made from Aluminium. The drift calculated with sensitivity analysis is 16 MHz while the measured frequency drift is 2 MHz more, which is due to the different height of post in the different cavity and the significant contribution of the cavity diameter made of Aluminium.

7.2. Future Scope

This concept of higher order mode of coaxial resonator filter extended to Q-band (38 to 43 GHz) and V-band (60GHz). This concept offer advantage as at that band size handling pose limitation of mechanical tunable filter. Moreover, the cavity filters at these band offer fixed frequency drift which gives less flexibility in design margin. The other higher order modes like TM_{01N} can be explore which further increase the Q-factor. The other mechanism of temperature

compensation to be explored to minimize the frequency drift near to zero, without impacting the RF performance of the filter. Moreover, other higher order dual modes of coaxial resonators can use for filter application which can minimize the filter footprint and save mass.

References

[1] [online]Available:https://www.hughes.com/who-we-are/resources/channels-newsletter/spring-2011/ka-band-the-future-of-satellite-broadband.

[2] I. Llamas-Garro, Y. Kim, C. Baek and Y. Kim, "A Planar High-Q Micromachined Monolithic Half-Coaxial Transmission-Line Filter," in *IEEE Transactions on Microwave Theory and Techniques*, vol. 54, no. 12, pp. 4161-4168, Dec. 2006, doi: 10.1109/TMTT.2006.886369.

[3] Wang Y, Ke M, Lancaster MJ, "38 GHz Micromachined Cavity Resonator and Filter with Rectangular-Coaxial Feed Lines." *IET microwave antenna and propagation* 3.1(2009):125-129.

[4] C. Wang and K. A. Zaki, "Dielectric Resonators and Filters," in *IEEE Microwave Magazine*, vol. 8, no. 5, pp. 115-127, Oct. 2007, doi: 10.1109/MMM.2007.903648.

[5] C. Kudsia, R. Cameron and W. -. Tang, "Innovations in Microwave Filters and Multiplexing Networks for Communications Satellite Systems," in *IEEE Transactions on Microwave Theory and Techniques*, vol. 40, no. 6, pp. 1133-1149, June 1992, doi: 10.1109/22.141345.

[6] K. Hano, H. Kohriyama and K. Sawamoto, "A Direct-Coupled Lambda/4-Coaxial Resonator Bandpass Filter for Land Mobile Communications," in *IEEE Transactions on Microwave Theory and Techniques*, vol. 34, no. 9, pp. 972-976, Sept 1986, doi: 10.1109/TMTT.1986.1133478.

[7] A. Morini, G. Venanzoni and T. Rozzi, "A New Adaptive Prototype for the Design of Side-Coupled Coaxial Filters with Close Correspondence to the Physical Structure," in *IEEE Transactions on Microwave Theory and Techniques*, vol. 54, no. 3, pp. 1146-1153, March 2006, doi: 10.1109/TMTT.2005.864112.

[8] X. Wang, G. Jang, B. Lee and N. Park, "Compact Quad-Mode Bandpass Filter Using Modified Coaxial Cavity Resonator With Improved Q-Factor," in *IEEE Transactions on Microwave Theory and Techniques*, vol. 63, no. 3, pp. 965-975, March 2015, doi: 10.1109/TMTT.2015.2389231.

[9] F. Chen, J. Qiu, S. Wong and Q. Chu, "Dual-Band Coaxial Cavity Bandpass Filter With Helical Feeding Structure and Mixed Coupling," in *IEEE Microwave and Wireless Components Letters*, vol. 25, no. 1, pp. 31-33, Jan. 2015, doi: 10.1109/LMWC.2014.2369965.

[10] Hung, CL., Yeh, Y. The Propagation Constants of Higher-Order Modes in Coaxial Waveguides with Finite Conductivity. *Int J Infrared Milli Waves* **26,** 29–39 (2005). https://doi.org/10.1007/s10762-004-2029-2

[11] A. E. Atia and A. E.Williams, "New Types of Waveguide Bandpass Filters for Satellite Transponders," Comsat Technical Review 1.1 (1971): 21–43.

[12] A. E. Atia and A. E. Williams, "Narrow-Bandpass Waveguide Filters," in *IEEE Transactions on Microwave Theory and Techniques*, vol. 20, no. 4, pp. 258-265, Apr. 1972, doi: 10.1109/TMTT.1972.1127732.

[13] A. E. Atia, A. E.Williams, and R.W. Newcom, "Synthesis of dual-mode filters," IEEE Transaction on Circuits and Systems 21(1974): 649–655, Sept.1974.

[14] S. Kallianteris and M. V. O'Donovan, "Technology Advances In The Realization of Filter Networks for Communication Satellites Operating above 10 GHz," 6th Communication Satellite System Conference, Montreal, QC, Canada, Apr. 1981.

[15] R. Tong and C. M. Kudsia. "Enhanced Performance and Increased EIRP in Communications Satellites Using Contiguous Multiplexers," in Proc. 10th AIAA Communication Satellite System Conference, Orlando, FL, Mar. 1984.

[16] A. E. Atia, "Computer-Aided Design of Waveguide Multiplexers," in *IEEE Transactions on Microwave Theory and Techniques*, vol. 24, pp. 332–336, 1974.

[17] J. D. Rhodes and R. Levy, "A Generalized Multiplexer Theory," in *IEEE Transactions on Microwave Theory and Techniques*, vol. 27, no. 2, pp. 99-111, Feb. 1979, doi: 10.1109/TMTT.1979.1129570.

[18] S. J. Fiedziuszko, I. C. Hunter, T. Itoh, Y. Kobayashi, T. Nishikawa, S. N.Stitzer, and K.Wakino, "Dielectric Materials, Devices, and Circuits," in

IEEE Transactions on Microwave Theory and Techniques, vol. 50, no. 3, pp. 706-720, March 2002, doi: 10.1109/22.989956.

[19] M. J. Lancaster. Passive Microwave Device Applications of High-Temperature Superconductors. Cambridge, U.K.: Cambridge Univ. Press, 1997.

[20] H. C. Nathanson, W. E. Newell, R. A. Wickstrom and J. R. Davis, "The Resonant Gate Transistor, " in *IEEE Trans. Electron Devices*, vol. 14, no. 3, pp. 117-133, March 1967, doi: 10.1109/T-ED.1967.15912.

[21] N. I. Dib, W. P. Harokopus, L. P. B. Katehi, C. C. Ling and G. M. Rebeiz, "Study of a Novel Planar Transmission Line," 1991 *IEEE MTT-S International Microwave Symposium Digest*, 1991, pp. 623-626 vol.2, doi: 10.1109/MWSYM.1991.147080.

[22] R. F. Drayton and L. P. B. Katehi, "Microwave Characterization of Microshield Lines," 40th *ARFTG Conference Digest*, 1992, pp. 171-176, doi: 10.1109/ARFTG.1992.327011.

[23] T. M. Weller, G. M. Rebeiz and L. P. B. Katehi, "Experimental Results on Microshield Transmission Line Circuits," 1993 *IEEE MTT-S International Microwave Symposium Digest*, 1993, pp. 827-830 vol.2, doi: 10.1109/MWSYM.1993.276747.

[24] R. F. Drayton and L. P. B. Katehi, "Experimental study of micromachined circuits," *Dig. 1993 Int. Symp. Space Terahertz Tech.*, Mar. 1993.

[25] R. F. Drayton and L. P. B. Katehi, "Micromachined Circuits for mm-Wave Applications," *Dig. 1993 Euro. Microwave Conf.*, Sept. 1993.

[26] T. M. Weller, L. P. B. Katehi and G. M. Rebeiz, "High Performance Microshield Line Components," in *IEEE Transactions on Microwave Theory and Techniques*, vol. 43, no. 3, pp. 534-543, March 1995, doi: 10.1109/22.372098.

[27] S. V. Robertson, L. P. B. Katehi and G. M. Rebeiz, "Micromachined W-band filters," in *IEEE Transactions on Microwave Theory and Techniques*, vol. 44, no. 4, pp. 598-606, April 1996, doi: 10.1109/22.491027.

[28] W. R. McGrath, C. Walker, M. Yap and Y. -. Tai, "Silicon Micromachined Waveguides for Millimeter-Wave and Submillimeter-Wave Frequencies,"

in *IEEE Microwave and Guided Wave Letters*, vol. 3, no. 3, pp. 61-63, March 1993, doi: 10.1109/75.205665.

[29] J. Papapolymerou, Jui-Ching Cheng, J. East and L. P. B. Katehi, "A Micromachined High-Q X-band Resonator," in *IEEE Microwave and Guided Wave Letters*, vol. 7, no. 6, pp. 168-170, June 1997, doi: 10.1109/75.585207.

[30] L. Harle and L. P. B. Katehi, "A Vertically Integrated Micromachined Filter," in *IEEE Transactions on Microwave Theory and Techniques*, vol. 50, no. 9, pp. 2063-2068, Sept. 2002, doi: 10.1109/TMTT.2002.802317.

[31] Lee Harle, J. Papapolymerou, J. East and L. P. B. Katehi, "The Effects of Slot Positioning on the Bandwidth of a Micromachined Resonator," 1998 *28th European Microwave Conference*, 1998, pp. 664-668, doi: 10.1109/EUMA.1998.338234.

[32] L. Harle and L. P. B. Katehi, "A silicon micromachined four-pole linear phase filter," in *IEEE Transactions on Microwave Theory and Techniques*, vol. 52, no. 6, pp. 1598-1607, June 2004, doi: 10.1109/TMTT.2004.828456.

[33] W. Gautier, A. Stehle, B. Schoenlinner, V. Ziegler, U. Prechtel and W. Menzel, "Low-Loss Micro-Machined Four-Pole Linear Phase Filter in Silicon Technology," *2009 European Microwave Conference (EuMC)*, 2009, pp. 1413-1416, doi: 10.23919/EUMC.2009.5296250.

[34] M. Stickel, P. C. Kremer and G. V. Eleftheriades, "High-Q Microstrip-Fed Bulk Micromachined Silicon Cavities," in *IEEE Antennas and Propagation Society International Symposium. Digest,* held in conjunction with: USNC/CNC/URSI North American Radio Sci. Meeting (Cat. No.03CH37450), 2003, pp. 632-635 vol.2, doi: 10.1109/APS.2003.1219316.

[35] M. Stickel, P. Kremer and G. V. Eleftheriades, "A Millimeter-Wave Bandpass Waveguide Filter Using a Width-Stacked Silicon Bulk Micromachining Approach," in *IEEE Microwave and Wireless Components Letters*, vol. 16, no. 4, pp. 209-211, April 2006, doi: 10.1109/LMWC.2006.872116.

[36] L. Pelliccia, P. Farinelli and R. Sorrentino, "Micromachined Filters in Multilayer Technology for On-Board Communication Systems in Ka-

band," *2013 IEEE MTT-S International Microwave Symposium Digest (MTT)*, 2013, pp. 1-3, doi: 10.1109/MWSYM.2013.6697473.

[37] P. Farinelli, L. Pelliccia, B. Margesin and R. Sorrentino, "Ka-band Surface-Mountable Pseudo-Elliptic Filter in Multilayer Micromachined Technology for On-Board Communication Systems," *2016 IEEE MTT-S International Microwave Symposium (IMS)*, 2016, pp. 1-4, doi: 10.1109/MWSYM.2016.7540055.

[38] Park, K.-Y., Lee, J.-C., Kim, J.-H., Lee, B., Kim, N.-Y., Park, J.-Y., Kim, G.-H., Bu, J.-U. and Chung, K.-W. (2001), A New Three-Dimensional 30 GHz Bandpass Filter Using the Liga Micromachined Process. Microw. Opt. Technol. Lett., 30: 199-201. https://doi.org/10.1002/mop.1264

[39] O. Glubokov, X. Zhao, J. Campion, U. Shah and J. Oberhammer, "Micromachined Filters at 450 GHz with 1% Fractional Bandwidth and Unloaded Q Beyond 700," in *IEEE Transactions on Terahertz Science and Technology*, vol. 9, no. 1, pp. 106-108, Jan. 2019, doi: 10.1109/TTHZ.2018.2883075.

[40] D. Deslandes and K. Wu, "Integrated Microstrip and Rectangular Waveguide in Planar Form," in *IEEE Microwave and Wireless Components Letters*, vol. 11, no. 2, pp. 68-70, Feb. 2001, doi: 10.1109/7260.914305.

[41] J. Hirokawa and M. Ando, "Single-Layer Feed Waveguide Consisting of Posts for Plane TEM Wave Excitation in Parallel Plates," in *IEEE Transactions on Antennas and Propagation*, vol. 46, no. 5, pp. 625-630, May 1998, doi: 10.1109/8.668903.

[42] H. Uchimura, T. Takenoshita and M. Fujii, "Development of a laminated waveguide," in *IEEE Transactions on Microwave Theory and Techniques*, vol. 46, no. 12, pp. 2438-2443, Dec. 1998, doi: 10.1109/22.739232.

[43] Li Yan, Wei Hong, Guang Hua, Jixin Chen, Ke Wu and Tie Jun Cui, "Simulation and Experiment on SIW Slot Array Antennas," in *IEEE Microwave and Wireless Components Letters*, vol. 14, no. 9, pp. 446-448, Sept. 2004, doi: 10.1109/LMWC.2004.832081.

[44] Y. D. Dong et al., "Development of Ultrawideband Antenna with Multiple Band-Notched Characteristics Using Half Mode Substrate Integrated

Waveguide Cavity Technology," in *IEEE Transactions on Antennas and Propagation*, vol. 56, no. 9, pp. 2894-2902, Sept. 2008, doi: 10.1109/TAP.2008.928792.

[45] G. Q. Luo, Z. F. Hu, L. X. Dong and L. L. Sun, "Planar Slot Antenna Backed by Substrate Integrated Waveguide Cavity," in *IEEE Antennas and Wireless Propagation Letters*, vol. 7, pp. 236-239, 2008, doi: 10.1109/LAWP.2008.923023.

[46] Zhen-Yu Zhang and Ke Wu, "Broadband Half-Mode Substrate Integrated Waveguide (HMSIW) Wilkinson Power Divider," *2008 IEEE MTT-S International Microwave Symposium Digest*, 2008, pp. 879-882, doi: 10.1109/MWSYM.2008.4632973.

[47] K. Song, Y. Fan and Y. Zhang, "Eight-Way Substrate Integrated Waveguide Power Divider with Low Insertion Loss," in *IEEE Transactions on Microwave Theory and Techniques*, vol. 56, no. 6, pp. 1473-1477, June 2008, doi: 10.1109/TMTT.2008.923897.

[48] Song, K. & Fan, Yizhi & Zhang, Y. (2006). Radial Cavity Power Divider Based on Substrate Integrated Waveguide Technology. *Electronics Letters*. 42. 1100- 1101. 10.1049/el: 20062012.

[49] G. H. Zhai et al., "Folded Half Mode Substrate Integrated Waveguide 3 dB Coupler," in *IEEE Microwave and Wireless Components Letters*, vol. 18, no. 8, pp. 512-514, Aug. 2008, doi: 10.1109/LMWC.2008.2001006.

[50] B. Liu, W. Hong, Y. Wang, Q. Lai and K. Wu, "Half Mode Substrate Integrated Waveguide (HMSIW) 3-dB Coupler," in *IEEE Microwave and Wireless Components Letters*, vol. 17, no. 1, pp. 22-24, Jan. 2007, doi: 10.1109/LMWC.2006.887244.

[51] Zhang Cheng Hao, Wei Hong, Xiao Ping Chen, Ji Xin Chen, Ke Wu and Tie Jun Cui, "Multilayered Substrate Integrated Waveguide (MSIW) Elliptic Filter," in *IEEE Microwave and Wireless Components Letters*, vol. 15, no. 2, pp. 95-97, Feb. 2005, doi: 10.1109/LMWC.2004.842836.

[52] H. J. Tang, W. Hong, J. Chen, G. Q. Luo and K. Wu, "Development of Millimeter-Wave Planar Diplexers Based on Complementary Characters of Dual-Mode Substrate Integrated Waveguide Filters With Circular and

Elliptic Cavities," in *IEEE Transactions on Microwave Theory and Techniques*, vol. 55, no. 4, pp. 776-782, April 2007, doi: 10.1109/TMTT.2007.893655.

[53] N. Grigoropoulos, B. Sanz-Izquierdo and P. R. Young, "Substrate Integrated Folded Waveguides (SIFW) and Filters," in *IEEE Microwave and Wireless Components Letters*, vol. 15, no. 12, pp. 829-831, Dec. 2005, doi: 10.1109/LMWC.2005.860027.

[54] X. Chen, W. Hong, T. Cui & K. Wu (2005) Substrate Integrated Waveguide (SIW) Asymmetric Dual-Mode Filter and Diplexer, *International Journal of Electronics*, 92:12, 743-753, DOI: 10.1080/00207210500304494

[55] X. Chen and K. Wu, "Substrate Integrated Waveguide Filter: Basic Design Rules and Fundamental Structure Features," in *IEEE Microwave Magazine*, vol. 15, no. 5, pp. 108-116, July-Aug. 2014, doi: 10.1109/MMM.2014.2321263.

[56] X. Chen, K. Wu and Z. Li, "Dual-Band and Triple-Band Substrate Integrated Waveguide Filters with Chebyshev and Quasi-Elliptic Responses," in *IEEE Transactions on Microwave Theory and Techniques*, vol. 55, no. 12, pp. 2569-2578, Dec. 2007, doi: 10.1109/TMTT.2007.909603.

[57] Y. Cheng, W. Hong and K. Wu, "Half Mode Substrate Integrated Waveguide (HMSIW) Directional Filter," in *IEEE Microwave and Wireless Components Letters*, vol. 17, no. 7, pp. 504-506, July 2007, doi: 10.1109/LMWC.2007.899309.

[58] Sung Tae Choi, Ki Seok Yang, K. Tokuda and Yong Hoon Kim, "A V-band Planar Narrow Bandpass Filter Using a New Type Integrated Waveguide Transition," in *IEEE Microwave and Wireless Components Letters*, vol. 14, no. 12, pp. 545-547, Dec. 2004, doi: 10.1109/LMWC.2004.837386

[59] H. J. Tang, W. Hong, Z. C. Hao, J. X. Chen, and K. Wu, "Optimal Design of Compact Millimetre-Wave SIW Circular Cavity Filters," *Electron. Lett.*, vol. 41, no. 19, pp. 1068-1069, Sep. 2005, DOI: 10.1049/el:20052251.

[60] X. P. Chen, and K. Wu, "Substrate Integrated Waveguide Crosscoupled Filter with Negative Coupling Structure," in *IEEE Transactions on*

Microwave Theory and Techniques, vol. 56, no. 1, pp. 142-149, Jan. 2008, doi: 10.1109/TMTT.2007.912222.

[61] Z. C. Hao, W. Hong, J. X. Chen, X. P. Chen, and K. Wu, "Compact Super-Wide Bandpass Substrate Integrated Waveguide (SIW) Filters," in *IEEE Transactions on Microwave Theory and Techniques*, vol. 53, no. 9, pp. 2968-2977, Sept. 2005, doi: 10.1109/TMTT.2005.854232.

[62] H.-Y. Chien, T.-M. Shen, T.-Y. Huang, W.-H. Wang, and R.-B. Wu, "Miniaturized Bandpass Filters with Double-Folded Substrate Integrated Waveguide Resonators in LTCC," in *IEEE Transactions on Microwave Theory and Techniques*, vol. 57, no. 7, pp. 1774-1782, July 2009, doi: 10.1109/TMTT.2009.2022591.

[63] C. A. Zhang, Y. J. Cheng, and Y. Fan, "Quadri-Folded Substrate Integrated Waveguide Cavity and its Miniaturized Bandpass Filter Applications," *Progress In Electromagnetics Research C*, Vol. 23, 1-14, 2011. doi:10.2528/PIERC11052401.

[64] L.-N. Chen, Y.-C. Jiao, Z. Zhang, and F.-S. Zhang, "Miniaturized Substrate Integrated Waveguide Dual-Mode Filters Loaded by a Series of Cross-Slot Structures," *Progress In Electromagnetics Research C*, Vol. 29, 29-39, 2012. doi:10.2528/PIERC12032302.

[65] A. Pourghorban Saghati, A. Pourghorban Saghati, and K. Entesari, "Ultraminiature SIW Cavity Resonators and Filters," in *IEEE Transactions on Microwave Theory and Techniques*, vol. 63, no. 12, pp. 4329-4340, Dec. 2015, doi: 10.1109/TMTT.2015.2494023.

[66] A. N. Alkhafaji, A. J. Salim, and J. K. Ali, "Compact Substrate Integrated Waveguide BPF for Wideband Communication Applications,"' in *Proc. Prog. Electromagn. Res. Symp. (PIERS)*, Prague, Czech Republic, Jul. 2015,pp. 135-139.

[67] H. Zhang, W. Kang and W. Wu, "Miniaturized Dual-Band SIW Filters Using E-Shaped Slotlines with Controllable Center Frequencies," in *IEEE Microwave and Wireless Components Letters*, vol. 28, no. 4, pp. 311-313, April 2018, doi: 10.1109/LMWC.2018.2811251.

[68] M. Danaeian, "Miniaturized half-mode substrate integrated waveguide diplexer based on SIR-CSRR unit-cell,"*Anal. Integr. Circuits Signal Process.*, vol. 102, pp. 555_561, Sep. 2019.

[69] Danaeian, M, Afrooz, K. Compact metamaterial unit-cell based on stepped-impedance resonator technique and its application to miniaturize substrate integrated waveguide filter and diplexer. *Int J RF Microw Comput Aided Eng*. 2019; 29:e21537. https://doi.org/10.1002/mmce.21537.

[70] T. Yang, P.-L. Chi, R. Xu, and W. Lin, "Folded Substrate Integrated Waveguide Based Composite Right/Left-Handed Transmission Line and its Application to Partial H-Plane Filters," in *IEEE Transactions on Microwave Theory and Techniques*, vol. 61, no. 2, pp. 789-799, Feb. 2013, doi: 10.1109/TMTT.2012.2231431.

[71] Y.-N. Yang, G. H. Li, L. Sun, W. Yang, and X. Yang, "Design of Compact Bandpass Filters Using Sixteenth Mode and Thirty-Second Mode SIW Cavities," *Progress In Electromagnetics Research Letters*, Vol. 75, 61-66, 2018.doi:10.2528/PIERL18021002.

[72] Y.-D.Wu, G. H. Li,W. Yang, and X. Yang, "Design of Compact Wideband QMSIW Band-Pass Filter with Improved Stopband," *Progress In Electromagnetics Research Letters*, Vol. 65, 75-79, 2017.doi:10.2528/PIERL16110301.

[73] Liu, Q., Zhou, D., Zhang, D., Bian, C., & Zhang, Y. (2020). Ultra-Compact Quasi-Elliptic Bandpass Filter Based on Capacitive-Loaded Eighth-Mode SIW cavities. *International Journal of Microwave and Wireless Technologies*, 12(2), 109-115. doi:10.1017/S175907871900120X

[74] A. R. Azad and A. Mohan. A Compact Sixteenth-Mode Substrate Integrated Waveguide Bandpass Filter with Improved Out-of-band Performance. *Microw. Opt. Technol. Lett.*, 2017; 59(7): 1728-1733. https://doi.org/10.1002/mop.30615.

[75] A. Iqbal, J. J. Tiang, S. K. Wong, M. Alibakhshikenari, F. Falcone and E. Limiti, "Miniaturization Trends in Substrate Integrated Waveguide (SIW) Filters: A Review," in *IEEE Access*, vol. 8, pp. 223287-223305, 2020, doi: 10.1109/ACCESS.2020.3044088.

[76] .R. Levy, "Theory of Direct-Coupled-Cavity Filters," in *IEEE Transactions on Microwave Theory and Techniques*, vol. 15, no. 6, pp. 340-348, June. 1967, doi: 10.1109/TMTT.1967.1126471.

[77] C. M. Kudsia and M. V. O'Donovan, "A Light Weight Graphite Fiber Epoxy Composite (GFEC) Waveguide Multiplexer for Satellite Applications," 1974 *4th European Microwave Conference*, 1974, pp. 585-589, doi: 10.1109/EUMA.1974.331987.

[78] J. C. Redd, H. C. Hyams and D. E. Collins, "Use of Graphite-Epoxy Pseudo-Elliptic Function Multiplexers for INTELSAT V," in *Proc. EASCON Conf.*, Washington, DC, 1978.

[79] J.E. Keigler, "RCA Satcom: An Example of Weight-Optimized, Satellite Design for Maximum Communications Capacity," *Acta Astronautics*, volume-5, issue 3-4, 1978, pages 219-242, https://doi.org/10.1016/0094-5765(78)90055-3

[80] W. G.Lin, "Microwave Filters Employing a Single Cavity Excited in More Than One Mode," *J. Appl. Phys.*, vol. 22, pp 989-1001, Aug. 1951. https://doi.org/10.1063/1.1700114.

[81] B. L. Blacier and A. R. Champeau, "Dual-Mode Circular and/or Square Waveguide Filters," U.S. Patent 3 697 898, issued Oct. 1972.

[82] A. E. Williams, "A Four-Cavity Elliptic Waveguide Filter," in *IEEE Transactions on Microwave Theory and Techniques*, vol. 18, no. 12, pp. 1109-1114, December 1970, doi: 10.1109/TMTT.1970.1127419.

[83] R. R. Bonetti and A. E. Williams, "Application of Dual TM-Modes to Triple and Quadruple Mode Filters," in *IEEE Transactions on Microwave Theory and Techniques*, vol. 35, no. 12, pp. 1143-1149, Dec 1987, doi: 10.1109/TMTT.1987.1133829.

[84] D. Siu, "Quadruple mode filter," Canadian Patent 1 218 122 issued Feb. 17, 1987.

[85] S. Kallianteris, "Low insertion loss wave guide filter," Canadian Patent 1 050 127, issued March 6, 1979.

[86] Ali E. Atia and Albert E. Williams, "General TE_{011}-Mode Waveguide Bandpass Filters," *IEEE-MTT-S International Microwave Symposium*, 1975, pp. 60-62, doi: 10.1109/MWSYM.1975.1123280.

[87] B. Yassini, M. Yu and B. Keats, "A Ka-Band Fully Tunable Cavity Filter," in *IEEE Transactions on Microwave Theory and Techniques*, vol. 60, no. 12, pp. 4002-4012, Dec. 2012, doi: 10.1109/TMTT.2012.2224367.

[88] B. Yassini and M. Yu, "A Novel Ka-band Dual Mode Super Q Cavity Filter," 2014 *IEEE MTT-S International Microwave Symposium* (IMS2014), 2014, pp. 1-3, doi: 10.1109/MWSYM.2014.6848452.

[89] B. Yassini and M. Yu, "Ka-band Dual-Mode Super Q Filters and Multiplexers," in *IEEE Transactions on Microwave Theory and Techniques*, vol. 63, no. 10, pp. 3391-3397, Oct. 2015, doi: 10.1109/TMTT.2015.2462822.

[90] R. M. Livingston, "Predistorted Waveguide Filters for Use in Communications Systems," 1969 *G-MTT International Microwave Symposium*, 1969, pp. 291-297, doi: 10.1109/GMTT.1969.1122705.

[91] A.E. Williams, W.G. Bush, R.R. Bonetti, "Predistortion Techniques for Multicoupled Resonator Filters," 1984 *IEEE MTT-S International Microwave Symposium Digest*, 1984, pp. 290-291, doi: 10.1109/MWSYM.1984.1131768.

[92] Ming Yu, Wai-Cheung Tang, A. Malarky, V. Dokas, R. Cameron and Ying Wang, "Predistortion Technique for Cross-Coupled Filters and Its Application to Satellite Communication Systems." in *IEEE Transactions on Microwave Theory and Techniques*, vol. 51, no. 12, pp. 2505-2515, Dec. 2003, doi: 10.1109/TMTT.2003.820172.

[93] Ming Yu, V. Dokas, Wai Cheung Tang, R. Cameron, "Novel Adaptive Predistortion Technique for Cross Coupled Filters," *IEEE MTT-S International Microwave Symposium Digest*, 2003, 2003, pp. 929-932 vol.2, doi: 10.1109/MWSYM.2003.1212521.

[94] M. Yu, R. Cameron, D. Smith, V. Dokas and Y. Wang, "Symmetrical Realization for Predistorted Microwave Filters," *IEEE MTT-S*

International Microwave Symposium Digest, 2005., 2005, pp. 245-248, doi: 10.1109/MWSYM.2005.1516571.

[95] Ming Yu, Vahid Miraftab, "Shrinking Microwave Filters," in *IEEE Microwave Magazine*, vol. 9, no. 5, pp. 40-54, Oct. 2008, doi: 10.1109/MMM.2008.927636.

[96] A. Guyette, I. Hunter and R. Pollard, "The Design of Microwave Bandpass Filters Using Resonators with Nonuniform Q," in *IEEE Transactions on Microwave Theory and Techniques*, vol. 54, no. 11, pp. 3914-3922, Nov. 2006, doi: 10.1109/TMTT.2006.884627.

[97] A. Guyette, I. Hunter and R. Pollard, "Exact Synthesis of Microwave Filters with Nonuniform Dissipation," 2007 *IEEE/MTT-S International Microwave Symposium*, 2007, pp. 537-540, doi: 10.1109/MWSYM.2007.380545.

[98] Marco L, "A Review of Temperature Compensated Techniques for Microwave Resonators and Filters." Micro and Millimeter wave Technology and Techniques Workshop 2014, Estec, Noordwijk, The Netherlands.

[99] Marco L, "Temperature Compensation of Microwave Resonators and Filters for Space Applications," *Microwave Journal* 57.11 (2015): 100-108.

[100] I. C. Hunter, L. Billonet, B. Jarry, and P. Guillon, "Microwave Filters Applications and Technology," in *IEEE Transactions on Microwave Theory and Techniques*, vol. 50, no. 3, pp. 794-805, March 2002, doi: 10.1109/22.989963.

[101] A. E. Atia, "A 14-GHz High-Power Filter," 1979 *IEEE MTT-S International Microwave Symposium Digest*, 1979, pp. 261-261, doi: 10.1109/MWSYM.1979.1124037.

[102] D. Rosowsky and D.Wolk, "A 450-W Output Multiplexer for Direct Broadcasting Satellites," in *IEEE Transactions on Microwave Theory and Techniques*, vol. 30, no. 9, pp. 1317-1323, Sep. 1982, doi: 10.1109/TMTT.1982.1131254.

[103] M. Klauda, T. Kässer, B. Mayer, C. Neumann, F. Schnell, B. Aminov, A. Baumfalk,H. Chaloupka, S. Kolesov, H. Piel, N. Klein, S. Schornstein, and

M. Bareiss, “Superconductors and Cryogenics for Future Communication Systems,” in *IEEE Transactions on Microwave Theory and Techniques*, vol. 48, no. 7, pp. 1227-1239, July 2000, doi: 10.1109/22.853466.

[104] E. R. Soares, J. D. Fuller, P. J. Marozick, and R. L. Alvarez, “Applications of High-Temperature-Superconducting Filters and Cryo-electronics for Satellite Communication,” in *IEEE Transactions on Microwave Theory and Techniques*, vol. 48, no. 7, pp. 1190-1198, July 2000, doi: 10.1109/22.853459.

[105] G. L. Matthaei, “Comb-line Band-Pass Filters of Narrow or Moderate Bandwidth,” *Microwave Journal*, vol. 6, pp. 82–91, Aug. 1963.

[106] G. L. Matthaei , “Interdigital Band-Pass Filters,” in *IRE Transactions on Microwave Theory and Techniques*, vol. 10, no. 6, pp. 479-491, November 1962, doi: 10.1109/TMTT.1962.1125556.

[107] G. Craven and C. K. Mok, “The Design of Evanescent Mode Waveguide Bandpass Filters for a Prescribed Insertion Loss Characteristic,” in *IEEE Transactions on Microwave Theory and Techniques*, vol. 19, no. 3, pp. 295-308, Mar. 1971, doi: 10.1109/TMTT.1971.1127503.

[108] C. Wang, K.A. Zaki, “Temperature Compensation of Combline Resonators and Filters,” 1999 *IEEE MTT-S International Microwave Symposium Digest* (Cat. No.99CH36282), 1999, pp. 1041-1044 vol.3, doi: 10.1109/MWSYM.1999.779566.

[109] D. J. Small and J. A. Lunn. “Temperature compensated high power bandpass filter.” U.S.Patent 6529104, Mar. 4, 2003.

[110] D. J. Small and J. A. Lunn. “Temperature compensated high power bandpass filter.” U.S. Patent 6232852, May15, 2001

[111] S. B. Lundquist. “Temperature compensated microwave filter.” U.S. Patent 815223, Feb. 2, 1999.

[112] W. Fitzpatrick, M. Yu, D. Smith, and A. Sivadas, “Microwave resonator having an external temperature compensator,” U.S. Patent 6 535 087, Mar. 18, 2003.

[113] V. Singh, P. K. Ambati, S. Soni and K. Karthik, “Enhancing Satellite Communications: Temperature-Compensated Filters and Their

Application in Satellite Technology," in *IEEE Microwave Magazine*, vol. 20, no. 3, pp. 46-63, March 2019, doi: 10.1109/MMM.2018.2885674.

[114] B. F. Keats, "Temperature compensation for cavity resonators using shape memory alloys," Master's thesis, University of Waterloo, Waterloo, Ontario, 2003.

[115] B. F. Keats, R. R. Mansour, and R. B. Gorbet, "Shape Memory Alloy Temperature Compensation for Resonators," IEEE Digest on Microwave Theory and Techniques Symposium. 2(2003): 1259–1262

[116] B. F. Keats, R. B. Gorbet, and R. R. Mansour, "Design and Testing of SMA Temperature-Compensated Cavity Resonators," in *IEEE Transactions on Microwave Theory and Techniques*, vol. 51, no. 12, pp. 2284-2289, Dec. 2003, doi: 10.1109/TMTT.2003.820166.

[117] Atia, A.E. and Williams, A.E., "Nonminimum-Phase Optimum-Amplitude Bandpass Waveguide Filters," in *IEEE Transactions on Microwave Theory and Techniques*, vol. 22, no. 4, pp. 425-431, Apr. 1974, doi: 10.1109/TMTT.1974.1128242.

[118] Atia, A.E., Williams, A.E., and Newcomb, R.W., "Narrow-Band Multiple-Coupled Cavity Synthesis," in *IEEE Transactions on Circuits and Systems*, vol. 21, no. 5, pp. 649-655, September 1974, doi: 10.1109/TCS.1974.1083913.

[119] Cameron RJ, Mansour RR, Kudsia CM. "Microwave filters for communication systems: Fundamental, design and Applications." Hoboken, NJ, USA: Wiley; 2007.

[120] Carlin, H.J., "The scattering matrix in network theory.," in *IRE Transactions on Circuit Theory*, vol. 3, no. 2, pp. 88-97, June 1956, doi: 10.1109/TCT.1956.1086297.

[121] Gantmacher, F.R. "The Theory of Matrices." vol. 1, NewYork, the Chelsea Publishing Co.:1959.

[122] Fröberg, C.E. "Introduction to Numerical Analysis." MA, Addison-Wesley: 1965.

[123] Hamburger, H.L. and Grimshaw, M.E. "Linear Transformations in n-Dimensional Space." London, Cambridge University Press: 1951.

[124] Tsukasa Yoneyama and Shigeo Nishida, "Non-radiative Dielectric Waveguide for Millimeter Wave Integrated Circuits," in *IEEE Transactions on Microwave Theory and Techniques*, vol. 29, no. 11, pp. 1188-1192, Nov. 1981, doi: 10.1109/TMTT.1981.1130529.

[125] T. Yoneyama, F. Kuroki, and S. Nishida, "Design of Nonradiative Dielectric Waveguide Filter," in *IEEE Transactions on Microwave Theory and Techniques*, vol. 32, no. 12, pp. 1659-1662, Dec. 1984, doi: 10.1109/TMTT.1984.1132909.

[126] J.C. Olivier and J.A.G Malherbe, "A Bandpass Filter Using Circular Discontinuities in Nonradiative Dielectric Waveguide," 1987 *IEEE MTT-S International Microwave Symposium Digest*, 1987, pp. 419-422, doi: 10.1109/MWSYM.1987.1132420.

[127] F. Boone and Ke Wu, "A Multiple Strip Nonradiative Dielectric Guide Filter Design," in Antenna - *Symposium on antenna technology and applied electromagnetic,* pages 815-818, Montreal, Quebec, Canada, August 6-9 1996

[128] J. Huang, K. Wu, T. Wang, and R.G. Bosisio, "Rigorous Fields Theoretical Design and Optimization of Novel Window-Coupled NRD-Guide Bandpass Filters," in *Proc. Asia-Pacific Microwave Conference*, pages 79-82, Tokyo, Japan, December 1994. vol. 1.

[129] T. Shimizu, Takashi & Yoneyama, Tsukasa. (2006). 60 GHz Bandpass Filter Using NRD Guide E-plane Resonators. *IEICE Transactions. 89-C.* 1851-1857. 10.1093/ietele/e89-c.12.1851.

[130] Smith DJ. "Filter utilizing a bar coupling." US Patent 6255919 B1, 2001.

[131] Ness JB, "A Unified Approach to Design, Measurement, and Tuning of Coupled-Resonator Filters," in *IEEE Transactions on Microwave Theory and Techniques*, vol. 46, no. 4, pp. 343-351, April 1998, doi: 10.1109/22.664135.

[132] Cst.com. (2018). CST-Computer Simulation Technology. [online] Available at: https://www.cst.com.

[133] Thomas JB, "Cross-Coupling in Coaxial Cavity Filters – A Tutorial Overview," in *IEEE Transactions on Microwave Theory and Techniques*, vol. 51, no. 4, pp. 1368-1376, April 2003, doi: 10.1109/TMTT.2003.809180.

[134] Kocbach J, Folgero K., "Design Procedure for Waveguide Filters with Cross-Couplings," *2002 IEEE MTT-S International Microwave Symposium Digest* (Cat. No.02CH37278), 2002, pp. 1449-1452 vol.3, doi: 10.1109/MWSYM.2002.1012128.

[135] Bornemann, J.; Rosenberg, U.; Amari, S.; Vahldieck, R.: "Tolerance Analysis of Bypass-, Cross- and Direct-Coupled Rectangular Waveguide Band-Pass Filters", *IEE Proceedings - Microwaves, Antennas and Propagation*, 2005, 152, (3), p. 167-170, DOI: 10.1049/ip-map:20041158

[136] S. Amari and U. Rosenberg, "Characteristics of Cross (Bypass) Coupling Through Higher/Lower Order Modes and Their Applications in Elliptic Filter Design," in *IEEE Transactions on Microwave Theory and Techniques*, vol. 53, no. 10, pp. 3135-3141, Oct. 2005, doi: 10.1109/TMTT.2005.855359.

[137] U. Rosenberg, S. Amari and J. Bornemann, "Inline TM/sub 110/-Mode Filters with High-Design Flexibility by Utilizing Bypass Couplings of Nonresonating TE/sub 10/01/ Modes," in *IEEE Transactions on Microwave Theory and Techniques*, vol. 51, no. 6, pp. 1735-1742, June 2003, doi: 10.1109/TMTT.2003.812577.

[138] N. Mohottige, O. Glubokov, U. Jankovic and D. Budimir, "Ultra Compact Inline E-Plane Waveguide Bandpass Filter Using Cross-Coupling," in *IEEE Transactions on Microwave Theory and Techniques*, vol. 64, no. 8, pp. 2561-2571, Aug. 2016, doi: 10.1109/TMTT.2016.2578329.

[139] Ruiz-Cruz JA, Zaki KA, Montejo-Garai JR, Rebollar JM, "Design of Elliptic Filters in Rectangular Waveguide with Capacitive and Inductive Irises and Integrated coaxial Excitation," *IEEE MTT-S Int. Microwave Symp. Digest*; 2005:1492-1452, doi:10.1109/MWSYM.2005.1516577.

[140] Ruiz-Cruz JA., Montejo-Garai JR, Rebollar JM, Zaki KA. Waveguide Filters with Elliptical Function Response: Overview and Results Of

Different Implementations. *International Journal of RF and Microwave Computer Aided Engineering*. 17 (2007): 63-69. doi:10.1002/mmce.20198

[141] J. R. M. Vaughan, "Multipactor," in *IEEE Transactions on Electron Devices*, vol. 35, no. 7, pp. 1172-1180, July 1988, doi: 10.1109/16.3387.

[142] M. Yu, "Power-Handling Capability for RF Filters," in IEEE Microwave Magazine, vol. 8, no. 5, pp. 88-97, Oct. 2007, doi: 10.1109/MMM.2007.904712.

[143] "Multipaction design and test," European Space Agency. Noordwijk, the Netherlands: ECSS-E-20-01A Rev.1; 2013.

[144] Woode A, Petit J., "Diagnostic investigations into the multipactor effect, Susceptibility zone measurements and parameters affecting a discharge," European Space Agency, Noordwijk, The Netherlands: ESTEC Working Paper 1556;1989.

[145] Woo R., "Final report on RF voltage breakdown in coaxial transmission lines," Jet Propulsion Lab, CA, U.S.A.:Tech. Rep.32-1500; 1970.

[146] Yu M., "Introduction to practical aspects of microwave filter design and realization,"Proc. IEEE Int,l Microwave Symp.,Workshop WMB:Filter II: Practical Aspects of Microwave Filter Design and Realization. Long Beach; 2005.

[147] SPARK 3D. [online] Available at: https://www.fest3d.com/rk3d.php